Isolation of paleofield information from the natural remanent magnetization of marine sediments using stratigraphic networks

Dissertation

Zur Erlangung des Doktorgrades der Naturwissenschaften

am Fachbereich Geowissenschaften der

Universität Bremen

vorgelegt von

Daniela Irene Hofmann

Bremen Juli 2008

Tag des Kolloquiums:

31. Oktober 2008

Gutachter:

Herr Prof. Dr. Ulrich Bleil

Frau PD Dr. Sabine Kasten

Prüfer:

Herr Prof. Dr. Heinrich Villinger

Herr Dr. habil. Karl Fabian

Abstract

Observations of the Earth's magnetic field discovered dramatic changes of its intensity. In the last ca. 100 years the dipole moment decreased by about 10 %. Such decreases of the geomagnetic field were observed already in the history of the Earth's magnetic field and even times were the polarity completely reverses. To understand more of the dynamics of such variations in intensity of the Earth's magnetic field high - resolution data from the ancient magnetic field are needed. Sedimentary sequences have become more and more interesting for paleointensity investigations because they give continuous records of the past variations of the Earth's magnetic field and have a reasonable global distribution. The mechanism of acquisition of natural remanent magnetization in sediments is strongly influenced by a variety of factors and the current state of knowledge about them is poor.

The aim of this study is to enhance the understanding of remanence acquisition in sediments. The complete study includes four publications, which are published or have been submitted for publication. The basis for this study are eight sediment series, recovered on a North-South profile across the Subtropical Front in the subtropical and subantarctic South Atlantic. Noticeable lithologic variations are observed between the different cores of the transect. Different water - masses strongly affect sediment accumulation and composition. Sedimentation rates decrease from South to North from about 4 cm/kyr to less than 1 cm/kyr. High - resolution measurements of magnetic and compositional data are performed for each core to form a multi - parameter data set. Newly adopted mathematical techniques are developed and by using multi - parameter signal correlations it is possible to define a high - resolution timescale for the eight sediment series. Taking into account correlations between all pairs of multi - parameter data sets, and correlation errors between core pairs (A,B) and (B,C) are controlled by comparison with (A,C). The final age model is called a stratigraphic network. The stratigraphic network provides to study the variations of paleomagnetic, paleoclimatic and oceanographic conditions during time of all sediment series. In addition, the results enable to trace temporal shifts of the Subtropical Front.

Based on this stratigraphic network it is possible to investigate high - resolution measurements of rock magnetic properties, the natural remanent magnetization (NRM) and artificial remanences like anhysteretic and isothermal remanent magnetization (ARM and IRM). Principal component analysis (PCA), which is a standard statistical tool to extract relevant information from a complex data set, is applied to isolate the predominant independent environmental signal components from the rock - magnetic parameters. This method reduces lithologic and climatic influence upon the relative paleointensity record. For the network cores a homogeneity interval, where remanences are only affected by a single environmental signal, was found. Relative paleointensity was determined in this homogeneity interval and the results were used to construct a first relative paleointensity stack for the central South Atlantic covering the last 300 ka. This stack connects southern and northern hemisphere relative paleointensity data.

The final aim of this study is to analyze the influence of lithology upon relative paleointensity, and to assess lithologic influences based on a comparison between many different recordings of the same field history. Due to the regional proximity of the records, they

have experienced approximately the same magnetic field history and variations between the single relative paleointensity signals are caused by their different lithologic composition. The performed studies upon rock - magnetic and compositional data as well as investigations of the relative paleointensity of the network cores provide a more detailed analysis of parameters, which influence the natural remanence of sediments. Therefore, a linear extension of the standard relative paleointensity determination is developed which enables to quantitatively test and compare the influence of different sediment properties and finally correct for such influences. The new relative paleointensity determination is used to construct a new corrected paleointensity stack for the central South Atlantic. This corrected paleointensity stack can be compared to other local and global paleointensity data. Another finding of this study is that the ratio between corrected and uncorrected relative paleointensity stack reveals a hidden climate signal, which indicates that climatic variations in sediment composition are present in non-ideal sediment sequences. The results contribute to the overall understanding of remanence acquisition in sediments and enhance the possibility to use sedimentary records as recorders of the ancient magnetic field.

Zusammenfassung

Das Erdmagnetfeld zeigt starke Variationen in der Intensität. In den letzten 100 Jahren hat die Intensität des Dipol-Moments um ca. 10 % abgenommen. In der Geschichte des Erdmagnetfeldes sind vergleichbare Abnahmen bereits öfter beobachtet worden. Auch Feldumkehrungen der magnetischen Pole sind häufige Ereignisse auf geologischen Zeitskalen. Zum besseren Verständnis der Dynamik dieser Variationen werden hochauflösende Daten des früheren Erdmagnetfeldes benötigt. Sedimente sind in den letzten Jahren immer interessanter für Paläointensitätsuntersuchungen geworden, da sie die Variationen des Erdmagnetfelds kontinuierlich und auf globaler Skala aufzeichnen. Der Mechanismus des Remanenzerwerbs in Sedimenten wird jedoch durch eine Vielzahl von Faktoren beeinflusst, die bisher noch nicht vollständig verstanden sind.

Ziel dieser Arbeit ist es, einen Beitrag zum Verständnis des Remanenzerwerbes in Sedimenten zu leisten. Sie umfasst vier international begutachtete Veröffentlichungen, die entweder bereits publiziert sind, oder zur Publikation eingesendet wurden.
Die Datengrundlage dieser Arbeit bilden acht Sedimentkerne, die entlang eines Nord - Süd Profiles gewonnen wurden, welches die Subtropische Front im subtropischen und subantarktischen Südatlantik kreuzt. Die Kerne zeigen deutliche Unterschiede in ihren lithologischen Zusammensetzungen. Das Untersuchungsgebiet wird von verschiedenen Wassermassen beeinflusst, die sowohl die Sedimentzusammensetzung als auch die Sedimentationsrate deutlich beeinflussen. Es ist eine Abnahme der Sedimentationsrate von Süden, mit ca. 4 cm/kyr, nach Norden, mit weniger als 1 cm/kyr, zu beobachten. Für jeden Sedimentkern wurden hochauflösende Messungen magnetischer Parameter sowie der Zusammensetzung des Sedimentes durchgeführt, um einen multi - parameter Datensatz zu gewinnen. Mit Hilfe neu entwickelter mathematischer Methoden wurde ein Programm zur Korrelation von multi - parameter Datensätzen entwickelt, mit dem ein hochauflösendes Altersmodell für die acht Sedimentkerne erstellt wurde. Dabei werden paarweise Korrelationen aller multi - parameter Datensätze berücksichtigt und Fehler zwischen der paarweisen Korrelation von Kernen (A,B) und (B,C) werden durch den Vergleich der Korrelation zwischen (A,C) entdeckt und ausgeglichen. Das daraus resultierende endgültige Altersmodell bildet ein stratigraphisches Netzwerk. Dieses stratigraphische Netzwerk ermöglicht es, die zeitlichen Variationen in paläomagnetischen, paläoklimatischen und ozeanographischen Gegebenheiten zu untersuchen. Insbesondere geben die Ergebnisse auch Aufschluss über die zeitliche Verschiebung der Subtropischen Front.

Basierend auf dem stratigraphischen Netzwerk können hochauflösende Messungen gesteinsmagnetischer Parameter, der natürlichen remanenten Magnetisierung (NRM) und
künstliche Remanenzen, wie der anhysteretischen und der isothermen remanenten Magnetisierung (ARM, IRM) durchgeführt werden. Durch Hauptkomponentenanalyse der gesteinsmagnetischen Parameter, welche eine statistische Methode zur Extraktion wichtiger Informationen eines komplexen Datensatzes ist, wurden die Komponenten der vorherrschenden, unabhängigen Umweltsignale isoliert. Mit dieser Methode kann der Einfluss lithologischer und klimatischer Faktoren auf die relative Paläointensität reduziert werden. Für die Kerne des stratigraphischen Netzwerkes wurde ein Homogenitätsintervall gefunden, in dem die Remanenzen nur von einem Umweltsignal beeinflusst werden. Die relative Paläointensität innerhalb dieses Homogenitätsintervalls wurde verwendet, um den ersten

relativen Paläointensitätsstack der letzen 300 ka, für den zentralen Südatlantik zu erstellen. Dieser Stack verknüpft relative Paläointensitätsdaten der nördlichen und südlichen Hemisphäre.
Das letztendliche Ziel dieser Arbeit ist die Analyse des Einflusses der Lithologie auf die relative Paläointensität und die Bestimmung dieses Einflusses, durch Vergleich vieler unterschiedlicher Aufzeichnungen mit der gleichen erdmagnetischen Geschichte. Aufgrund der regionalen Nachbarschaft der Sedimentkerne, kann angenommen werden, dass alle das gleiche Magnetfeld erfahren haben und Unterschiede zwischen den einzelnen relativen Paläointensitätssignalen durch die unterschiedliche lithologische Zusammensetzung bedingt werden. Die bisherigen Untersuchungen der gesteinsmagnetischen Parameter, der Zusammensetzung des Sedimentes sowie der relativen Paläointensität der Kerne des Netzwerkes ermöglichen eine detailierte Analyse der Parameter, die einen Einfluss auf die natürliche remanente Magnetisierung haben. Durch lineare Erweiterung der bisher üblichen relativen Paläointensitätbestimmung ist es möglich, den Einfluss verschiedener Sedimentparameter quantitativ zu bestimmen. Die neu entwickelte Methode zur relativen Paläointensitätsbestimmung wird verwendet, um einen neuen korrigierten Paläoinensitätsstack zu erstellen. Dieser korrigierte Paläointensitätsstack kann mit anderen lokalen und globalen Paläointensitätsdaten verglichen werden. Ein unerwartetes Ergebnis dieser Arbeit ist, dass das Verhältnis zwischen korrigiertem und unkorrigiertem relativen Paläointensitätsstack ein nicht direkt sichtbares Klimasignal zeigt. Solche klimatischen Variationen sind in der Sedimentzusammensetzung aller nicht-idealer Sedimente vorhanden. Die Resultate tragen somit zum allgemeinen Verständnis des Remanenzgewinns in Sedimenten bei und verbessern die Möglichkeit, Sedimente zur Untersuchung des Erdmagnetfeldes zu verwenden.

Contents

1 Introduction

1.1 Variations of the Earth's magnetic field

The study of the Earth's magnetic field is one of the oldest in geophysical disciplines. During the last 150 years the geomagnetic field has been analyzed and the data have been published as global maps. In the last 40 years standardized methods were applied for the analysis of the data, resulting in the International Geomagnetic Reference Field (IGRF). The intensity of the earth magnetic field was observed to vary considerable on different time scales from million of years to seconds. Studies on lava flows found, that the Earth's magnetic field even completely reverses in intervals ranging from tens of thousands to many million years. The last event, the so called Matuyama - Brunhes reversal, occured ~ 0.780 million years ago. On basis of such events it was possible to create a geomagnetic polarity time scale (Figure 1, [1]), which is used to correlate records from different locations to create a common time scale.

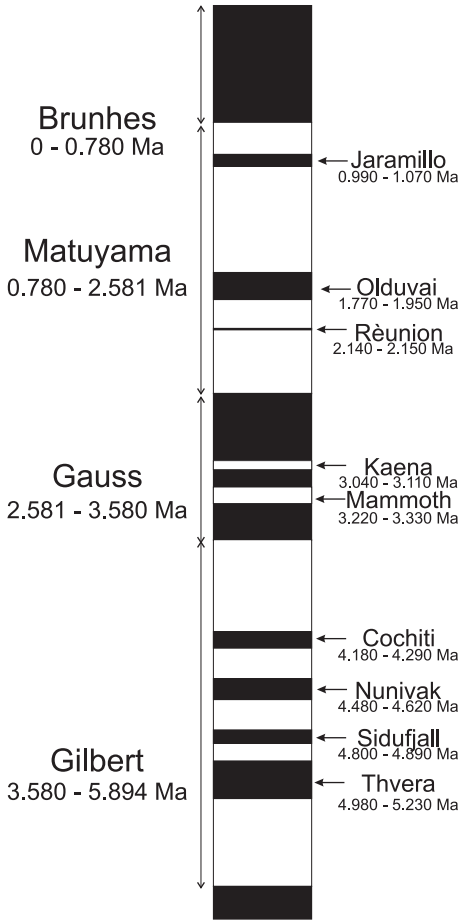

Figure 1: Polarity changes of the geomagnetic field during the last 5 Ma. Black shows times with normal polarity (like today's polarity), white with reversed polarity (after [1])

.

Since the last reversal $\sim$ 0.780 million years ago, there were several attempts to reverse the field, the so called excursions. The last one is the Laschamp excursion $\sim$ 41000 years ago. The excursions are periods with a duration of several thousand years where the field is relatively weak and seems to reverse in some parts of the globe whereas in other parts only a strong secular variation is present. The process in the Earth core, which causes such excursions and field reversals is still not understood, therefore to study the variations of the ancient Earth magnetic field is of global interest and paleointensity data are needed to achieve a better understanding how the geomagnetic field reverses its polarity, how and why geomagnetic excursions occur and to understand the mechanisms driving paleosecular variations. Further estimating the ancient intensity of the geomagnetic field is important for understanding long-term field evolution and for constraining models of the Earth's magnetic dynamo. In recent times more and more numerical dynamo models have been produced but still no complete theory exists of how the Earth's magnetic field is generated and what causes the variations of the magnetic field. To advance such dynamo models and to understand more of the processes in the Earth interiors, continuous paleointensity data are needed.

1.2 Sedimentary magnetism

Magnetic minerals have the capability to carry a stable permanent magnetization and therefore they can be used as recorders of the recent and the ancient Earth's magnetic field. Lava flows were used for paleointensity determination, but volcanic rocks are produced only in irregularly time intervals and do not yield a continuous record of the ancient magnetic field. In the last years sedimentary sequences have become increasingly interesting for paleointensity investigations because they give continuous records of the past variations of the Earth magnetic field and have a reasonable global distribution. Determining paleointensity from sediments is restricted by the quality of sedimentary records and the lack of a common theory of how sediments record the paleointensity. The here presented study gives an attempt to enhance sedimentary records for paleointensity investigations. The natural remanent magnetization (NRM), present in a rock sample prior to laboratory treatment is the main magnetic parameter used for paleomagnetic studies. NRM depends on the geomagnetic field and has been acquired by a variety of mechanisms during rock formation and during the geological history of the rock. NRM is typically composed of more than one component. The NRM component acquired during rock formation is referred to as primary NRM and is the component sought in most paleomagnetic investigations. Secondary NRM components may be acquired subsequent to rock formation and can alter or obscure the primary NRM. Three basic forms of primary NRM are (1) thermoremanent magnetization (TRM), which is acquired during cooling from high temperature, (2) chemical remanent magnetization (CRM), formed by growth of ferrimagnetic grains below the Curie temperature and (3) detrital remanent magnetization (DRM), acquired during accumulation of sedimentary rocks containing detrital ferrimagnetic minerals. The latter becomes important while studying remanence acquisition in sediments. A classical DRM is acquired by a single magnetic particle which tend to align with the ambient magnetic field while settling through the water column and after deposition retain a DRM. This occurs very quickly, even when Brownian motion is taken into account [2]. In marine environments, the above single-grain sedimentation is unrealistic also, because small magnetic particles are likely to reach the sediment-water interface in bigger flocculated or coagulated compounds within which the particles are already mechanically or electrostatically bound.

The relative remanence directions of the magnetic particles within such a compound are probably uncorrelated and the coupling upon the compound due to the total remanence is negligible in comparison to the mechanical coupling due to irregular shape or turbulent flow [3, 4, 5]. When the particles reach the sediment/water boundary the particles can undergo secondary or so called post-depositional processes. Such post-depositional processes can be for example bioturbation or some mechanical or chemical processes (Figure 2). The DRM does not survive in the mixed layer of the sediment, therefore all sedimentary NRM must be considered to be a post-depositional remanent magnetization (pDRM). It is unknown how magnetic particles are fixed and whether they still can acquire a pDRM, although the latter is likely. At the so - called "lock - in - depth", the grains become consolidated (Figure 2). Below the "lock - in - depth"the particles undergo some compaction processes. Due to compaction the magnetic particles may rotate in response, which can lead to inclination shallowing ([6, 7, 8]). A broad study on effects influencing magnetic particles during sedimentation is given in [9].

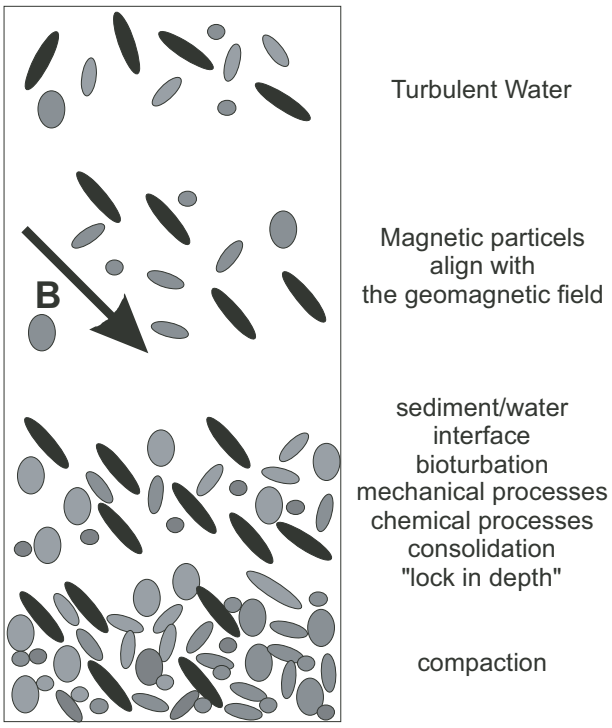

Figure 2: Schematic drawing of the journey of magnetic particles from the water column to burial. Magnetic particles (black) tend to align with the ambient geomagnetic field. At the water/sediment boundary secondary processes. like bioturbation is possible, in the "lock-in-depth" the particles are locked in in the sediment matrix and then they undergo some compaction processes.

1.3 Determination of relative paleointensity

Sedimentary magnetization is related to the quantity and type of magnetizable material within the sediment. The common method of determining paleointensity from sediments is to divide the intensity of the natural remanent magnetization (NRM) left after removal of any viscous components by a normalizer which represents the variability in the mag-

netization potential of sediments [6, 9]. The ideal normalizer activates the same grains as those which carry the NRM, thereby compensating for down core variations in the concentration of remanence carrying grains. The anhysteretic remanent magnetization, the isothermal remanent magnetization (ARM, IRM), and the low field susceptibility (κ) are commonly used as normalizers. Advantages and disadvantages of ARM, IRM or κ as normalizing parameters are still widely discussed [9, 10, 11, 12, 13, 14]. Seemingly the most reliable normalizers are ARM and IRM because they are remanence based, as the NRM, and resemble the NRM in their demagnetization behavior. Susceptibility also encompasses paramagnetic, superparamagnetic and large multi - domain grains, which contribute nothing or very little to the NRM. However, our knowledge of the processes responsible for the magnetization of marine sediments is far from being complete, and a number of non-geomagnetic phenomena can affect the magnetic record in sediments, such as changes in grain size and mineralogy variations, and/or diagenetic processes in the sedimentary column [15, 16, 17]. A number of quality criteria have been proposed to select sediments suitable for paleointensity determination [9, 11]. Common requirements are that the main remanence carrier is magnetite, and that of the sediment is homogeneous with respect to composition and grain size. Variations in concentration of the magnetic carrier must be less than an order of magnitude, and the grain size of the magnetic mineral assemblage should be in the range of 1 – 15 μm. Finally, the NRM should exhibit no inclination error and no diagenetic overprint. In recent times relative paleointensity has been determined from sedimentary records from all over the world to constrain changes in regional or global magnetic field intensity and to allow a separation of geomagnetic and environmental signal ([12, 18, 19, 20, 21]). Further, approaches have been made to improve relative paleointensity records [22, 23, 24, 25, 26, 27]. The here presented study tries to contribute to the understanding of the mechanism of remanence acquisition in sediments, and to improve the methods for creating relative paleointensity records.

2 Objective and methods

Sedimentary sequences are the most important continuous archives of the past variations of the Earth's magnetic field. Yet, the fundamental problem to understand the physics of remanence acquisition in sediments has not been solved. Relative paleointensity determination is still very descriptive and qualitative. In this study a quantitative method is developed to estimate the influence of sediment composition upon relative paleointensity records. A set of sediment series from a constraint area but with very different sediment compositions is used. These sediment series are combined in a high - resolution stratigraphic network (**S**outh **A**tlantic **S**tratigraphic **Net**work - SASNET) and high - resolution records of many different physical, chemical and magnetic parameters have been generated. The stratigraphic network was set up by using a newly developed computer aided multi-parameter correlation tool which allows synchronous correlation of different sediment parameters. This provides equally good correlation between all cores. The cores from the SASNET where then used for a detailed study of natural remanence and rock - magnetic properties.

2.1 Oceanographic setting and sediment composition

During R/V Meteor Cruise M46/4 a set of 29 gravity cores were recovered from the western flank of the Mid Atlantic Ridge (MAR) and in the adjacent basins including the Argentine Basin, the Cape Basin and the Brasil Basin [28]. Lithologic description and shipboard measurements of magnetic susceptibility and wet bulk density [28] were used to select eight apparently continuous and undisturbed gravity cores for further study. The

Table 1: Sampling site, recovered length, water depth, age and estimated average sedimentation rate $\sigma_{\text{est.}}$ of the eight selected cores.

GeoB	Latitude [S]	Longitude [W]	Length [m]	Depth [m]	Age [ka]	$\sigma_{\text{est.}}$ [cm/kyr]
6428-1	32°30.60'	24°14.91'	7.26	4015	1801	0.4
6426-1	33°30.00'	24°01.50'	13.31	4385	1323	1.0
6425-2	33°49.51'	23°35.24'	10.89	4352	1028	1.0
6422-1	35°42.45'	22°44.01'	5.45	3972	297	1.8
6421-2	36°26.70'	22°26.70'	9.60	4220	442	2.2
6407-1	42°02.70'	19°30.00'	5.45	3384	388	1.4
6408-4	43°36.85'	20°26.46'	10.57	3797	302	3.5
6405-6	42°00.00'	21°51.19'	12.12	3862	302	4.0

coring sites are located between 32°S, 19°W and 42°S, 24°W at water depths ranging from 3380 m to 4385 m (Table 1). The core locations form a N-S profile across the Subtropical Front (STF), separating the subtropical South Atlantic in the North from the subantarctic South Atlantic in the South (Figure 3).

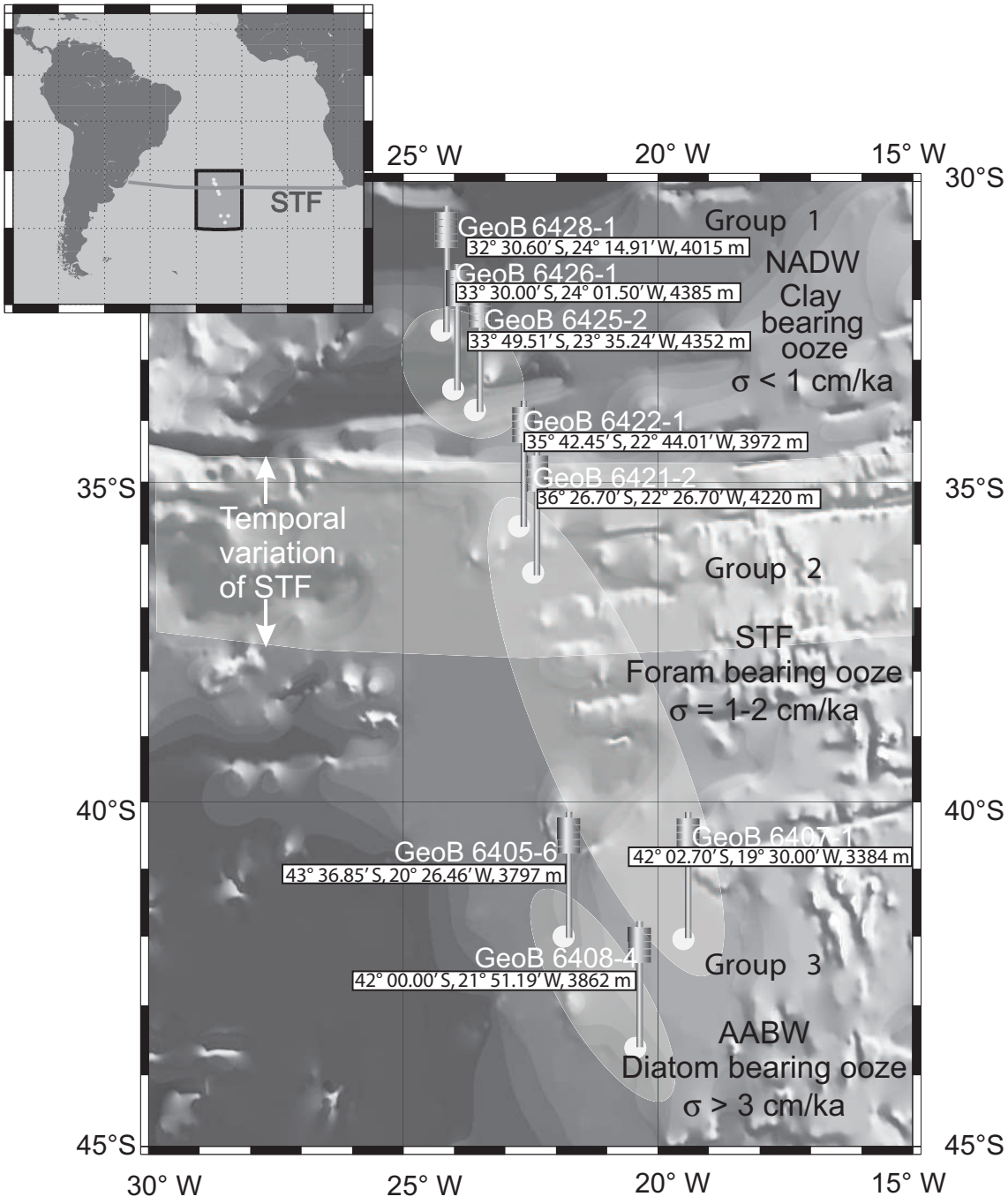

Figure 3: Location, water depth, average sedimentation rates and grouping of the network cores. The inset shows the approximate current position of the sub-tropical front (STF).

The Subtropical Front is characterized by a sharp surface temperature and salinity discontinuity of at least 4°C and 0.005 ‰. At the Subtropical Front the Subantarctic Surface Water (SASW) subducts beneath the northern South Atlantic Central Water (SACW) and merges with the Antarctic Intermediate Water (AAIW). The prevailing deep water masses are nutrient poor North Atlantic Deep Water (NADW) in the northern part and nutrient rich Antarctic Bottom Water (AABW) in the South [29, 30, 31, 32]. The differences between these water masses strongly affect sediment accumulation and composition (Table 1).

This results in noticeable lithologic variations between different cores of the transect. Also within single sediment series which recorded the temporal shifts of the STF during the Quaternary strong lithologic variations are present. Accordingly, the eight cores can be divided into three types of lithology [28, 33]. The influence of the different water masses causes different sedimentation rates with very low rates in the North, where the nutrient poor NADW prevails and with higher rates towards the South, where the nutrient rich AABW influences the sediment series. The northernmost cores GeoB 6425-2, GeoB 6426-1 and GeoB 6428-1 lie in the oligotrophic subtropical South Atlantic north of the STF and contain mainly clay bearing nannofossil ooze. The foram bearing nannofossil ooze of cores GeoB 6407-1, GeoB 6421-2, GeoB 6422-1 are characterized by a higher carbonate content. While cores GeoB 6421-2 and GeoB 6422-1 lie in the vicinity of the STF, core GeoB 6407-1 is located further south close to cores GeoB 6405-6 and GeoB 6408-4 but at shallower water depth (Table 1). It could be assumed that core GeoB 6407-1 show similar composition like the two southern cores, but because it was recovered from a lower water-depth it lies above the carbonate compensation depth (CCD) and therefore is associated to the cores GeoB 6421-2 and GeoB 6422-1. The southernmost cores GeoB 6405-6 and GeoB 6408-4 contain diatom bearing nannofossil ooze.

2.2 Rock-magnetic and composition measurements

High - resolution measurements of physical, chemical and magnetic parameters have been obtained to form the basis of this study.

2.2.1 Magnetic volume susceptibility

Magnetic volume susceptibility κ was measured in 1 cm intervals along the surface of split cores using a Bartington spot sensor type M.S.2.F mounted on a computer controlled positioning system. The instrumental drift was controlled by separate background (zero) readings in air after each single measurement. It is the most widely used parameter to quantify concentration changes of the magnetic mineral fraction, mainly magnetite, in marine sediments [34, 35, 36]. Magnetic susceptibility subsumes ferri-, para- and diamagnetic contributions. For magnetite, κ is relatively constant for grain sizes between 0.1 and 10000 μm, but increases towards smaller superparamagnetic (SP) grains [37]. In the here investigated South Atlantic sediments, variation of κ is mainly due to changes of (titano-) magnetite concentration. Thus, κ can be used as a proxy for terrigenous input in this region [38]. Additionally room temperature frequency dependent susceptibility in sediments indicates the relative concentration of particles in a certain superparamagnetic (SP) grain size range [39]. It was measured on discrete samples using a Bartington bulk sensor M.S.2.B connected to a M.S.2 susceptibility meter, which applies an alternating

field of 0.5 mT at a low frequency of 460 Hz (for κ_{lf}) and a high frequency of 4600 Hz (for κ_{hf}). All data were normalized to a sample volume of 6.2 cm^3

2.2.2 XRF measurements

To measure the elemental composition of the sediment records a X-ray fluorescence (XRF) scanner is used. High-resolution records of elements from potassium through strontium have been determined using an X-ray fluorescence (XRF) scanner developed and built at the Netherlands Institute for Sea Research [40]. The obtained XRF spectra are processed with the software toolbox KEVEX^{TM} [41] calculating relative element intensities in counts per second (cps).

The XRF Fe-records, similar to magnetic susceptibility, correspond to terrigenous content, while Ca-records indicate variations in biogenic carbonate input.

2.2.3 Wet bulk density

Wet bulk density ρ is inferred from electric resistivity measurements performed directly after core splitting with a resolution of 2 cm [28]. According to the empirical Archie's equation, the ratio between measured sediment resistivity R_s and known pore water resistivity R_w can be approximated by a power function

$$R_s/R_w \;=\; k\Phi^{-m}, \tag{1}$$

where Φ denotes the sediment porosity. Following the study of [42], who used the values of $k = 1.30$ and $m = 1.45$ are used to determine Φ which subsequently can be converted into an estimate of wet bulk density ρ [43] by setting

$$\rho \;=\; \Phi\ \rho_{\mathrm{f}} \;+\; (1-\Phi)\ \rho_{\mathrm{m}}. \tag{2}$$

Here, average pore fluid density is $\rho_{\mathrm{f}} \;=\; 1030\ \mathrm{kg/m^3}$ and average matrix density is $\rho_{\mathrm{m}} \;=\; 2670\ \mathrm{kg/m^3}$.

Wet bulk density reflects a combination of compaction and variations in particle size and texture of the sediment matrix.

2.2.4 Hysteresis measurements

Sub-samples for hysteresis measurements were taken from cores GeoB 6405-6, GeoB 6407-1, GeoB 6408-4, and GeoB 6422-1 and prepared using the technique described by von Dobeneck [44]. Measurements were carried out using a PMC M2900 alternating field gradient force magnetometer (AGFM), and then were processed with the program HYSTEAR [44]. Standard hysteresis parameters were determined in order to calculate the magnetogranulometric indicative ratios of saturation remanence to saturation magnetization (σ_{rs}/σ_s) and coercivity of remanence to coercive force (B_{cr}/B_c).

2.2.5 Determining high coercivity minerals

To determine the presence of high coercivity minerals, IRM acquisition curves were measured in 27 steps up to a peak field of 2.5 T. A back field of -300 mT was imparted after the 1 and 2.5 T steps, in order to calculate the S-parameter $S_{-0.3T}$ after Bloemendal et al. [45]. $S_{-0.3T}$ quantifies the fraction of SIRM acquired in 300 mT and varies between

0 for extremely high coercive, and and 1 for low coercive samples. In sediments, 1 usually represents pure magnetite, while lower $S_{-0.3T}$ indicates increasingly larger magnetic influence of hematite or goethite.

2.2.6 Magnetic Remanence measurements

Oriented cubic samples with a volume of 6.2 cm^3, were taken from all sediment series at 5 cm intervals on board immediately after core recovery [28]. In the lab onshore natural remanent magnetization (NRM) was systematically alternating field (AF) demagnetized in first 5 mT steps up to a peak field of 30 mT, and then in 10 mT steps up to a peak field of 100 mT. Anhysteretic and isothermal remanent magnetization (ARM and IRM) were also measured on the same cubic samples as NRM. ARM, acquired in a 40 μT bias field and a 100 mT peak AF, was subsequently demagnetized to a peak AF of 100 mT, using the same field steps as for NRM demagnetization. IRM acquisition curves were measured at room temperature in 18 steps up to 250 mT. Subsequently AF demagnetization of IRM was measured using again the same steps as for NRM demagnetization, and four additional field steps at 125, 150, 200 and 250 mT. Remanence measurements for all samples were performed with an automated 2G SQUID rock magnetometer (Model 755 R) of the Marine Geophysics Division at the Department of Geosciences, University of Bremen.
Based on this high - resolution rock - magnetic and compositional data it is possible to quantitatively test and compare the influence of different sediment properties upon the natural remanent magnetization. In the following chapter the results of this study are presented in four peer-reviewed publications.

3 Publications

This thesis comprises four publications which are published or have been submitted for publication. The first publication (**Section 3.1**) presents a new method to construct a precise common age model, a so - called "stratigraphic network", for multi - parameter records. The stratigraphic network is established from eight sediment cores from the subtropical and subantarctic South Atlantic ocean. A new developed computer aided multi-parameter correlation tool was used to construct a precise common age model. The eight contiguous sediment cores are located on a North - South profile across the subtropical front and widely different lithologies. The correlation is based on high - resolution data sets of magnetic susceptibility κ, density ρ, X-ray fluorescence measurements (Fe, Ca concentration) and the oxygen isotope δ^{18}O. Correlation between all pairs of multi-parameter sequences are performed, and correlation errors between core pairs (A,B) and (B,C) are controlled by comparison with (A,C). The final age model is called a stratigraphic network. The maximum intrinsic error is about 5 ka. This stratigraphic network forms the basis for all further investigations. Additionally the XRF data set together with the high - resolution age model is used to trace the temporal shifts of the subtropical front.
The second publication (**Section 3.2**) uses the stratigraphic network cores for a detailed study of natural remanence and rock - magnetic properties. Based on a linear model of the sediment matrix a principal component analysis of natural remanent magnetization (NRM), anhysteretic and isothermal remanent magnetization (ARM and IRM) was performed in order to determine a homogeneity interval, where remanences are only affected by a single environmental signal. This homogeneity interval for the given network cores is the 30 to 80 mT alternating field demagnetization interval. This reduces lithologic and climatic influence upon the relative paleointensity records. For each single core the relative paleointensity (RPI) record was estimated and by direct averaging a stack for the last 300 kyrs for the South Atlantic (SAS-300) was developed. This stack then was compared to other paleointensity series such as Sint-800, or the RPI records from ODP Sites 1089 (subantarctic South Atlantic) and 983 (Gardar Drift) [46, 18, 47]. The SAS - 300 provides the first field intensity record for the central South Atlantic and can be used as link between southern and northern RPI records.
The third publication (**Section 3.3**) exhibits a complete new method for determining relative paleointensity. The eight network cores from the SAS-300 show very different sediment composition. They were recovered in a constraint area in the subtropical and subantarctic South Atlantic and thus should have seen the same paleofield. This fact provides to correct relative paleointensity records for variations in sediment composition. Little is known how varying sediment compositions and environmental conditions during deposition affect the NRM. In this study a new attempt is made to identify and quantify such sedimentary influences. Based on high - resolution rock - magnetic and compositional data, from the previous studies, it is possible to quantitatively test and compare the influences of different sediment properties upon the NRM. It is found that magnetic grain size, as measured by the magnetic parameter ARM/IRM, is most influential for ARM-based RPI determination and weak to moderate reductive diagenesis, as measured by the parameter Fe/κ, has less influence. For IRM-based RPI determination it turns out that grain size has less and diagenesis is the most influential parameter. Based on the extended linear RPI theory a corrected RPI stack (SASC - 300) for the investigated cores is constructed. The correction improves the correlation with independent global paleointensity stacks in comparison to

the previous uncorrected RPI stack [48]. The ratio between corrected and uncorrected RPI stacks reveals a hidden global climate signal, which indicates that climatic variations in sediment composition are inevitably present in non-ideal sediment sequences.
In a fourth publication (**Section 3.4**) a statistical analysis was performed to test how lithology influences relative paleointensity records. For 90 samples from the network cores a combined paleomagnetic and sedimentological dataset was established. Different parameters, including carbonate, opal and terrigenous content, grain size distribution and clay mineral composition, where determined. Their Bi- and multivariate correlations with the RPI signal were statistically investigated using standard techniques and criteria. A moderately correlation is found with opal, illite and kaolinite with the relative paleointensity estimate NRM/ARM, weak correlation is found for clay grain size and chlorite. The kaolinite/illite ratio is detected to be the most influential sedimentological factor.

3.1 A stratigraphic network from the subtropical and subantarctic South Atlantic: Multiparameter correlation of magnetic susceptibility, density, X-ray fluorescence measurements and δ^{18}O

Daniela I. Hofmann, K. Fabian, F. Schmieder, B. Donner, U. Bleil,

Available online at www.sciencedirect.com
SCIENCE DIRECT®
Earth and Planetary Science Letters 240 (2005) 694–709
EPSL
www.elsevier.com/locate/epsl

A stratigraphic network across the Subtropical Front in the central South Atlantic: Multi-parameter correlation of magnetic susceptibility, density, X-ray fluorescence and $\delta^{18}O$ records

Daniela I. Hofmann, Karl Fabian *, Frank Schmieder, Barbara Donner, Ulrich Bleil

University of Bremen, Department of Geoscience, Postbox 330440, 28334 Bremen, Germany

Received 27 May 2005; received in revised form 26 August 2005; accepted 26 September 2005
Available online 7 November 2005
Editor: V. Courtillot

Abstract

Computer aided multi-parameter signal correlation is used to develop a common high-precision age model for eight gravity cores from the subtropical and subantarctic South Atlantic. Since correlations between all pairs of multi-parameter sequences are used, and correlation errors between core pairs (A, B) and (B, C) are controlled by comparison with (A, C), the resulting age model is called a *stratigraphic network*. Precise inter-core correlation is achieved using high-resolution records of magnetic susceptibility κ, wet bulk density ρ and X-ray fluorescence scans of elemental composition. Additional $\delta^{18}O$ records are available for two cores. The data indicate nearly undisturbed sediment series and the absence of significant hiatuses or turbidites. After establishing a high-precision common depth scale by synchronously correlating four densely measured parameters (Fe, Ca, κ, ρ), the final age model is obtained by simultaneously fitting the aligned $\delta^{18}O$ and κ records of the stratigraphic network to orbitally tuned oxygen isotope [J. Imbrie, J. D. Hays, D. G. Martinson, A. McIntyre, A. C. Mix, J. J. Morley, N. G. Pisias, W. L. Prell, N. J. Shackleton, The orbital theory of Pleistocene climate: support from a revised chronology of the marine $\delta^{18}O$ record, in: A. Berger, J. Imbrie, J. Hays, G. Kukla, B. Saltzman (Eds.), Milankovitch and Climate: Understanding the Response to Orbital Forcing, Reidel Publishing, Dordrecht, 1984, pp. 269-305; D. Martinson, N. Pisias, J. Hays, J. Imbrie, T. C. Moore Jr., N. Shackleton, Age dating and the orbital theory of the Ice Ages: development of a high-resolution 0 to 300.000-Year chronostratigraphy, Quat. Res. 27 (1987) 1-29.] or susceptibility stacks [T. von Dobeneck, F.Schmieder, Using rock magnetic proxy records for orbital tuning and extended time series analyses into the super-and sub-Milankovitch Bands, in: G. Fischer, G. Wefer (Eds.), Use of proxies in paleoceanography: Examples from the South Atlantic, Springer-Verlag, Berlin (1999), pp. 601-633.]. Besides the detection and elimination of errors in single records, the stratigraphic network approach allows to check the intrinsic consistency of the final result by comparing it to the outcome of more restricted alignment procedures. The final South Atlantic stratigraphic network covers the last 400 kyr south and the last 1200 kyr north of the Subtropical Front (STF) and provides a highly precise age model across the STF representing extremely different sedimentary regimes. This allows to detect temporal shifts of the STF by mapping δMn/Fe. It turns out that the apparent STF movements by about 200 km are not directly related to marine oxygen isotope stages.

Keywords: signal correlation; chronostratigraphy; oxygen isotope records; magnetic susceptibility; XRF; Subtropical Front; South Atlantic

1. Introduction

Ice cores, marine, lacustrine and continental sediments continuously record climatic and environmental

* Corresponding author. Tel.: +49 421 218 8956.
E-mail addresses: danhof@uni-bremen.de (D.I. Hofmann), karl.fabian@uni-bremen.de (K. Fabian).

0012-821X/$ - see front matter © 2005 Elsevier B.V. All rights reserved.
doi:10.1016/j.epsl.2005.09.048

changes as well as geomagnetic variations [1,4–9]. Precise and accurate dating is of paramount importance to combine these records into a global geological archive, [2,10–12]. Temporal calibration of single stratified records is commonly based on either layer counting techniques [13,14] or time-series modelling of variations in $\delta^{18}O$ coupled to orbital-forcing climate theory [2,3,15,16]. Reversals of the Earth magnetic field recorded in the natural remanent magnetization (NRM) of marine sediments that at least recorded one geomagnetic reversal, enables dating by comparison to the geomagnetic polarity timescale [17]. For the Brunhes chron it has been proposed to use relative paleointensity records in comparison to a global paleointensity stack as a dating tool [18]. Dating by radiogenic isotopes (U–TH, K–Ar, $^{40}Ar/^{39}Ar$) or cosmogenic nuclides (^{14}C) is commonly precluded by the lack of adequate material in deep-sea deposits. In addition to the above dating methods, physical properties become more and more accepted parameters for chronostratigraphy, because they can be measured relatively quickly and with high resolution [11,19–21]. Dating problems arise from deficient temporal resolution of the defining parameter or from secondary processes of biological, physical or chemical origin which overprint or alter the original sedimentary stratification. All these approaches compare single sediment records of a single parameter to some calibrated reference curve. Here, two steps are introduced to improve upon this procedure. First, an automatic signal correlation algorithm has been developed which considerably simplifies multi-parameter correlation between pairs of sediment records or calibrated reference curves. Second, instead of dating single records, a *stratigraphic network* of several sediment cores is constructed by first optimizing the correlation between all pairs of the network cores. Only then the optimal common depth scale is used for comparison with the calibrated reference curve. The new method is demonstrated in a comprehensive case study on eight gravity cores from the subtropical and subantarctic South Atlantic. These cores show considerable variations in lithology and sedimentation rates. They were selected for detailed rock magnetic and relative paleointensity studies [22] requiring a common highly accurate age model.

2. Investigated area

During R/V Meteor Cruise M46/4 a set of 29 gravity cores were recovered from the western flank of the Mid Atlantic Ridge (MAR) and in the adjacent basins including the Argentine Basin, the Cape Basin and the Brasil Basin [23]. Lithologic description and shipboard measurements of magnetic susceptibility and wet bulk density [23] were used to select eight apparently continuous and undisturbed gravity cores for further study. The coring sites are located between 32°S, 19°W and 42°S, 24°W at water depths ranging from 3380 to 4385 m (Table 1). The core locations form a N–S profile across the Subtropical Front (STF), separating the subtropical South Atlantic in the North from the subantarctic South Atlantic in the South (Fig. 1). The STF is indicated by a sharp surface temperature and salinity discontinuity of at least 4°C and 0.005. At the STF the Subantarctic Surface Water (SASW) subducts beneath the northern South Atlantic Central Water (SACW) and merges with the Antarctic Intermediate Water (AAIW). The prevailing deep water masses are nutrient poor North Atlantic Deep Water (NADW) in the northern part and nutrient rich Antarctic Bottom Water (AABW) in the south [24–27]. The differences between these water masses strongly affect sediment accumulation and composition. This results in noticeable lithologic variations between different cores of the transect. Also within single sediment series which recorded the temporal shifts of the STF during the Quaternary strong lithologic variations are present. Accordingly, the eight cores can be divided into three types of lithology [23,28]. The northernmost cores GeoB 6425-2, GeoB 6426-1 and GeoB 6428-1 lie in the oligotrophic subtropical South Atlantic north of the STF and contain mainly clay bearing nannofossil ooze. The foram bearing nannofossil ooze of cores GeoB 6407-1, GeoB 6421-2, GeoB 6422-1 has a higher carbonate content. While cores GeoB 6421-2 and GeoB 6422-1 lie in the vicinity of the STF, core GeoB 6407-1 is located further south close to cores GeoB 6405-6 and GeoB 6408-4 but at shallower water depth (Table 1). The southernmost

Table 1
Sampling site, recovered length, water depth, preliminary age and estimated average sedimentation rate σ_{est} of the eight selected cores

GeoB	Latitude (S)	Longitude (W)	Length (m)	Depth (m)	Age (ka)	σ_{est} (cm/kyr)
6428-1	32°30.60′	24°14.91′	7.26	4015	1801	0.4
6426-1	33°30.00′	24°01.50′	13.31	4385	1323	1.0
6425-2	33°49.51′	23°35.24′	10.89	4352	1028	1.0
6422-1	35°42.45′	22°44.01′	5.45	3972	297	1.8
6421-2	36°26.70′	22°26.70′	9.60	4220	442	2.2
6407-1	42°02.70′	19°30.00′	5.45	3384	388	1.4
6408-4	43°36.85′	20°26.46′	10.57	3797	302	3.5
6405-6	42°00.00′	21°51.19′	12.12	3862	302	4.0

Ages and average sedimentation rates are roughly estimated by matching susceptibility records to SUSAS [3].

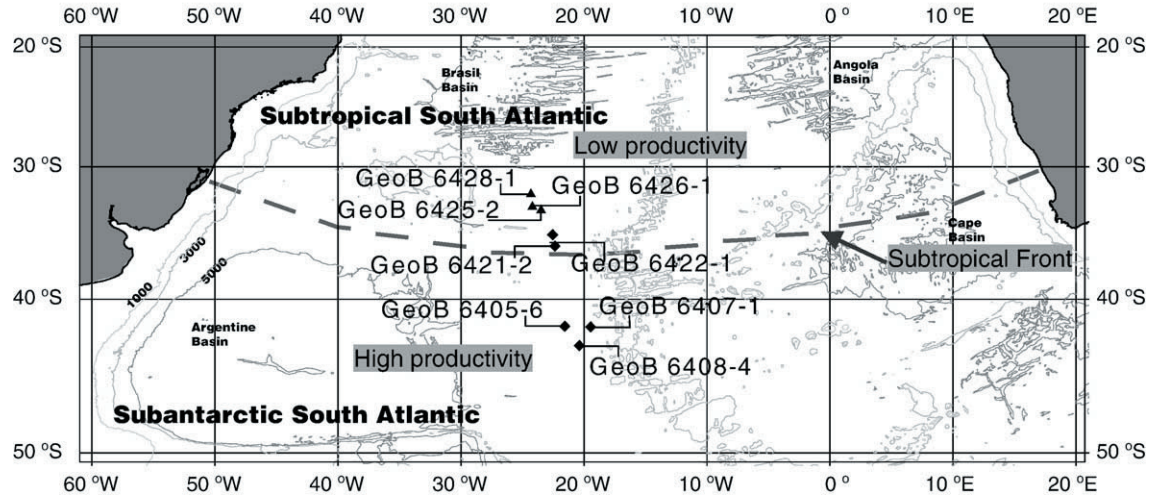

Fig. 1. Location of the eight gravity cores used to build the stratigraphic network. The dashed line indicates the approximate current position of the Subtropical Front as derived from satellite data of pigment distribution in surface waters [29].

cores GeoB 6405-6 and GeoB 6408-4 contain diatom bearing nannofossil ooze.

3. Measurements and parameters

Setting up a multi-parameter stratigraphic network requires compatible high-resolution measurements of the same parameters for all network cores. Sufficient resolution is achieved by primarily using automated scanning measurements as described below. Care has been taken to ensure that the depth scales for all parameters measured on the same core, but at different instruments, agree to a precision of at least 1 cm.

3.1. Magnetic volume susceptibility

Magnetic volume susceptibility κ was measured in 1 cm intervals along the surface of split cores using a Bartington spot sensor type M.S.2.F mounted on a computer controlled positioning system. The instrumental drift was controlled by separate background (zero) readings in air after each measurement. Magnetic susceptibility subsumes ferri-, para- and diamagnetic contributions.

It is the most widely used parameter to quantify concentration changes of the magnetic mineral fraction in marine sediments [30–32]. For magnetite, κ is relatively constant for grain sizes between 0.1 and 10,000 μm, but increases towards smaller superparamagnetic (SP) grains [33]. In the here investigated South Atlantic sediments, variation of κ is mainly due to changes of (titano-) magnetite concentration. Thus, κ is a proper proxy for terrigenous input in this region [11]. A first approximate chronostratigraphy (Table 1, Fig. 2) was constructed by correlating the susceptibility records with the Subtropical South Atlantic susceptibility stack (SUSAS) [3].

3.2. Elemental records from XRF measurements

High-resolution records of elements from potassium through strontium have been determined using an X-ray flouorescence (XRF) scanner developed and built at the Netherlands Institute for Sea Research [34]. The obtained XRF spectra are processed with the software toolbox KEVEX™ [35] calculating relative element intensities in counts per second (cps).

The XRF Fe-records, similar to magnetic susceptibility, correspond to terrigenous content, while Ca-records indicate variations in biogenic carbonate input. Therefore, Fe should essentially mirror the variations of κ, while the Ca records are inverse to both (Fig. 3). Nonetheless, there are small differences in signal variation between the κ, Fe and Ca records. These are consistent over different cores and thus very specifically for obtaining a precise correlation. XRF records of other elements are not used for chronostratigraphy because element concentrations and consequently the signal-to-noise ratios are too low to provide reliable tie-points. However, it will be shown in the discussion that at least the Mn-record contains additional oceanographic information, which together with the final age model, allows to infer the temporal variation of the STF.

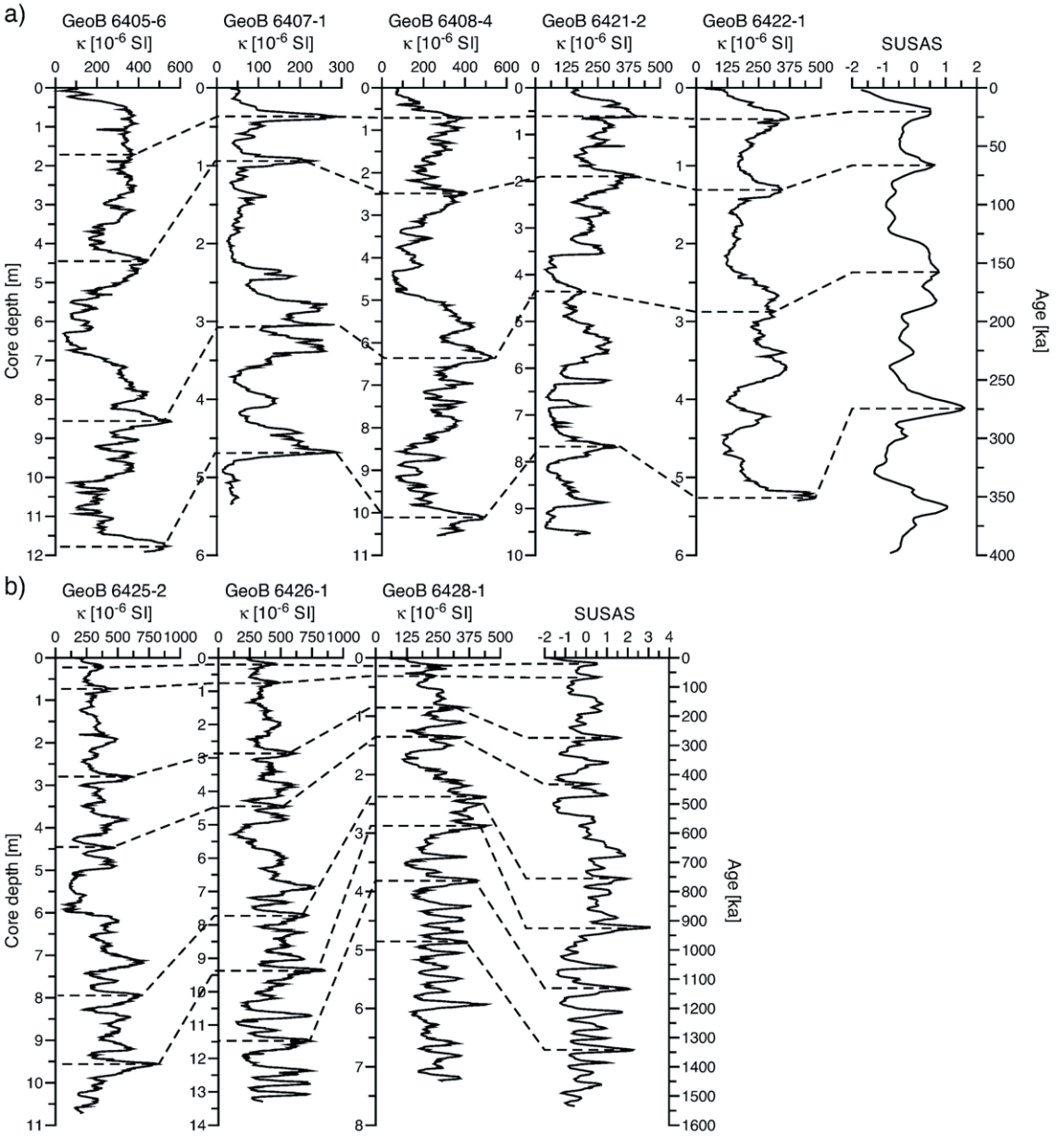

Fig. 2. (a) Magnetic susceptibility records of the southern sediment cores. Highest κ values are found in cores GeoB 6405-6 and GeoB 6408-4, while GeoB 6407-1 has the lowest values. Four major tie points (dashed lines) indicate correlation among the cores and with the Subtropical South Atlantic Susceptibility Stack (SUSAS, [3]). (b) Magnetic susceptibility records from the northern sediment series, showing overall higher κ values than the southern cores, only core GeoB 6428-1 has lower susceptibility values. Eight major tie points (dashed lines) indicate correlation between the cores and with SUSAS.

3.3. Wet bulk density

Wet bulk density ρ is inferred from electrical resistivity measurements performed directly after core recovery with a resolution of 2 cm [23]. It reflects a combination of compaction and variations in particle size and texture of the sediment matrix. Due to the higher intrinsic density of calcareous nannofossil ooze as compared to silicates, ρ essentially correlates with Ca for all cores.

3.4. Stable oxygen isotopes

Stable oxygen isotopes are evaluated on hand-picked specimens of the benthonic foraminifer *Cibicides wuellerstorfi* from sites GeoB 6408-4 and

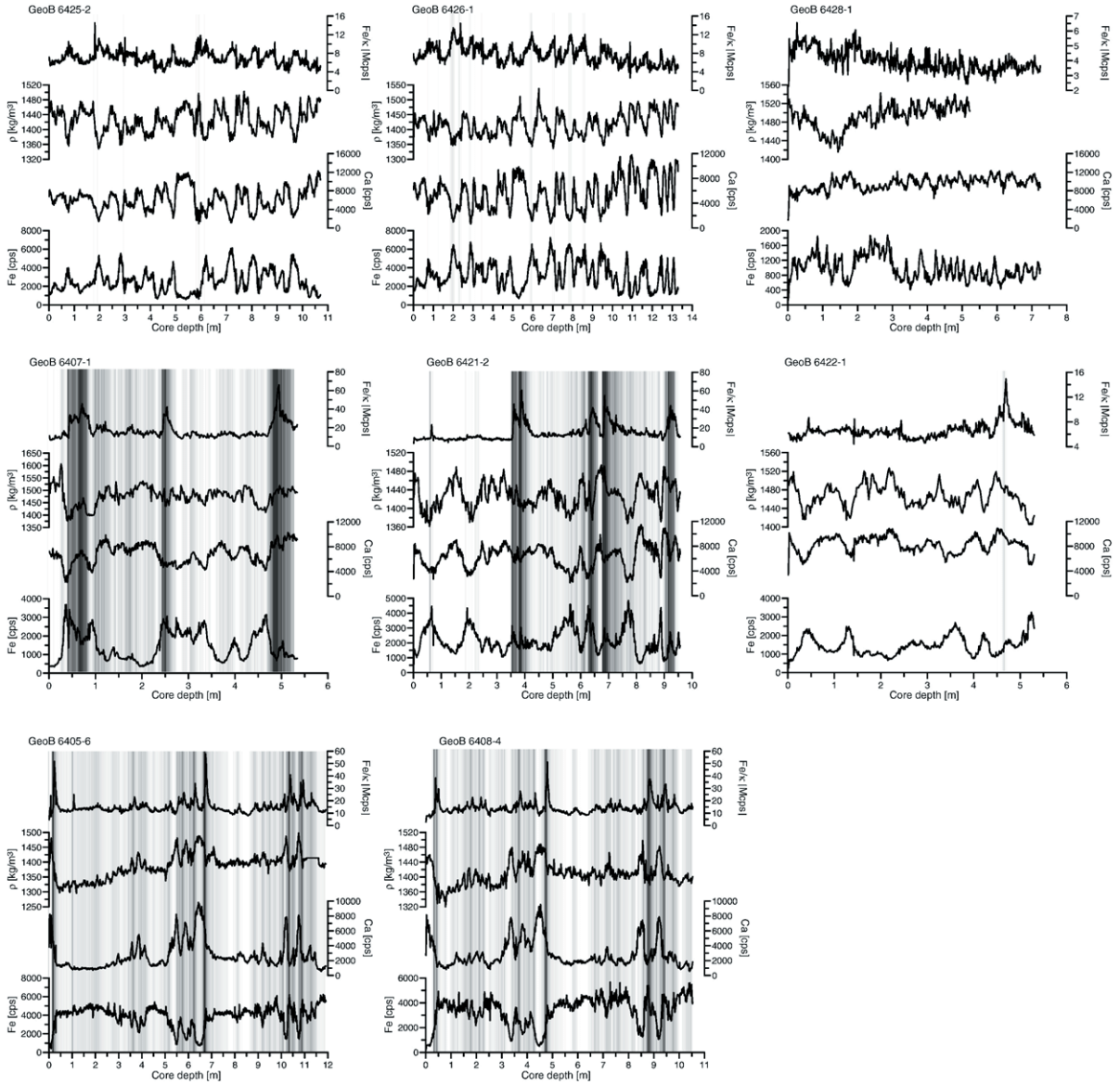

Fig. 3. Wet bulk density ρ, Iron (Fe) and Calcium (Ca) records for eight sediment series. High Fe values are related to low Ca values and vice versa in all cores. Density correlates with Ca for all cores, except for GeoB 6428-1. The ratio Fe/κ, indicating reductive diagenesis, is presented as a background linear gray scale from $Fe/\kappa \leq 10$ Mcps (white) to $Fe/\kappa \geq 40$ Mcps (black).

GeoB 6421-2 using a Finnigan MAT251 mass spectrometer, equipped with an automated Kiel carbonate preparation line. Calibration of the lab internal standard to a PDB standard scale (PeeDee Belemnite) was achieved using the NBS 19 standard (National Bureau of Standards, Vienna, Austria). Analytical precision is better than 0.07‰. $\delta^{18}O$ records of the benthonic foraminifer of cores GeoB 6408-4 and GeoB 6421-2 correlate well with SPECMAP and the stack of Martinson et al. [1,2] (Fig. 4).

3.5. Assessing the influence of reductive diagenesis

Post-depositional chemical alteration is a major error source for stratigraphic correlation. Ferric iron minerals, are dissolved due to sedimentary iron reduction, which transforms Fe^{3+}-ions, originating mainly from ferri- or antiferro-magnetic minerals like magnetite or hematite, into Fe^{2+}-ions typically related to paramagnetic minerals [36]. Since magnetic susceptibility κ primarily reflects the ferrimagnetic mineral concentration it is easily af-

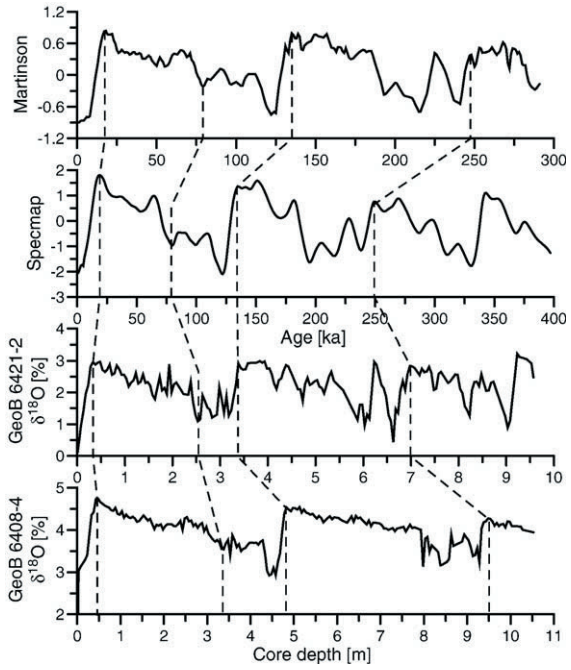

Fig. 4. Benthonic $\delta^{18}O$ records of GeoB 6408-4 and GeoB 6421-2. The two records apparently correlate well with SPECMAP [1] and the Martinson et al. [2] curve. Four major tie points are presented.

fected by reductive diagenesis. Because alteration may occur at different age levels in different cores, it diminishes the worth of magnetic susceptibility as a chronostratigraphic parameter. While on one hand the sensitivity of κ with respect to diagenesis is an unwanted effect, it can be used on the other hand to detect diagenetic processes. This can be done by observing that the strong correlation between κ and Fe results from a time independent ratio of ferrimagnetic to paramagnetic Fe compounds of the terrigenous iron source region. Postdepositional reductive diagenesis can reduce ferrimagnetic iron minerals to paramagnetic iron compounds whereby κ is noticeably diminished. Since diffusion rates are small, the local Fe concentration remains nearly constant during this process. Consequently, reductive diagenesis increases the ratio Fe/κ above the constant value characteristic for the undisturbed terrigenous phase [36]. To avoid a possible singularity of Fe/κ for $\kappa=0$ it was suggested to correct κ for an estimated average diamagnetic contribution from the sediment matrix [36]. In our case, κ is used directly, since it is positive throughout and much larger than the suggested correction of $15 \cdot 10^{-6}$ SI. Fig. 3 shows that in the studied cores low reductive diagenesis is associated with values of Fe/κ below 10 Mcps. Values above 40 Mcps indicate substantial reductive diagenesis. To identify diagenetic influence in the records, a linear gray scale plot of Fe/κ is used as background shading in Fig. 3. Here, black colors indicate values above 40 Mcps and white color values below 10 Mcps. Fig. 3 also documents that on average diagenetic influence increases from North to South.

4. Signal correlation method

4.1. Computer aided multi-parameter correlation

Manual multi-parameter correlation requires the simultaneous overview over several wiggle-matching tasks while keeping track of the list of common tie points on various depth axes. Apparently, this is a time-consuming and visually challenging undertaking that can be considerably simplified and accelerated by using a specially designed computer algorithm. The program ASC (*A*utomatic *S*ignal *C*orrelation) has been developed to either support the above described manual task of multi-parameter signal correlation, or to propose an automatic correlation. Thereby, it finally allows to construct a transfer function between depth or age scales from two sediment series by synchronous wiggle matching based on any number of parameters.

Manual correlation in ASC is iteratively done by stepwise adding new tie-points between the multi-parameter records at any position using any of the available parameters. After each step the change in correlation effected by the new tie-point is immediately shown and each single parameter record is mapped to the new scale. This manual iterative matching already improves on previous single-parameter correlation programs.

In addition, ASC also can calculate an automatic multi-parameter signal correlation. Automatic signal correlation of geological time series is a difficult and not completely solved problem. As already noted by Martinson et al. [37], a major problem in geological signal correlation is the request of finding a globally — as opposed to a mere locally — optimal match between two given records. A more practical problem is computation speed. In geological applications the final result always must be manually confirmed and corrected. Therefore a sufficiently rapid automatic fitting procedure is essential to allow for interactive work. Here a dynamic time warping (DTW) algorithm is used for globally minimizing a prescribed distance function. DTW has been originally developed in the context of speech recognition [38], but it turns out to be especially suited for geological time series. As in the recent approach by Lisiecki and Lisiecki [39], DTW is based on dynamic programming [40] to perform a fast global optimization of the multi-parameter correlation instead of locally improving a prescribed initial guess.

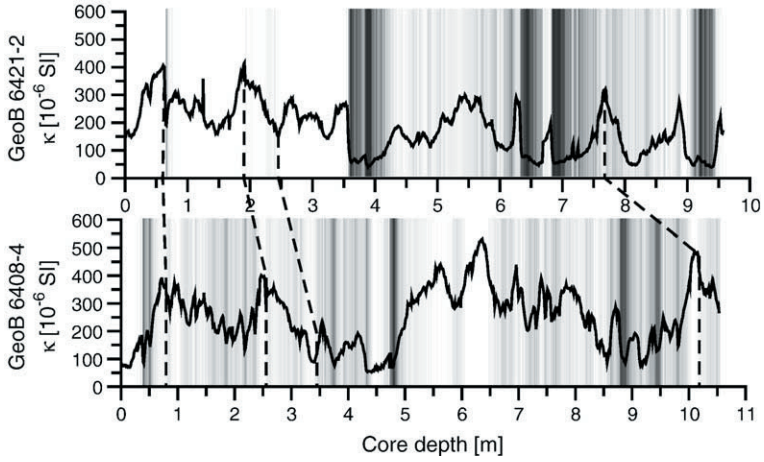

Fig. 5. Magnetic susceptibility records of cores GeoB 6408-4 and GeoB 6421-2. As in Fig. 3 the background shading represents the variation of Fe/κ. In the undisturbed regions the κ records correlate well. Dashed lines indicate prominent synchronous signal patterns. No reliable correlation is found in the parts where Fe/κ indicates considerable diagenesis.

The use of multi-parameter records for pattern matching considerably reduces the chances of misalignment during the automated fitting process. However, the quality of the fit still depends on the measurements signal-to-noise ratios, on preceding smoothing, normalization and detrending procedures and on the function that is used to calculate the distance between two multi-parameter signals. Our experience shows, that least-square distance is the best choice even for multiple parameters, but each parameter should be weighed according to its actual information content. This requires not only insight into data quality (noisy data should have less weight), but also should take into account systematic dependencies between seemingly different parameters like Fe and κ. The DTW algorithm also includes the possibility to impose slope constraints [38]. They restrict the possible slope of the transfer function to some interval $[1/n, n]$ and thereby prevent unrealistic jumps. This can be used

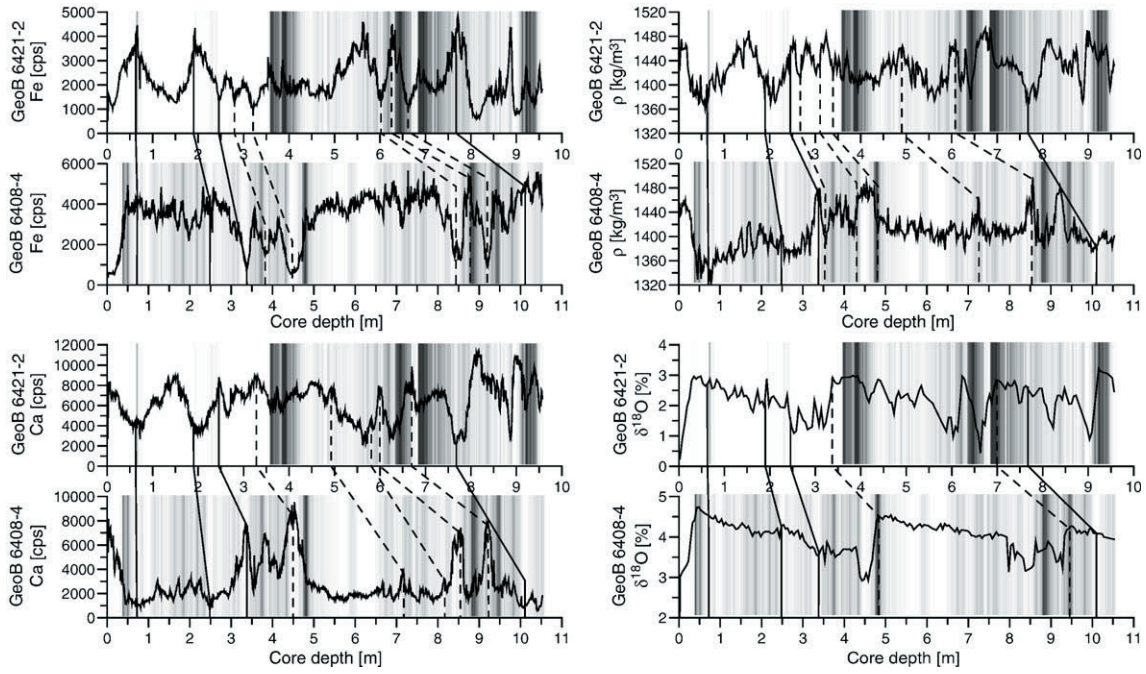

Fig. 6. Correlating Fe, Ca, ρ and $\delta^{18}O$ for GeoB 6408-4, GeoB 6421-2. Solid lines indicate the tie points from Fig. 5. Dashed lines represent additional tie points. Again, Fe/κ is represented by the background shading as in Fig. 3.

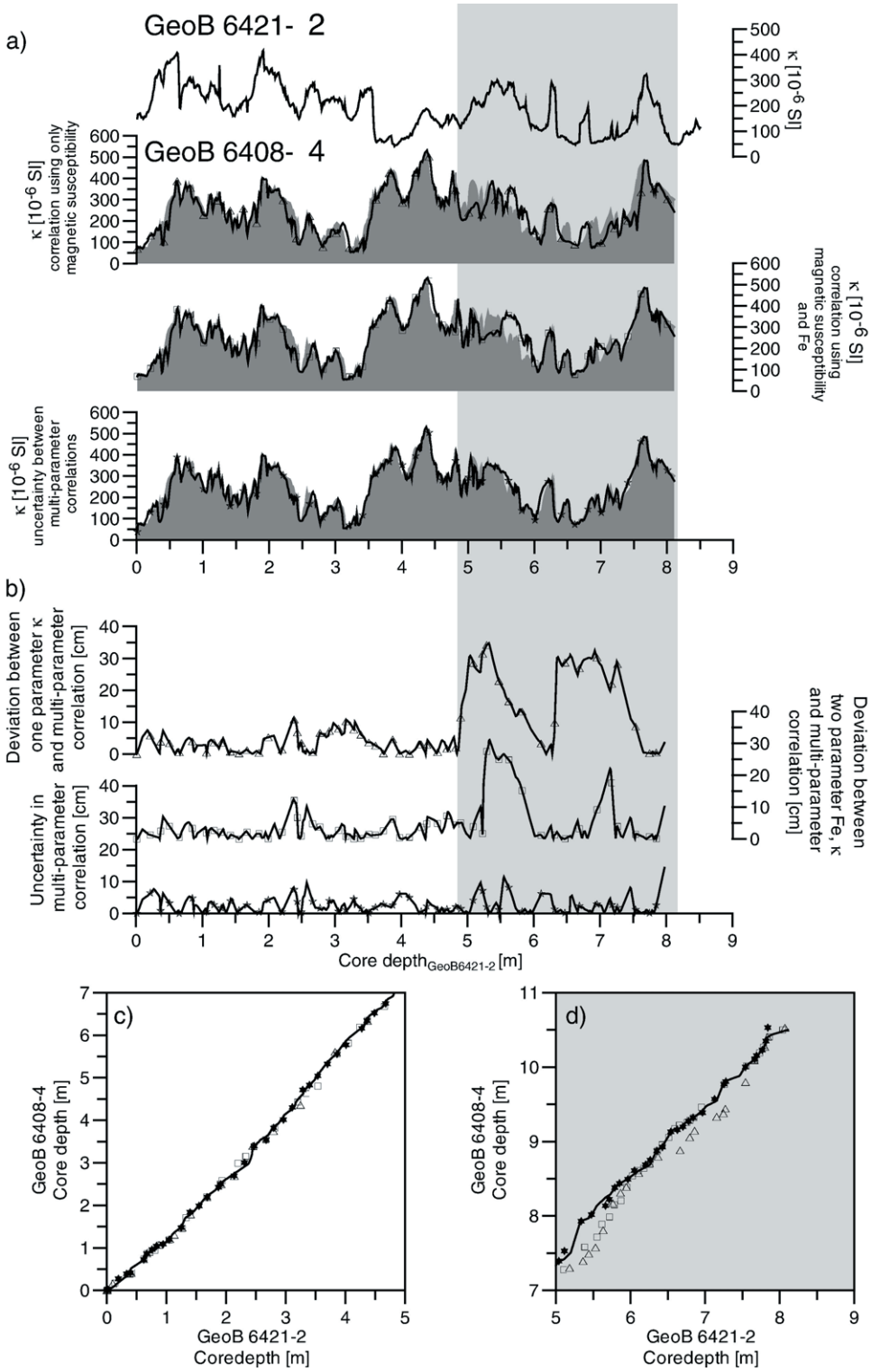

Fig. 7. (a) Magnetic susceptibility versus the different depth scales obtained by matching either only κ (triangles), κ and Fe (squares) or all available parameters (stars) between GeoB 6408-4 and GeoB 6421-2. The different depth models are compared to the final network multi-parameter correlation (filled background plot). (b) shows the corresponding deviation between the depth-to-depth correlations. The intrinsic error is minimized using all available parameters (stars). In (c) and (d) the transfer functions for the different correlation approaches are presented. (c) shows the nearly undisturbed upper part of the core and (d) the altered part below 5 m core depth (gray).

to avoid noise fitting that may occur in the unconstraint case. On the other hand, a strong slope constraint hinders the global optimization of highly distorted signals. The best trade-off is found by starting with unconstraint fitting and by afterwards stepwise introduction of stronger slope constrains.

In case of the *South Atlantic stratigraphic network* automatically found correlations were merely used to survey the correlation properties of all core pairs and to rapidly detect similarities and problematic regions between the stratigraphic sequences. All final correlations have been manually checked and refined to optimally include all relevant information.

4.2. Intrinsic error estimates in multi-parameter correlation

The alignment of GeoB 6408-4 and GeoB 6421-2 provides a typical example for improving the correlation by using a multi-parameter data set. These cores are especially important for the network chronology because only for them $\delta^{18}O$ records are available.

The κ record of GeoB 6421-2 (Fig. 5) shows a sharp decrease at 3.5 m core depth. Without the clear indication of diagenetic alteration by Fe/κ at this depth, it would be tempting to erroneously align this decrease with the drop in κ of GeoB 6408-4 at 4.3 m. Only in the undisturbed regions some clear pattern similarities of the κ records can be reliably aligned (dashed lines in Fig. 5). By including ρ, $\delta^{18}O$, Fe and Ca records into the correlation process, the alignment becomes much more detailed. The dashed lines in Fig. 6 delineate for each of the four additional parameters some newly found pattern similarities which step-by-step improve upon the initial tie-points from Fig. 5 (solid lines in Fig. 6). Already by adding the less diagenetically influenced Fe-record it is possible to resolve the potential mismatch at 3.5 m core depth of GeoB 6421-2. In the alignment shown in Fig. 6, all parameters are aligned simultaneously using ASC and each additional tie-point restricts the degrees of freedom of the following ones. Thus, most of the shown tie-points effect only a tiny shift with respect to the previously correlated depth-scale. They align peaks or slopes of already close patterns and the consistency of their position with the other parameters is immediately checked.

As illustrated in Fig. 7a the multi-parameter approach also allows for an intrinsic error estimate of the alignment process itself. The idea is to assess the alignment error of a correlation process restricted to a smaller parameter set, by comparing it to the final multi-parameter correlation, which is considered to be the optimal estimate.

Fig. 7a depicts the results of the alignments by transferring the magnetic susceptibility signal of GeoB 6408-4 to the depth scale of GeoB 6421-2 using the various correlation results (triangles, squares, stars) compared to the final multi-parameter correlation (gray plot). The most simple case is the correlation obtained by using only κ (triangles). While at low depths both approaches coincide very well, there are discrepancies up to 40 cm below 5 m core depth in GeoB 6421-2. The deviation between both correlations is plotted in the top row of Fig. 7b (triangles). It increases at depths where correlation is most heavily deteriorated by diagenesis. Including also Fe in the correlation process (central rows of Fig. 7a and Fig. 7b, squares) the alignment is improved but the transfer function still deviates up to 30 cm from the final solution between 5 and 6 m core depth in GeoB 6421-2. The remaining intrinsic uncertainty within the final transfer function itself is estimated by comparing two separately performed alignments of the same multi-parameter data set (stars in bottom rows of Fig. 7a and b). The result demonstrates that the intrinsic error is everywhere below 10 cm. Fig. 7c shows the transfer functions for the nearly undisturbed upper parts of the cores where all different correlation approaches lead to nearly identical results. In contrast, the transfer functions for the bottom parts of the cores (Fig. 7d) distinctly deviate between the different correlation approaches. The largest deviation occurs when only susceptibility (triangles) is matched, while deviation is continuously reduced by using an increasing number of parameters (squares and stars). This provides strong evidence that the parallel use of several parameters is highly efficient for obtaining a reliable high-resolution pattern alignment.

5. Constructing the SASNET

Before the methods of the previous section are applied to extend the preliminary common depth scale of GeoB 6408-4 and GeoB 6421-2 to the final stratigraphic network, the core set is divided into two groups which are treated differently as sketched in Fig. 8.

The first group contains the northern cores with low sedimentation rate and negligible diagenetic overprint. An optimal age model for these cores has already been developed in a previous study by correlating characteristics of their magnetic susceptibility records to SUSAS [11]. Since all northern cores recorded at least the Brunhes–Matuyama geomagnetic boundary at their base, the age model is additionally constraint by magnetostratigraphic tie-points [11]. Only the remaining five southern cores require detailed multi-parameter

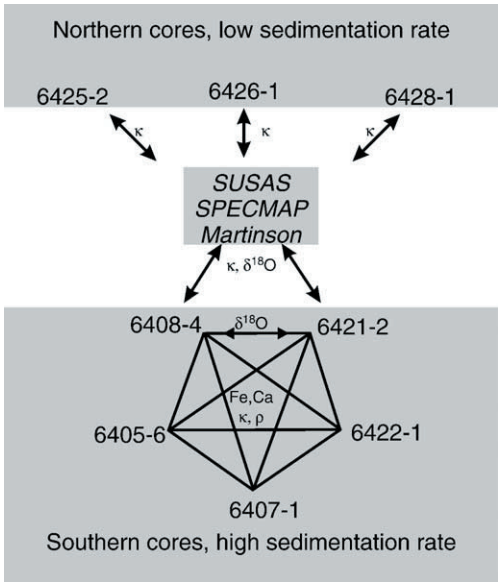

Fig. 8. Correlation structure of the network age model. Magnetic susceptibilities of the northern cores were correlated with SUSAS in the former study [11] (upper part). For the southern cores the parameters κ, ρ, Fe, Ca and $\delta^{18}O$ are correlated using ASC. For these cores firstly a common depth scale was defined by taking into account correlations between all cores. Afterwards, κ and $\delta^{18}O$ records of cores GeoB 6408-4 and GeoB 6421-2 were correlated with the master signals of SPECMAP, Martinson stack and SUSAS [1–3]. The obtained network age model was then assigned to all southern cores.

correlation. Here, κ alone is not sufficient for reliable dating since diagenetic alteration substantially distorts the records and considerably deteriorates their correlation with SUSAS. Moreover, the higher sedimentation rates allow to discern more small scale features that can be used for detailed pattern matching.

The lower part of Fig. 8 indicates that all pairwise correlations of the five southern cores are evaluated to construct the age model. Starting from the preliminary common depth scale of GeoB 6408-4 and GeoB 6421-2 from the previous section (Fig. 7), records of other cores are iteratively included into the existing depth scale by synchronous comparison of all available parameters. This approach aims to obtain optimal correlation among each set of three cores A, B, C, by ensuring that after pairwise multi-parameter correlation of (A, B) and (B, C) also the correlation between (A, C) is of the same quality. All tie-points of the correlations are displayed in Fig. 9. Between two tie-points the sedimentation rate is assumed to be constant, which allows to compare the signal patterns of all used parameters and cores on the common depth scale of GeoB 6421-2 in Fig. 9.

Based on the precise depth correlation between the southern cores, it is possible to construct a common age model by assigning ages to each depth level of GeoB

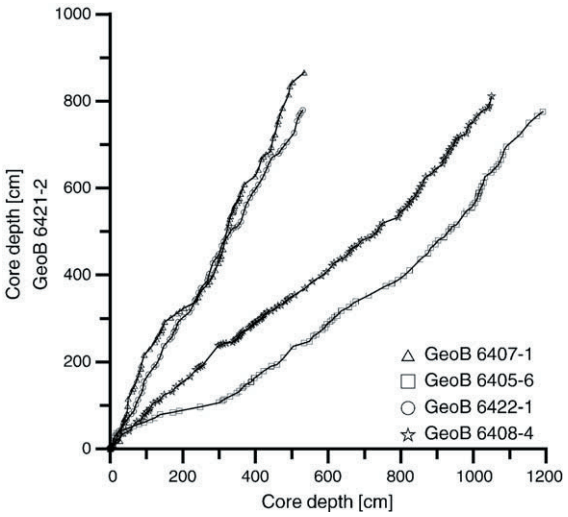

Fig. 9. Depth-to-depth correlation between GeoB 6421-2 and the other four southern network cores.

6421-2. This again is done by a multi-parameter correlation between the $\delta^{18}O$ and κ records of GeoB 6408-4 and GeoB 6421-2 on one hand and with SPECMAP and Martinson [1,2] as well as SUSAS [3,11] on the other hand. The SUSAS age model takes into account a phase lag between $\delta^{18}O$ and susceptibility, which has been determined using a $\delta^{18}O$ time scale of the SUSAS-core GeoB 1211-3. In this core susceptibility leads $\delta^{18}O$ by 3.4 kyr in the obliquity band and there-

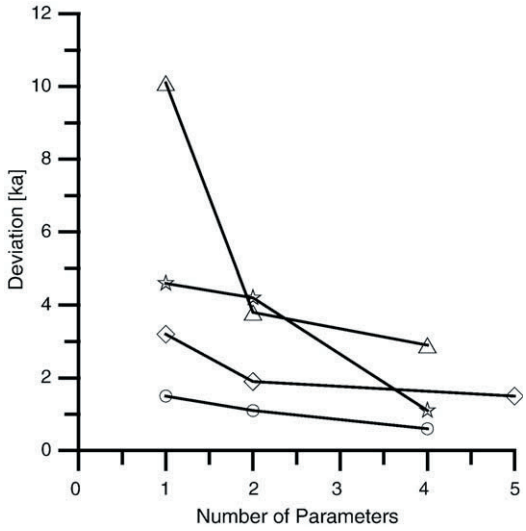

Fig. 10. The median intrinsic deviation from the final network age model of the different correlation approaches, which use an increasing number of parameters. For all correlation pairs, GeoB 6405-6 and GeoB 6421-2 (circles), GeoB 6408-4 and GeoB 6421-2 (diamonds), GeoB 6407-1 and GeoB 6421-2 (triangles), GeoB 6422-1 and GeoB 6421-2 (stars), the median intrinsic deviation is diminished by using more parameters.

fore lags the corresponding insolation forcing by 7.9 − 3.4 kyr = 4.5 kyr [3].

To document the improvement in precision of the common age model, which arises from the use of multiple parameters, the depth–depth correlation has been performed several times, while each time one or two new parameters were included into the correlation process. Fig. 10 shows the resulting decrease of median deviation from the final model. The first data points have been obtained by solely using the κ-records. In the next steps were added Fe, then Ca and ρ, and finally δ^{18}O. All deviations are transformed to ages by the same final age model. Even though lithology varies considerably between the five cores, it is possible to obtain high internal consistency that ensures a relative median age error of less then 5 ka.

The absolute error of the age model depends not only on the internal resolution of the parameters used for the correlation, but also on precision and accuracy of the alignment with the reference signals (SUSAS, SPECMAP, Martinson). Since these are stacks of several cores, small scale local features are averaged out and cannot be precisely correlated to higher resolving signals. While this effect reduces the accuracy of the age model, it does not influence the internal precision of the network core alignment. Fig. 11 presents time dependent sedimentation rates of core GeoB 6408-4, reconstructed using the different correlation approaches. Obviously only small differences between these approaches are observed. This is confirmed for all cores by comparing the average sedimentation rates inferred from the different correlation approaches that are collected in Table 2. The bottom plot of Fig. 11 additionally shows the summer insolation at 65°N, which indicates that sedimentation rates are higher during glacial and lower during interglacial times. This pattern was confirmed for all studied cores.

Table 2
Average sedimentation rates obtained using correlation approaches with different numbers of parameters

GeoB	σ (κ)	σ (κ, Fe)	σ (κ, Fe, Ca, ρ, δ^{18}O)	σ (final)
6405-6	4.2	4.3	4.3	4.2
6407-1	1.4	1.4	1.4	1.4
6408-4	3.3	3.3	3.3	3.4
6422-1	1.9	1.9	1.9	1.9

The parameters used for correlation are given in parentheses. σ (final) refers to the final network age model.

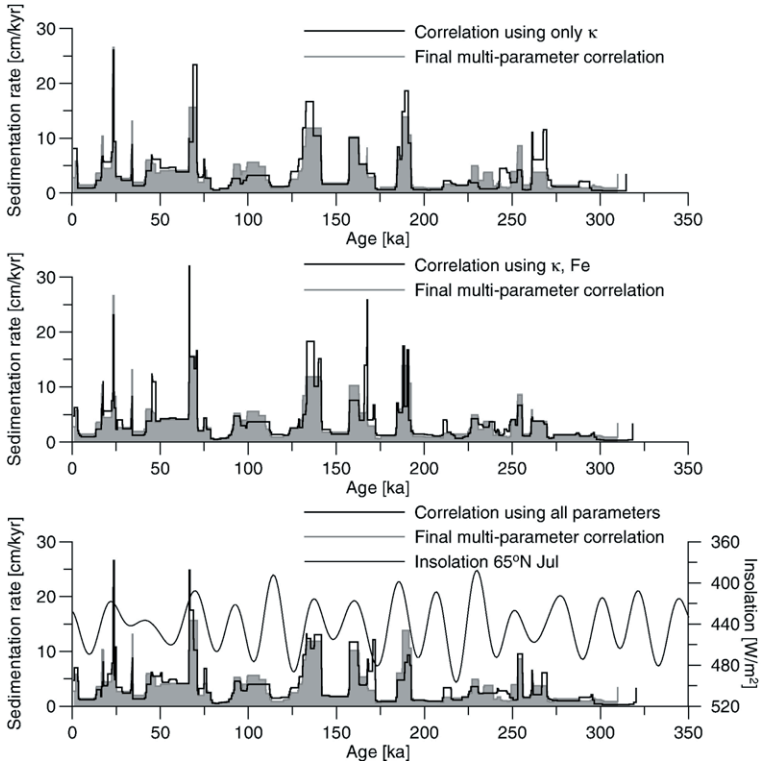

Fig. 11. Differences in sedimentation rates using the different correlation approaches are presented for core GeoB 6408-4. Only small variations between the different correlation approaches are found. Comparison with the summer insolation record at 65°N documents higher sedimentation rates during glacial than during interglacial times.

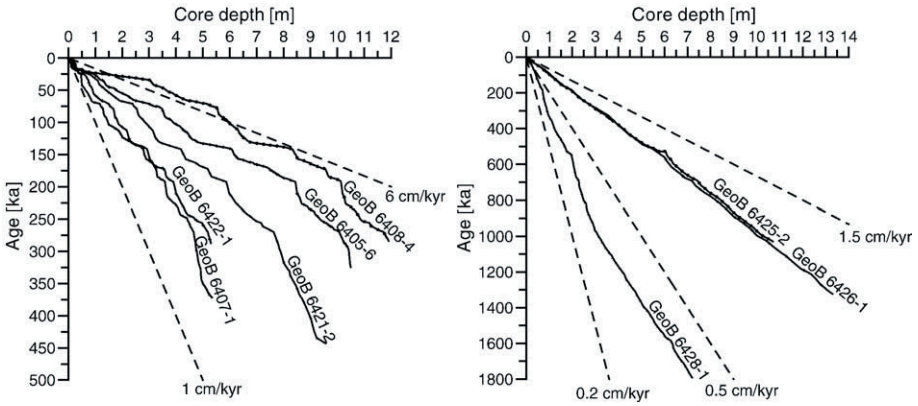

Fig. 12. Age-to-depth transfer functions for all network cores. The northern cores are much older than the southern cores, while the southern cores have higher sedimentation rates. Dashed lines depict different sedimentation rates. Note the different age and depth scales of the two diagrams.

Fig. 12 collects the final age-to-depth relations for the stratigraphic network, which now consistently documents the sedimentation chronology of the last 400 kyr south of the STF, and of the last 1200 kyr north of the STF. The average parameter values based on this age model are given in Table 3.

6. Discussion

After setting up the age model for the stratigraphic network, it is now possible to discuss the paleoclimatic and oceanographic conditions that are reflected by the temporal variation of all available records. Apart from the κ, ρ, Ca and Fe records which are shown in Fig. 13, this includes the complete XRF data set.

The gray shaded areas in Fig. 13 mark the glacial periods of the marine oxygen isotope stages (MIS) according to [1]. In all cores κ and Fe values are higher during cold than during warm oxygen isotope stages, while Ca and ρ values show an opposite pattern. This correlation reflects climatic variation in biogenic and lithogenic sediment components, which indicate shifts in carbonate production and concurrent changes in terrigenous input. Similar variations are found in sediments from the Ceará Rise [41]. In general, these climatic variations are linked to a northward movement of the polar front during glacial periods and the corresponding sea level low. Both effects intensify erosion on land and lead to higher terrigenous input into the central South Atlantic. However, large scale climatic changes alone cannot explain the significant differences between the climatic responses of the network cores along the South–North profile. The large deviations, as observed in Fig. 13 and Table 3, even between neighboring cores, are also a consequence of dissimilar water masses that dominate sedimentation at different water depths in this region.

Table 3
Mean values of κ, Fe and Ca, ρ, Fe/κ and sedimentation rate σ for the network cores

GeoB	κ (10^{-6} SI)	Fe (cps)	Ca (cps)	ρ (kg/m^3)	Fe/κ	σ (cm/kyr)
6428-1	247	980	9567	1490	4.0	0.4
6426-1	421	3263	5547	1416	7.8	1.0
6425-2	357	2532	6179	1426	7.1	1.0
6422-1	224	1456	8272	1466	6.5	1.9
6421-2	178	2180	6375	1427	12.3	2.2
6407-1	100	1471	6825	1475	14.7	1.4
6408-4	250	3357	2895	1407	13.4	3.4
6405-6	279	3877	2698	1388	13.9	4.2

A most pronounced example is the southern group with its very similar records of GeoB 6405-4 and GeoB 6408-4, which differ clearly from the nearby core GeoB 6407-1 (Fig. 13). Especially their κ-records deviate substantially, and in the upper part, GeoB 6407-1 has a much lower sedimentation rate than the other two cores. The reason for these differences is that GeoB 6405-6 and GeoB 6408-4 are deposited under influence of nutrient rich AABW at a water depth around 3800 m below the carbonate compensation depth (CCD), whilst the slightly shallower position of GeoB 6407-1 already provides a completely different sedimentary environment. This is most clearly demonstrated by the high diatom content along with reduced carbonate content in GeoB 6405-6 and GeoB 6408-4, which fits to the known facts that the AABW transports large amounts of diatoms [42], and that in this region the boundary between the AABW and the NADW coincides with the CCD [43]. On the other hand, the low sedimentation rate, and the high content of calcareous nannofossil ooze [23] indicates that

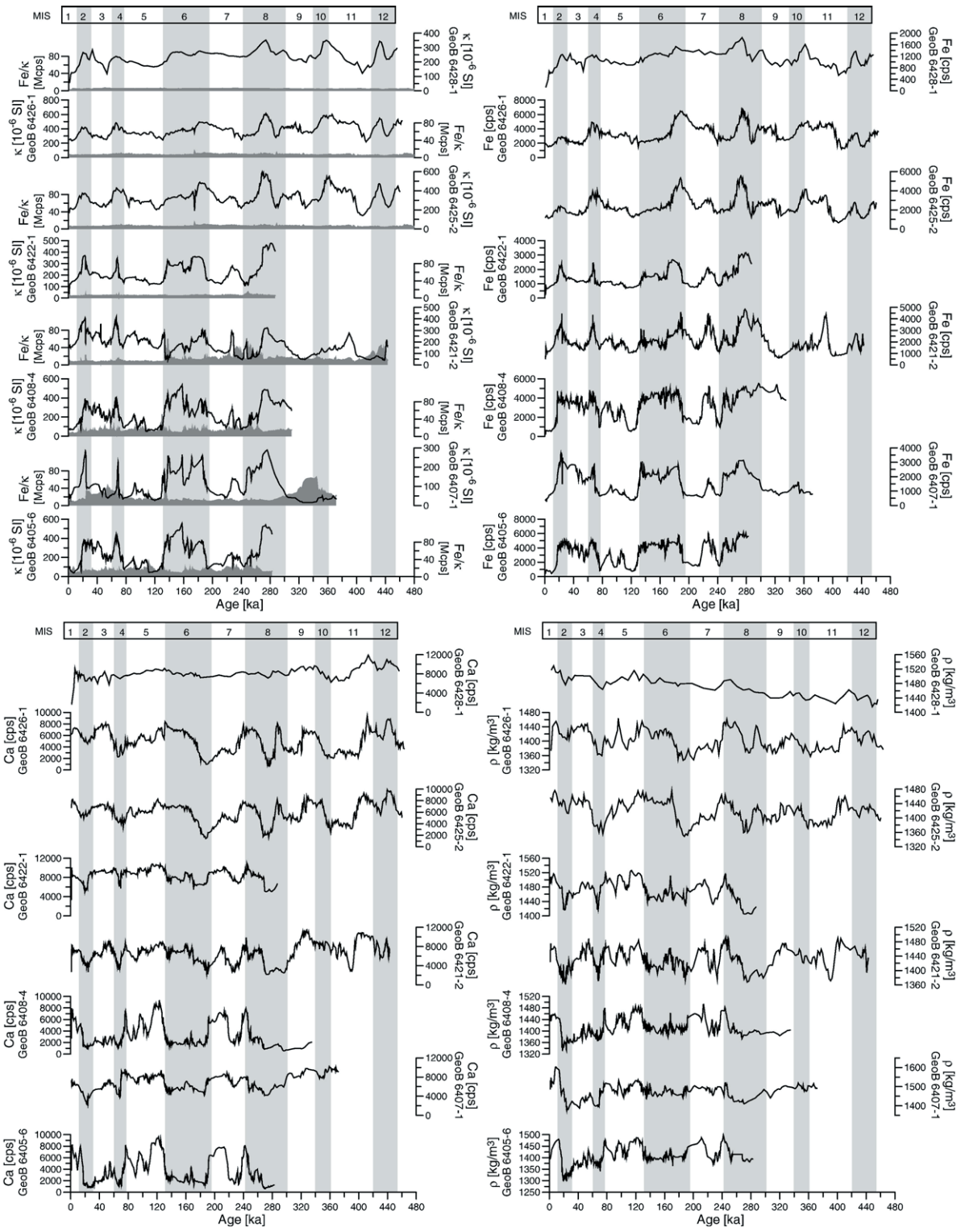

Fig. 13. Magnetic susceptibility, Fe/κ (gray plot), Fe, Ca and wet bulk density records for all cores versus the common network age scale. All cores show similar signal patterns. Gray shading indicates cold oxygen isotope stages.

GeoB 6407-1 lies above the CCD within the realm of the nutrient poor NADW.

The variations within the central group of the network cores are, at least partly, connected to yet another different phenomenon. Berger and Wefer [29] proposed, that the STF is likely to move northward during glacial periods, but no clear record of such a shift is available. Using the age model of the stratigraphic network, a search for an indication of a STF shift has been performed by systematically plotting the available parameters from the XRF measurements, and their ratios, versus the same highly precise time scale. It turned out that the ratio

$$\delta\mathrm{Mn/Fe} \equiv (\mathrm{Mn} - \mathrm{Mn_0})/\mathrm{Fe}$$

with $\mathrm{Mn_0} = 40$ cps, shows distinct differences between the cores in terms of their position relative to the STF. The value of $\mathrm{Mn_0}$ describes a constant manganese background that is independent of Fe concentration and has been found not to differ significantly between the network cores. As displayed in Fig. 14, δMn/Fe is approximately constant for all cores which are either definitely north of the STF (first group in Table 3), or definitely south of the STF (third group in Table 3). The average δMn/Fe values lie above 7% in the northern cores, and below 2% in the southern cores. This difference in δMn/Fe apparently is due to a lithogenic manganese source which contributes to the sedimentation north of the STF, but delivers no input to the cores south of the STF. Therefore, δMn/Fe allows to decide whether the central cores (second group in Table 3) are rather influenced by the regime south or north of the STF. GeoB 6407-1 has δMn/Fe ratios below 2% throughout its whole record and accordingly lies definitely in the southern realm with respect to this parameter. This is in contrast to most of its other physical properties, which closely resemble the central core GeoB 6422-1 in the second group in Table 3. This demonstrates that δMn/Fe is indeed a geographic signal that is not influenced by water depth relative to the CCD.

As demonstrated in Fig. 14, the δMn/Fe records of GeoB 6421-2 and GeoB 6422-1 are strongly modulated. By interpreting the change of their δMn/Fe values as switching in time between typical values for northern or southern regime, respectively, these cores provide clear evidence for a movement of the STF. Both have high δMn/Fe values at their tops, which agrees with the current position of the STF lying south of them. While the existence of STF shifts confirms the prediction of Berger and Wefer [29], the timing of the STF movements apparently is not directly linked to the marine isotope stages (Fig. 14).

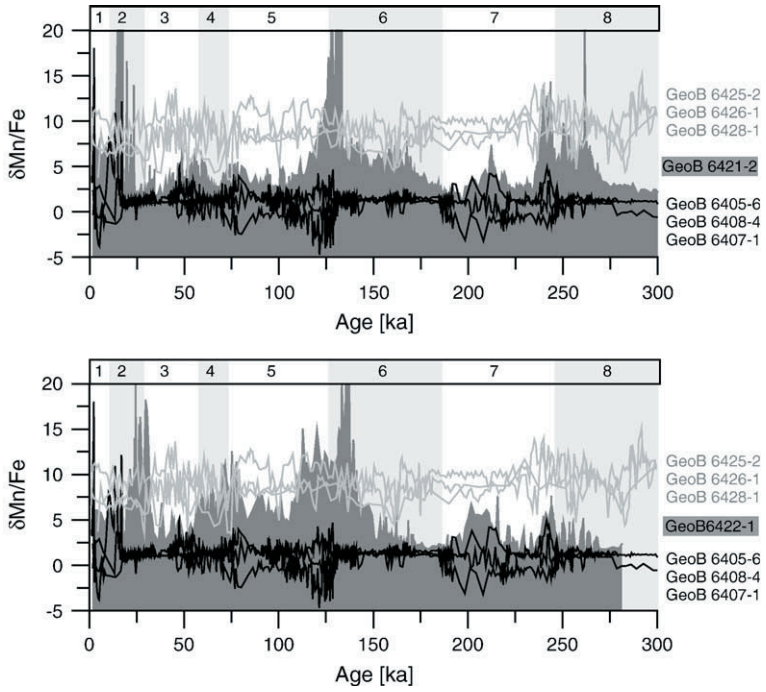

Fig. 14. δMn/Fe ratios of cores GeoB 6421-2 and GeoB 6422-1 (gray background) as compared to the nearly constant ratios of about 7% for the northern cores (light gray) and 2% for the southern cores (black). The temporal changes in δMn/Fe probably reflect shifts of the STF which apparently are not directly linked to the marine isotope stages.

A third reason for variation of the physical properties within the SASNET is a general increase of diagenetic influence from North to South. Average values of Fe/κ are highest in core GeoB 6407-1 and lowest in the northernmost core GeoB 6428-1 (Table 3). Strong diagenetic overprint is focussed at redox horizons. In core GeoB 6421-2 (Fig. 13), a sharp decrease of magnetic susceptibility related to an increase in Fe/κ provides a typical example for this effect which also produces a Mn peak slightly above the diagenetic front [36]. This event coincides with the boundary between stages 5 and 6 (Termination II). Increasing Fe/κ values at the boundaries of stages 7–8 (Termination III) and 11–12 (Termination V) are remnants of earlier locations of diagenetic redox events.

7. Conclusion

This study presents a precise common age model for eight contiguous sediment cores which cover widely different lithologies. They are located on a N–S profile across the Subtropical Front, separating the subtropical from the subantarctic South Atlantic. Based on high resolution data sets of magnetic susceptibility, Fe, Ca, wet bulk density and $\delta^{18}O$, a stratigraphic network (SASNET) is constructed which provides equally good correlation between all possible core pairs from the network. To obtain a precise network age model in spite of the considerable lithologic variety, a newly developed program for multi-parameter correlation is applied. This makes it possible to optimize all pairwise correlations between the network cores. Moreover, intrinsic error estimates for inter-core correlation have been obtained, which for the final age model limit the average inconsistency to 2 ka, and indicate that the maximum intrinsic error is about 5 ka. The XRF data set of the SASNET together with the new age model is used to trace temporal shifts of the STF, which are shown to manifest themselves in changes of the $\delta Mn/Fe$-ratios of the central SASNET cores GeoB 6421-2 and GeoB 6422-1. While a more detailed description of the multi-parameter correlation program ASC will be published elsewhere, a beta version of ASC is available from the second author (KF) upon request.

Acknowledgements

We thank Thomas Frederichs and Christian Hilgenfeld for technical support and valuable discussions. We further thank Ulla Röhl for supporting the XRF scanner measurements. Thoughtful comments of two anonymous reviewers are gratefully acknowledged. We thank crew and scientific party of METEOR cruise M46-4 for their cooperation. Financial support was provided by grant Fa 408/1 in the framework of the DFG priority program “Geomagnetic Variations” and by the DFG-Research Center ‘Ocean Margins’ of the University of Bremen No. RCOM0340.

References

[1] J. Imbrie, J.D. Hays, D.G. Martinson, A. McIntyre, A.C. Mix, J.J. Morley, N.G. Pisias, W.L. Prell, N.J. Shackleton, The orbital theory of Pleistocene climate: support from a revised chronology of the marine $\delta^{18}O$ record, in: A. Berger, J. Imbrie, J. Hays, G. Kukla, B. Saltzman (Eds.), Milankovitch and Climate: Understanding the Response to Orbital Forcing, Reidel Publishing, Dordrecht, 1984, pp. 269–305.

[2] D. Martinson, N. Pisias, J. Hays, J. Imbrie, T.C. Moore Jr., N. Shackleton, Age dating and the orbital theory of the Ice Ages: development of a high-resolution 0 to 300,000-year chronostratigraphy, Quat. Res. 27 (1987) 1–29.

[3] T. von Dobeneck, F. Schmieder, Using rock magnetic proxy records for orbital tuning and extended time series analyses into the super- and sub-Milankovitch bands, in: G. Fischer, G. Wefer (Eds.), Use of Proxies in Paleoceanography: Examples from the South Atlantic, Springer-Verlag, Berlin, 1999, pp. 601–633.

[4] N. Opdyke, Paleomagnetism of deep-sea cores, Rev. Geophys. Space Phys. 10 (1972) 213–249.

[5] L. Tauxe, Sedimentary records of relative paleointensity: theory and practice, Rev. Geophys. 31 (1993) 319–354.

[6] Y. Guyodo, J.-P. Valet, Relative variations in geomagnetic intensity from sedimentary records: the past 200,000 years, Earth Planet. Sci. Lett. 143 (1996) 23–36.

[7] F. Chen, J. Bloemendal, J. Wang, J. Li, F. Oldfield, High-resolution multi-proxy climate records from Chinese loess: evidence for rapid climatic changes over the last 75 kyr, Palaeogeogr. Palaeoclimatol. Palaeoecol. 130 (1997) 323–335.

[8] C. Hammer, P. Mayewski, D. Peel, M. Stuiver, Preface, J. Geophys. Res. 102 (1997) 26315–26316.

[9] S. Johnson, D. Dahle-Jensen, N. Gundestrup, J. Stefeensen, H. Clausen, H. Miller, V. Masson-Delmotte, A. Sveinbjörnsdottir, J. White, Oxygen isotope and paleotemperature records from six Greenland ice-core stations: Camp Century, Dye-3, GRIP, GISP2, Renland and NorthGRIP, J. Quat. Sci. 16 (2001) 299–307.

[10] D. McMillan, C. Constable, R. Parker, Limitations on stratigraphic analyses due to incomplete age control and their relevance to sedimentary paleomagnetism, Earth Planet. Sci. Lett. 201 (2002) 509–523.

[11] F. Schmieder, Magnetic signals in Plio-Pleistocene sediments of the South Atlantic: chronostratigraphic usability and paleoceanographic implication, in: G. Wefer, S. Mulitza, V. Ratmeyer (Eds.), The South Atlantic in the Late Quaternary: Reconstruction of Material Budgets and Current Systems, Springer-Verlag, Berlin, 2004, pp. 269–305.

[12] H. Guillou, B. Singer, C. Laj, C. Kissel, S. Scaillet, B. Jicha, On the age of the Laschamp geomagnetic excursion, Earth Planet. Sci. Lett. 227 (2004) 331–343.

[13] R. Alley, C. Shuman, D. Meese, A. Gow, K. Taylor, K. Cuffey, J. Fitzpatrick, P. Grootes, G. Zielinski, M. Ram, G. Spinelly, B.

Elder, Visual-stratigraphic dating of the GISP2 ice core: basis, reproducibility, and application, J. Geophys. Res. 102 (C12) (1997) 26367–26381.
[14] U. von Raad, M. Schaaf, K. Michels, H. Schulz, W. Berger, F. Sirocko, A 5000-yr record of climate change in varved sediments from the oxygen minimum zone off Pakistan, Northeastern Arabian Sea, Quat. Res. 51 (1999) 39–53.
[15] M. Milankovitch, Die astronomische Theorie der Klimaschwankungen, in: W. Kppen, R. Geiger (Eds.), Handbuch der Klimatologie, Gebrder Borntrger, Berlin, 1936.
[16] N. Pisias, D. Martinson, T. Moore, G. Bod, High resolution stratigraphic correlation of benthic oxygen isotope records spanning the last 300,000 years, Mar. Geol. 56 (1984) 119–136.
[17] S. Cande, D. Kent, Revised calibration of the geomagnetic polarity time scale for the Late Cretaceous and Cenozoic, J. Geophys. Res. 100 (1995) 6093–6095.
[18] J. Stoner, J. Channell, D. Hodell, C. Charles, A ~580 kyr paleomagnetic record from the sub-Antarctic South Atlantic (Ocean Drilling Program Site 1089), J. Geophys. Res. 108 (1998).
[19] N. Shackleton, S. Crowhurst, T. Hagelberg, N. Pisias, D. Schneider, A new Late Neogene time scale: application to Leg 138 sites, Proc. ODP Sci. Results 138 (1995) 73–101.
[20] D. Heslop, C. Langereis, M. Dekkers, A new astronomical timescale for the loess deposits of northern China, Earth Planet. Sci. Lett. 184 (2000) 125–139.
[21] H. Kuhlmann, T. Freudenthal, P. Helmke, H. Meggers, Reconstruction of paleoceanography off NW Africa during the last 40,000 years: influence of local and regional factors on sediment accumulation, Mar. Geol. 207 (2004) 209–224.
[22] D. Hofmann, K. Fabian, A stratigraphic network from the subtropical and subantarctic South Atlantic: rockmagnetism and relative paleointensity investigations (in preparation).
[23] G. Wefer, cruise participants, Report and preliminary results of Meteor Cruise M46/4, Mar del Plata (Argentina)-Salvador da Bahia (Brazil), February 10– March 13, 2000. With partial results of Meteor cruise M46/2, Berichte, FB Geowissenschaften, Universität Bremen 173.
[24] J. Reid, On the total geostrophic circulation of the South Atlantic Ocean: flow patterns, tracers, and transports, Prog. Oceanogr. 23 (1989) 149–244.
[25] L. Talley, Antarctic intermediate water in the South Atlantic, in: G. Wefer, W.D. Siedler (Eds.), The South Atlantic: Present and Past Circulation, Springer Verlag, Berlin, 1996, pp. 219–238.
[26] L. Stramma, R. Peterson, The South Atlantic current, J. Phys. Oceanogr. 20 (1990) 846–859.
[27] L. Stramma, M. England, On the water masses and mean circulation of the South Atlantic Ocean, J. Geophys. Res. 104 (C9) (1999) 20863–20883.
[28] C. Franke, D. Hofmann, T. von Dobeneck, Does lithology influence the paleointensity record? A statistical analysis on South Atlantic pelagic sediments, Phys. Earth Planet. Inter. 147 (2004) 285–296.
[29] W. Berger, G. Wefer, Central themes of South Atlantic circulation, in: G. Wefer, W. Berger, G. Siedler, D. Webb (Eds.), The South Atlantic: Present and Past Circulation, Springer Verlag, Berlin, 1996, pp. 1–11.
[30] S. Robinson, The Late Pleistocene paleoclimatic record of North-Atlantic deep sea sediments revealed by mineral magnetic measurements, Phys. Earth Planet. Inter. 42 (1986) 22–47.
[31] S. Robinson, Applications for whole-core-magnetic susceptibility measurements of deep-sea sediments, Proc. ODP Sci. Results 115 (1990) 737–771.
[32] R. Thompson, F. Oldfield, Environmental Magnetism, Allen and Unwin, London, 1986, pp. 1–227.
[33] F. Heider, A. Zitzelberger, K. Fabian, Magnetic susceptibility and remanent coercive force in grown magnetite crystals from 0.1 μm to 6 mm, Earth Planet. Sci. Lett. 93 (1996) 239–256.
[34] J. Jansen, S. van der Gaast, B. Koster, A. Vaars, CORTEX, a shipboard XRF-scanner for element analysis in split sediment cores, Mar. Geol. 151 (1998) 143–153.
[35] U. Roehl, L. Abrams, High resolution, downhole, and nondestructive core measurements from sites 999 and 1001 in the Caribbean Sea: application to the Late Paleocene thermal maximum, Proc. ODP Sci. Results 165 (2000) 191–203.
[36] J. Funk, T. von Dobeneck, A. Reitz, Integrated rock magnetic and geochemical quantification of redoxomorphic iron mineral diagenesis in Late Quaternary sediments from the equatorial Atlantic, in: G. Wefer, S. Mulitza, V. Ratmeyer (Eds.), The South Atlantic in the Late Quaternary: Reconstruction of Material Budgets and Current Systems, Springer-Verlag, Berlin, 2004, pp. 237–260.
[37] D. Martinson, W. Menke, P. Stoffa, An inverse approach to signal correlation, J. Geophys. Res. 87 (B6) (1982) 4807–4818.
[38] H. Sakoe, S. Chiba, Dynamic programming algorithm optimization for spoken word recognition, IEEE Trans. Acoust. Speech Signal Process. 26 (1978) 43–49.
[39] L.E. Lisiecki, P.A. Lisiecki, Application of dynamic programming to the correlation of paleoclimate records, Paleoceanography 17 (2002) 1049, doi:10.1029/2001PA000733.
[40] R. Bellman, S. Dreyfus, Applied Dynamic Programming, Princeton University Press, 1962.
[41] U. Bleil, T. von Dobeneck, Late Quaternary terrigenous sedimentation in the western equatorial Atlantic South American versus African provenance discriminated by magnetic mineral analysis, in: G. Wefer, S. Mulitza, V. Ratmeyer (Eds.), The South Atlantic in the Late Quaternary: Reconstruction of Material Budgets and Current Systems, Springer-Verlag, Berlin, 2004, pp. 213–236.
[42] O. Romero, C. Hensen, Oceanographic control of biogenic opal and diatoms in surface sediments of the southwestern Atlantic, Mar. Geol. 186 (2002) 263–280.
[43] M. Frenz, R. Höppner, J.-B. Stuut, T. Wagner, R. Henrich, Surface sediment bulk geochemistry and grain size composition related to the oceanic circulation along the South American continental margin in the southwest Atlantic, in: G. Fischer, G. Wefer (Eds.), The South Atlantic in the Late Quaternary: Reconstruction of Material Budgets and Current Systems, Springer-Verlag, Berlin, 2004, pp. 374–383.

3.2 Rock-magnetic properties and relative paleointensity stack for the last 300 ka based on a stratigraphic network from the subtropical and subantarctic South Atlantic

Daniela I. Hofmann, K. Fabian,

Available online at www.sciencedirect.com
ScienceDirect
Earth and Planetary Science Letters 260 (2007) 297–312
EPSL
www.elsevier.com/locate/epsl

Rock magnetic properties and relative paleointensity stack for the last 300 ka based on a stratigraphic network from the subtropical and subantarctic South Atlantic

Daniela I. Hofmann [a,*], K. Fabian [a,b]

[a] *Department of Geoscience, University Bremen, Postbox 330440, 28334 Bremen, Germany*
[b] *NGU, Geological Survey of Norway, Leiv Eirikssons vei 39, 7491 Trondheim, Norway*

Received 17 July 2006; received in revised form 20 May 2007; accepted 21 May 2007
Available online 31 May 2007
Editor: M.L. Delaney

Abstract

We present a detailed study of natural remanence and rock magnetic properties of eight sediment cores from a South–North profile across the subtropical front (STF) in the South Atlantic, which previously have been combined into a stratigraphic network. Based on these measurements, we construct a first relative paleointensity (RPI) stack for the central South-Atlantic (SAS-300) covering the last 300 ka. The degree of down-core homogeneity of magnetic mineral concentration as well as magnetic mineral content and grain sizes vary between all cores and are quantified by high-resolution rock magnetic measurements. In the cores north of and close to the STF, the magnetic remanence is mainly carried by magnetite. The cores in the south also contain a high coercive mineral fraction. Based on a linear model of the sediment matrix, we propose to apply principal component analysis (PCA) of natural remanent magnetization (NRM), anhysteretic, and isothermal remanent magnetization (ARM and IRM) to determine a homogeneity interval, where remanences are only affected by a single environmental signal. This reduces lithologic and climatic influence upon the relative paleointensity record. For our data set PCA indicates that all remanences in the 30 mT to 80 mT demagnetization interval are dominated by a single environmental influence. Single core RPI estimates are then obtained by normalizing the NRM fraction in this homogeneity interval with respect to either IRM, ARM in the same interval, or by κ. By direct averaging, we obtain the stack SAS-300, which is compared to other paleointensity series such as Sint-800, or the RPI records from ODP Sites 1089 (Subantarctic South Atlantic) and 983 (Gardar Drift). The detailed documentation of environmental influences combined with the presentation of seven different recordings of the same geomagnetic signal allows to connect southern and northern hemisphere RPI data, also with respect to possible common environmental distortions.

Keywords: NRM; relative paleointensity; South Atlantic; sediment lithology

1. Introduction

Sedimentary sequences continuously record the past variations of the Earth magnetic field. Normalized records of sedimentary natural remanent magnetization (NRM) are interpreted as representing the relative paleointensity (RPI) of the geomagnetic field (King et al., 1983; Tauxe, 1993). The quality of individual RPI determinations is assessed in terms of mineralogic and rock magnetic uniformity, possible diagenetic alteration, and any residual correlation of the normalized record to rock magnetic parameters

* Corresponding author.
E-mail address: danhof@uni-bremen.de (D.I. Hofmann).

0012-821X/$ - see front matter © 2007 Elsevier B.V. All rights reserved.
doi:10.1016/j.epsl.2007.05.042

(King et al., 1983; Tauxe, 1993; Valet, 2003). Many RPI records have been obtained from marine sedimentary sequences for time intervals spanning a few thousand to several million years (Meynadier et al., 1992; Tauxe and Shackleton, 1994; Stoner et al., 1995; Yamazaki et al., 1995; Lehman et al., 1996; Channell et al., 1997; Guyodo et al., 1999; Stoner et al., 2000; Guyodo et al., 2001; Thouveny et al., 2004). These studies refine our understanding of the temporal geomagnetic field variations, and provide data to constrain geodynamo models. Individual high quality RPI records from different sites have been combined into stacks which are available at both global (e.g. SINT-800) and regional scales (e.g. NAPIS) (Stoner et al., 1995; Lehman et al., 1996; Guyodo and Valet, 1996; Channell et al., 1997; Channell, 1999; Laj et al., 2000; Stoner et al., 2002b; Channell et al., 2002). A recent compilation of RPI records from sedimentary sequences recovered by Ocean Drilling Program (ODP) cruises all over the world by Lund et al. (2006) shows a large data gap in the central South Atlantic. In this region the sedimentation environment is very complex. Partly because the corrosive Antarctic bottom water together with oligotrophic conditions results in very low sedimentation rates, but also due to climatic variations of terrigenous influx, and movements of the subtropical front. Due to these complications, no reliable sedimentary magnetic records are available from this area.

During Meteor cruise M46/4, 29 sediment cores were recovered from this critical region close to the Mid-Atlantic Ridge across the subtropical front (Wefer and cruise participants, 2001). Out of this collection, we selected eight most appropriate sediment series and combined them into a stratigraphic network (Hofmann et al., 2005). Here we present the results of high-resolution paleomagnetic and rock magnetic measurements carried out on these network cores. Because of the highly variable oceanographic regimes the eight investigated sediment cores have widely varying sedimentary compositions, which for the reconstruction of geomagnetic variation is a most unwanted feature.

However, the cores were taken from a region small enough to assume a spatially uniform external field and it can be supposed that by stacking the RPI records, much of the compositional variation is effectively suppressed. Besides using standard reliability criteria for RPI estimation, we develop and apply a principal component analysis (PCA) of NRM and rock magnetic records. This PCA analysis takes into account the different sediment compositions, and detects and singles out signal components which relate to independent but concurrent environmental signals. Consequently, for each individual core a remanence fraction is identified which should give the optimal RPI estimate. The individual RPI records were stacked by using the arithmetic mean over the time interval of the last 300 ka. Thereby, a first direct RPI stack (SAS-300) for the central South-Atlantic is defined. Although SAS-300 averages over variable sediment compositions it cannot be expected to be completely independent of climatic influences in the region. Yet, it shows distinct similarities with other RPI stacks like SINT-800 (Guyodo et al., 1999), SAPIS (Stoner et al., 2002b), or the nearby RPI record from ODP Site-1089 (Stoner et al., 2002a). While most signal characteristics which can be related are probably of geomagnetic origin, it is likely that some features, and especially the signal amplitudes are linked to local or global environmental effects. In this sense, SAS-300 provides a first link between RPI records of the southern and northern hemispheres, but it still cannot fully resolve the issue of environmental distortion.

However, the story does not end here. Since the eight cores recorded the same field history in eight different, but closely related lithologies, it is possible to compare the natural in situ recording properties of these sedimentary recording media, and to derive a correction method which allows to identify the environmental distortion. This is the topic of a forthcoming study, which will assess the reliability of existing RPI quality criteria, and tries to correct the individual RPI records for lithological variations.

2. Sedimentary regimes and timescale of the stratigraphic network

In this section we briefly recapitulate geography, sedimentary environment, and chronostratigraphy of the here investigated stratigraphic network as developed in Hofmann et al. (2005).

2.1. Sampling area and core lithology

All eight network cores are located west of the Mid-Atlantic ridge in the subtropical and subantarctic South Atlantic across the subtropical front (STF) and have been recovered during the single expedition M46/4 (Wefer and cruise participants, 2001).

Core locations, water depths, ages and sedimentary environments are summarized in Fig. 1 (details are summarized in Table 1 of the electronic appendix).

At the STF northern and southern water masses collide, and create a characteristic productivity gradient with low sedimentation rates in the North, and higher sedimentation rates south of the STF (Reid, 1989; Stramma and Peterson, 1990; Talley, 1996; Stramma and England, 1999; Hofmann et al., 2005). Shipboard lithologic description and measurements of κ and density confirm that the

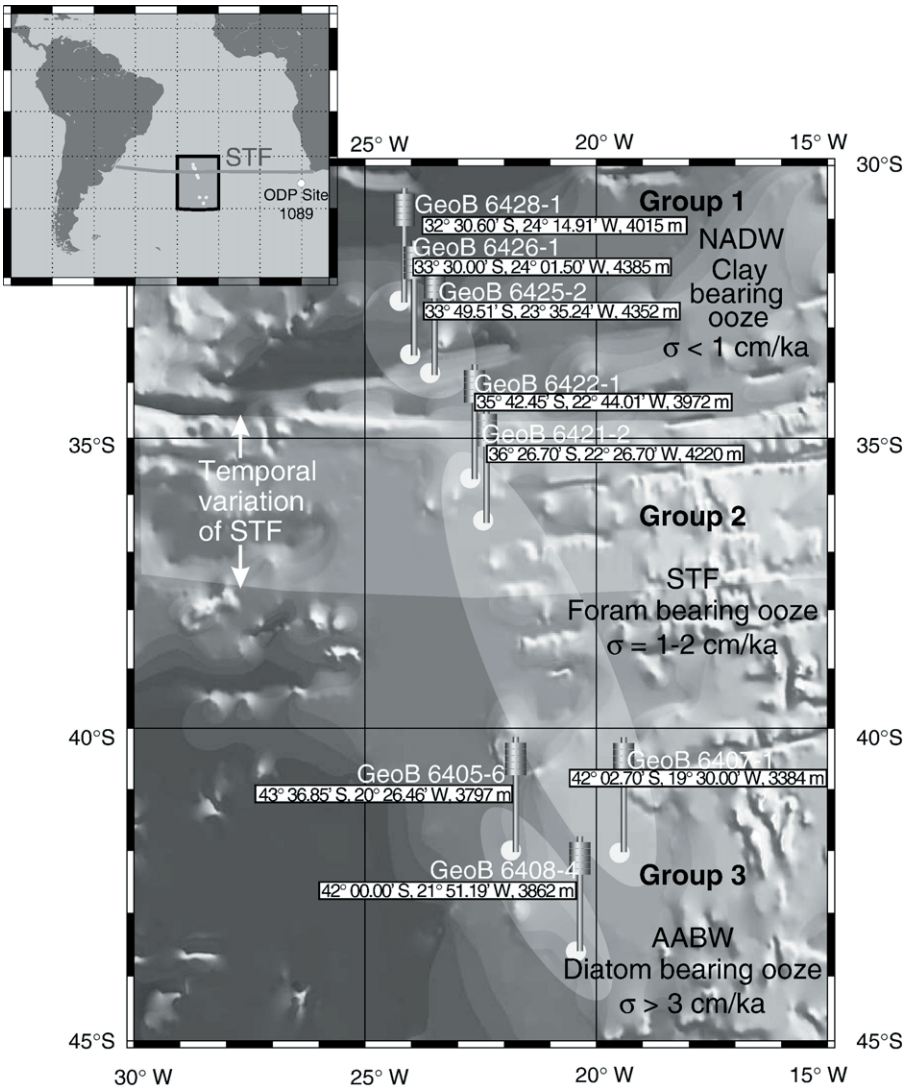

Fig. 1. Location, water depth average sedimentation rates σ and grouping of the network cores. The inset shows the approximate current position of the STF as inferred from satellite productivity mapping. The band of temporal STF variation roughly represents our previous conclusion from δMn/Fe measurements.

selected eight cores have continuous and undisturbed lithologies, which can be ordered into three groups (Wefer and cruise participants, 2001; Hofmann et al., 2005). The two southernmost cores GeoB 6405-6 and GeoB 6408-4 are influenced by the Antarctic bottom water (AABW) and lie below the calcium carbonate compensation depth (CCD). They are classed as diatom bearing nannofossil ooze. Because the nearby core GeoB 6407-1 was taken from a shallower water depth (3384 m), its sediment composition rather resembles cores GeoB 6421-2 and GeoB 6422-1 from the vicinity of the STF. All three cores of this second group lie above the CCD and contain mainly foram bearing nannofossil ooze. The remaining cores, GeoB 6425-2, GeoB 6426-1, and GeoB 6428-1, come from the oligotrophic subtropical South Atlantic north of the STF. They reflect the sedimentation history of the nutrient poor nutrient-poor NADW where, due to low carbonate or opal influx, clay minerals are dominant.

2.2. The stratigraphic network

A detailed age model for the three northern cores has been developed in Schmieder (2004) by correlating small scale characteristics of their magnetic susceptibility records to the Subtropical South Atlantic Susceptibility Stack (SUSAS) (von Dobeneck and Schmieder, 1999). Since all northern cores recorded at least the Brunhes–Matuyama geomagnetic boundary at their base, the age

model is additionally constrained by magnetostratigraphic tiepoints (Schmieder, 2004). The age model for the remaining five cores was constructed using computer aided multiparameter signal correlation (Hofmann et al., 2005). In this approach precise intercore correlation is achieved by synchronously matching high-resolution records of magnetic susceptibility κ, wet bulk density ρ, and X-ray fluorescence scans of elemental composition. Moreover, $\delta^{18}O$ records have been matched in the same process for the two cores where they are available. An optimal network correlation between all pairs of multi-parameter sequences has been obtained by controlling the correlation errors between core pairs (A, B) and (B, C) through comparison with the correlation (A, C). The network correlation was then provided with an absolute age model by synchronously correlating the $\delta^{18}O$ and κ records of GeoB 6408-4 and GeoB 6421-2 with SPECMAP, Martinson (Imbrie et al., 1984; Martinson et al., 1987) and SUSAS (von Dobeneck and Schmieder, 1999; Schmieder, 2004). Even though lithology varies considerably between the cores, it was thus possible to obtain high internal consistency which ensures a relative median age error of less than 5 ka (Hofmann et al., 2005).

3. Methods

Magnetic susceptibility κ was measured on the archive halves of the cores at 1 cm intervals using a Bartington spot sensor type M.S.2.F mounted on a computer controlled positioning system. The instrument drift was controlled by a separate background reading in air for each measurement. High-resolution records of elements from potassium (K, atomic number 19) through strontium (Sr, atomic number 38) have been determined using an X-ray fluorescence (XRF) scanner developed and built at the Netherlands Institute for Sea Research (NIOZ, Texel) (Jansen et al., 1998). The obtained XRF spectra are processed with the software toolbox KEVEX™ (Roehl and Abrams, 2000) calculating relative element intensities in counts per second (cps). Oriented cubic samples with a volume of 6.2 cm^3, were taken from all sediment series at 5 cm intervals, on board immediately after recovery (Wefer and cruise participants, 2001). Natural remanent magnetization (NRM) was systematically alternating-field (AF) demagnetized in first 5 mT steps up to a peak field of 30 mT, and then in 10 mT steps up to a peak field of 100 mT. Anhysteretic and isothermal remanent magnetization (ARM and IRM) were both measured on cubic samples. ARM, acquired in a 40 μT bias field and a 100 mT peak AF, was subsequently demagnetized to a peak AF of 100 mT, using the same field steps as for NRM demagnetization. IRM acquisition curves were measured at room temperature in 18 steps up to 250 mT. Subsequently AF demagnetization of IRM was measured using again the same steps as for NRM demagnetization, but with four additional field steps at 125, 150, 200 and 250 mT. Remanence measurements for all samples were performed with an automated 2G SQUID rock magnetometer (Model 755 R) of the Marine Geophysics Division at the Department of Geosciences, University of Bremen. Sub-samples for hysteresis measurements were taken from cores GeoB 6405-6, GeoB 6407-1, GeoB 6408-4, and GeoB 6422-1 and prepared using the technique described by von Dobeneck (1996). Measurements were carried out using a PMC M2900 alternating field gradient force magnetometer (AGFM), and then were processed with the program HYSTEAR von Dobeneck (1996). Standard hysteresis parameters were determined in order to calculate the magnetogranulometric indicative ratios of saturation remanence to saturation magnetization (σ_{rs}/σ_s) and coercivity of remanence to coercive force (B_{cr}/B_c).

Room temperature frequency dependent susceptibility in sediments indicates the relative concentration of particles in a certain superparamagnetic (SP) grain size range (Worm, 1998). It was measured on discrete samples using a Bartington bulk sensor M.S.2.B connected to a M.S.2 susceptibility meter, which applies an alternating field of 0.5 mT at a low frequency of 460 Hz (for κ_{lf}) and a high frequency of 4600 Hz (for κ_{hf}). All data were normalized to a sample volume of 6.2 cm^3.

To determine the presence of high coercivity minerals, IRM acquisition curves were measured in 27 steps up to a peak field of 2.5 T. A back field of −300 mT was imparted after the 1 and 2.5 T steps, in order to calculate the *S*-parameter $S_{-0.3\ T}$ after Bloemendal et al. (1992). $S_{-0.3\ T}$ quantifies the fraction of SIRM acquired in 300 mT and varies between 0 for extremely high coercive, and 1 for low coercive samples. In sediments, 1 usually represents pure magnetite, while lower $S_{-0.3\ T}$ indicates increasingly larger magnetic influence of hematite or goethite.

3.1. Quality tests for relative paleointensity

Several standard criteria are in use to ensure the reliability of sediments for relative paleointensity investigations (King et al., 1983; Tauxe, 1993). Common requirements are that the main remanence carrier is magnetite, and that the sediment is homogenous with respect to composition and grain size. Further, variations in magnetic carrier concentration must be less than an order of magnitude, and the grain size of the magnetic mineral assemblage should be in the range of 1–15 μm. Finally, the NRM should exhibit no inclination error and no diagenetic overprint. In the following these reliability criteria are

evaluated for the network cores. Median inclinations were calculated using Fisher statistics and except for core GeoB 6428-1 they correspond well to the values expected for a geocentric axial dipole field (Fig. 2). To detect and quantify reductive diagenesis we use the parameter Fe/κ of Funk et al. (2004) which has been evaluated for all cores (Hofmann et al., 2005). It is used as background shading in Fig. 3 on a linear gray scale from Fe/$\kappa \leq 10$ Mcps (white) indicating low and Fe/$\kappa \geq 40$ Mcps (black) for higher reductive diagenesis. On average, diagenetic influence increases from north to south across the subtropical front. Homogeneity of the magnetic mineral fraction as reflected by κ, κ_{ARM} and IRM (Fig. 3) changes throughout the cores, with higher variability in the South. This also is confirmed by the core ratios ARM_{min}/ARM_{max}, which for the northern cores is below the commonly suggested limit of 10, while in the southern cores it achieves values of more than 30. In our previous study κ was found to assume higher values during cold, and lower values during warm oxygen isotope stages (Hofmann et al., 2005). The parameters κ_{ARM} and IRM closely resemble this pattern (Fig. 3) which indicates that the concentration of all magnetic minerals is higher during glacial and lower during interglacial times. The data also provide evidence that low values of κ, κ_{ARM} and IRM are related to higher Fe/κ, which supports the interpretation of the latter ratio as indicating a diagenetic transformation of ferrimagnetic to paramagnetic iron minerals.

Both grain size sensitive ratios, ARM/IRM and κ_{ARM}/κ, coincide very well in all network cores (Fig. 3). As with concentration, also the variations in magnetic grain size are more substantial in the southern cores than in the northern cores. The average ARM/IRM value of 0.031 for the northern cores indicates that their remanence carriers are slightly coarser than in the vicinity of the STF, where average ARM/IRM is 0.041, or south of the STF, where

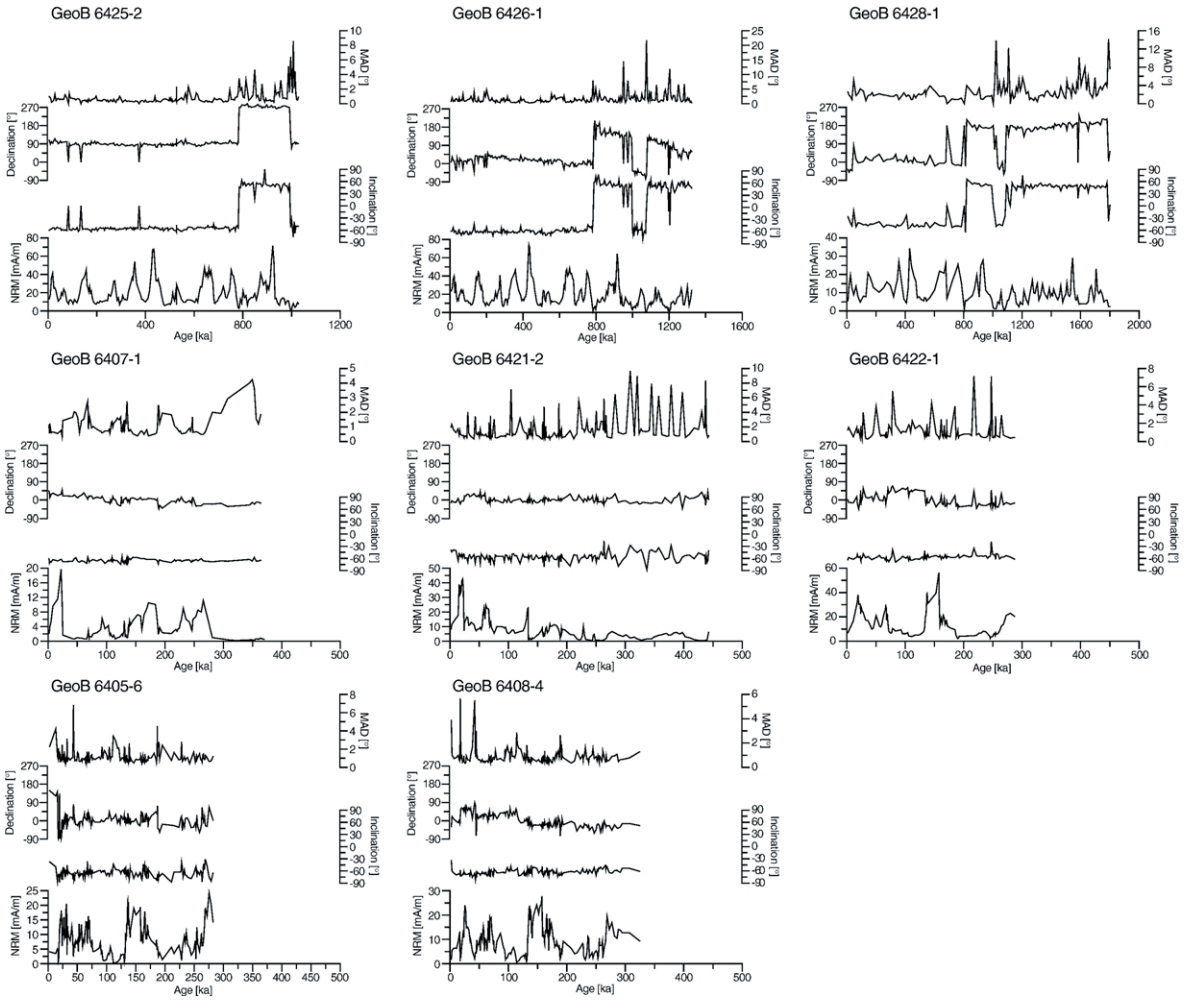

Fig. 2. NRM30, inclination and declination records of the ChRM and their MAD of the cores from the stratigraphic network.

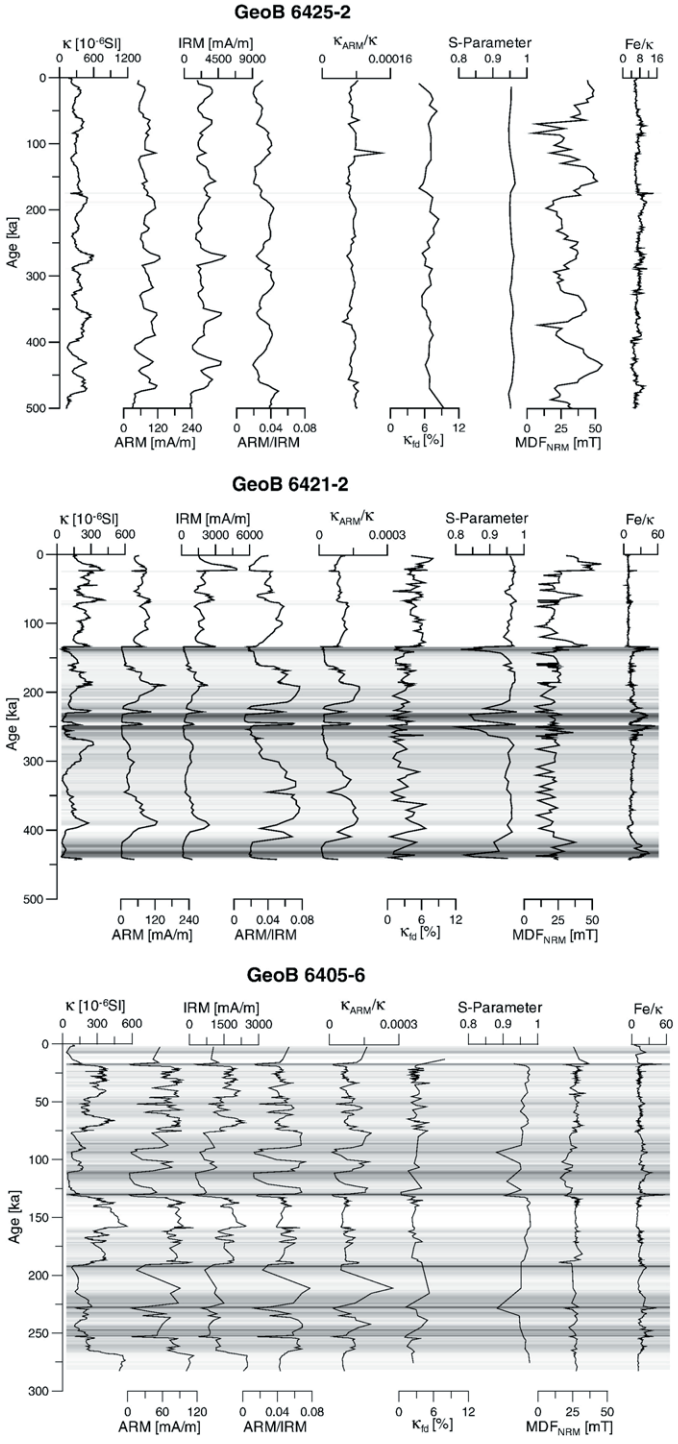

Fig. 3. Concentration and grain size dependent parameters for core GeoB 6425-2, representing the northern cores, core GeoB 6421-2 for the cores within the STF and core GeoB 6405-6, representing the southern cores. Clearly the variations in the different parameters decrease from south to north. On a background linear gray scale from $Fe/\kappa \leq 10$ Mcps (white) and $Fe/\kappa \geq 40$ Mcps (black), the ratio Fe/κ, which indicates reductive diagenesis (Funk et al., 2004; Hofmann et al., 2005), is presented. High Fe/κ values correspond with low values in the concentration dependent parameters related to larger magnetite grain sizes.

average ARM/IRM is 0.046. Low ARM/IRM values significantly correlate with higher Fe/κ values, which can be explained by a loss of fine grained magnetic minerals during reductive diagenesis. In GeoB 6421-2 below an age of ~150 ka ARM/IRM displays a step-like increase. Since no signs of diagenetic coarsening are visible in Fe/κ above this age, there must have occurred a change in source or transport path around this time. This interpretation is supported by our δMn/Fe data which imply that before 150 ka the STF was located north, and afterwards mostly south of GeoB 6421-2 (Hofmann et al., 2005). (The rock magnetic parameters of all cores are presented in the electronic appendix Figs. 10–12.) For four of the network cores we also performed hysteresis measurements for magnetic grain size determinations according to Day and Fuller (1977). While most of the samples plot within the pseudo-single domain (PSD) field of the Day plot (Fig. 4), some diagenetically influenced samples from cores GeoB 6405-6 and GeoB 6407-1 show multi-domain (MD) characteristics with B_{cr}/B_c values above 4. Superparamagnetic (SP) content, as represented by the frequency dependent susceptibility κ_{fd}, varies around 3–8% for all network cores (Fig. 3). Probably related to diagenesis, κ_{fd} on average decreases from North to South across the STF. The generally high S-parameters, between 0.95 and 1, imply that the magnetic mineralogy of the network cores is dominated by low coercive magnetite (Fig. 3). Yet, the cores south of the STF and core GeoB 6421-2 contain intervals where high coercive minerals are more prominent ($S_{-0.3T} \leq 0.9$). Here, the coincidence of low $S_{-0.3T}$-values with high Fe/κ leads us to the conclusion that the magnetite phase is dissolved by diagenesis, whereas the high coercive components remain, and thereby appear relatively enriched.

The above quality considerations are not conclusive because the network cores with respect to most criteria are just at the border of the admissibility region, whereby unfortunately cores with higher sedimentation rate are rather of lower quality. This leaves us with the unsatisfactory choice to either dismiss the higher resolving sequences on the basis of some empirical limits, or to include possibly biased records into the relative paleointensity evaluation. For three reasons we decided to carefully follow the second path. First, by analyzing the normalized NRM records, we found that the high ranked northern cores display the highest amplitude variations and do not appear to be the best RPI records from the network. Second, the final aim of our stratigraphic network project is to analyze the influence of lithology upon RPI, and to assess lithologic influences based on a comparison between many different recordings of the same field history. Third, a theoretical study showed that even an inhomogeneous sediment could yield a true RPI record if NRM acquisition and sediment composition are both linearly influenced by a single environmental signal (Fabian, 2006). In the spirit of the last consideration, we now apply principal component analysis (PCA) to isolate the predominant signal components from the rock magnetic parameters.

3.2. Principal component analysis of ARM and IRM

PCA is a standard statistical tool to extract relevant information from complex data sets. Its main idea is to optimally adapt an orthogonal coordinate system into a high dimensional set of data points. The coordinate axes are sorted, such that the first axis coincides with the direction of maximal data variance, the second with the direction of maximal residual variance and so on. A good introduction to PCA can be found in Lay (2000). Here PCA is applied to determine the principal independent environmental signals which influence our rock magnetic measurements. We explain this method for the IRM demagnetization of GeoB 6408-4, but it equally applies for ARM, NRM and all other cores. First, from the direct demagnetization curves $IRM_k(z)$ for the AF-field steps H_k (Fig. 5a) we determine the difference curves $\Delta IRM_k(z) = IRM_k(z) - IRM_{k+1}(z)$ (Fig. 5b). Since we wish to focus on the hard magnetite fraction, we constrain our investigation to the demagnetizing interval between 30 and 80 mT, which is covered by five difference curves $\Delta IRM_k(z)$. Though we believe that in this interval magnetite contributes most, we cannot exclude that coercivities of other unwanted mineral fractions also overlap into this range. By PCA we can assess to which extent the five $\Delta IRM_k(z)$-curves are explained by their first principal component, which is interpreted as the predominant environmental signal $s(z)$ governing magnetic mineral composition and remanence acquisition in this coercivity range. In an ideal sediment all concentrations vary with one predominant environmental signal $s(z)$, while in more complex (real) sediments there may be two or more environmental signals (Fabian, 2006). For the northern and the southern cores ARM and IRM are represented by mainly one component (97%). The ARM of the cores from the STF is also represented by one component, while for IRM a small second component (3–6%) is required to explain the IRM.

4. Natural remanent magnetization

Primary remanence acquisition in sediments occurs by alignment of magnetic particles within the external field. This depositional or post-depositional alignment

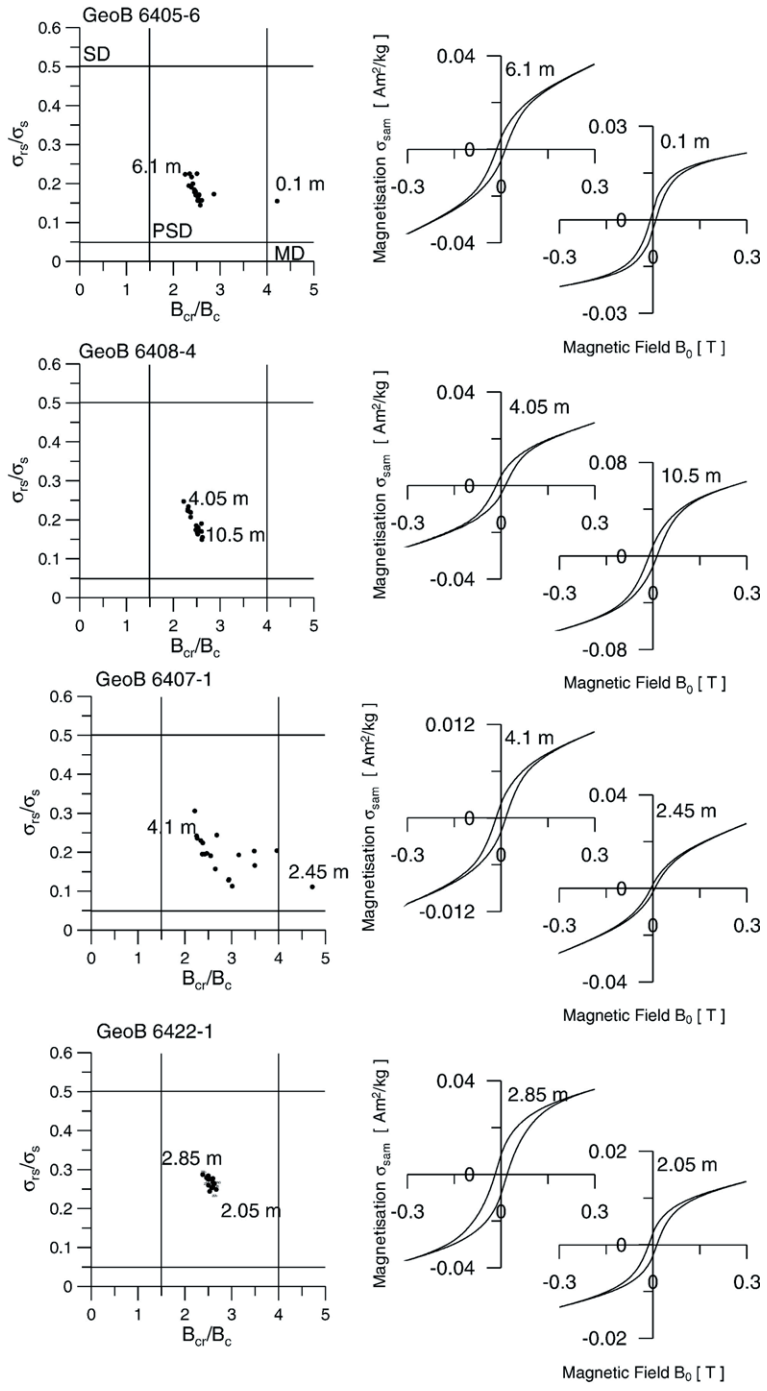

Fig. 4. Grain size determination using Day plots (Day and Fuller, 1977). Most samples have PSD characteristics. Only cores GeoB 6405-6 and GeoB 6407-1 contain single samples where hysteresis data indicate MD properties.

occurs over a depth interval denoted as lock-in depth λ. Accordingly, the natural remanent magnetization (NRM) measured at a certain core depth is a weighted average of the field history over a time span of about λ/σ, where σ denotes the sedimentation rate. Using an optimistic value of $\lambda \approx 2$ cm and an average $\sigma \approx 2$ cm/ka for our network cores yields an optimal temporal resolution of about 1 kyr independent of sampling density. The final NRM also comprises chemical or viscous overprints, but, outside of some clearly defined redox

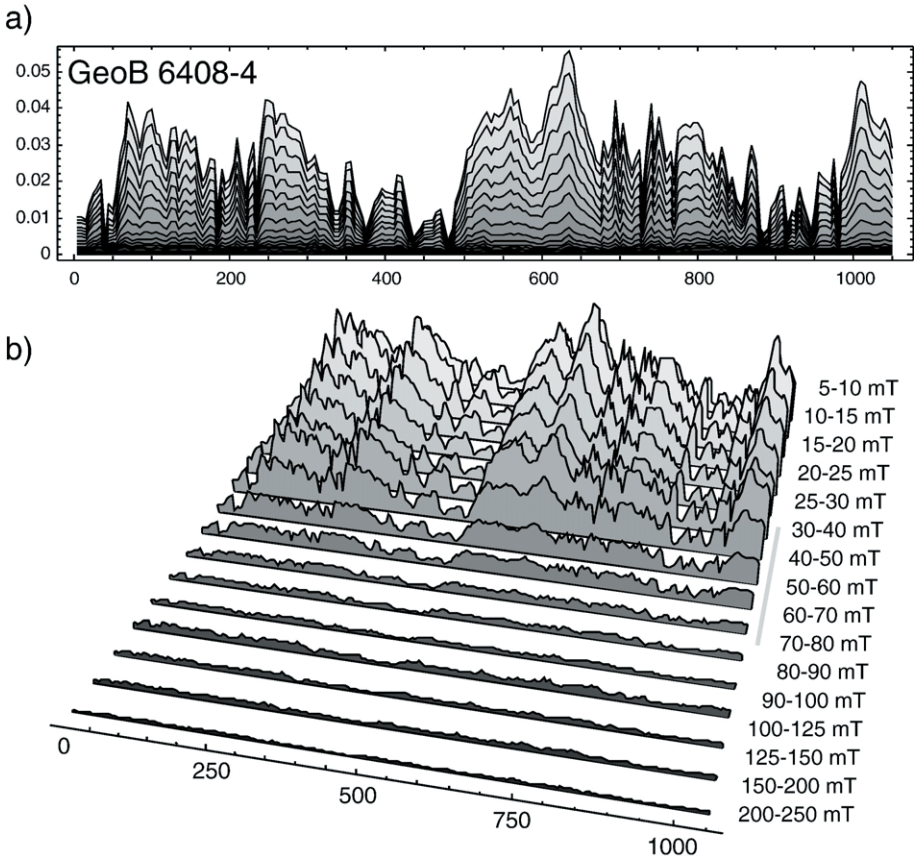

Fig. 5. The IRM demagnetization steps of GeoB 6408-4 form a decreasing sequence of magnetization curves (a). The differences between subsequent steps (b) contain independent information about different coercivity fractions. Applying PCA to the five coercivity intervals from 30 to 80 mT allows to assess if the magnetic mineral fraction with coercivity in this range is dominated by a single environmental signal.

horizons, these factors appear to be negligible in our cores. Additional systematic effects of gravitational forces, which could lead to inclination shallowing, are also unlikely, since the average inclination of each core is consistent with the expected geocentric dipole inclination at its respective latitude. Therefore, the network NRM records constitute slightly smoothed, but otherwise reliable series of local paleomagnetic field directions (declination, inclination). Yet, the quality of these recordings with respect to paleointensity also depends on mineralogy, concentration and grain size of the magnetic mineral assemblage, and on the mechanical mode of remanence acquisition. Depth dependent variations of these factors could substantially distort the recorded intensity as compared to the true geomagnetic field signal. It is therefore necessary to independently ensure the homogeneity of the NRM intensity records used for paleointensity reconstruction.

As an indication of the variability of the NRM demagnetization curves within the single records, the background plots in Fig. 6 contain all AF demagnetization curves for each core as gray lines. The solid black lines highlight single typical curves together with their related orthogonal projections (Zijderveld, 1967).

In each core we find NRM demagnetization curves (solid line with circles), which are almost completely demagnetized in fields of 100 mT. They are characteristic for a low coercive magnetic mineral (e.g. magnetite) and display a stable single component normal remanence direction (circles in Fig. 6). For some samples (triangles) the NRM demagnetization curve is not fully demagnetized at AF fields of 100 mT, indicative of a higher coercive magnetic mineral. The demagnetization curve for the sample at 2.7 m in core GeoB 6428-1 shows a stable single component with reversed polarity and a low coercive over-print with normal polarity. For cores GeoB 6421-2 through GeoB 6428-1 Fig. 6 presents additional demagnetization curves (squares) where a stable single component remanence is overprinted by a weak viscous remanence, which is demagnetized above fields of 30 mT. The median destructive field of the NRM (MDF_{NRM}) for

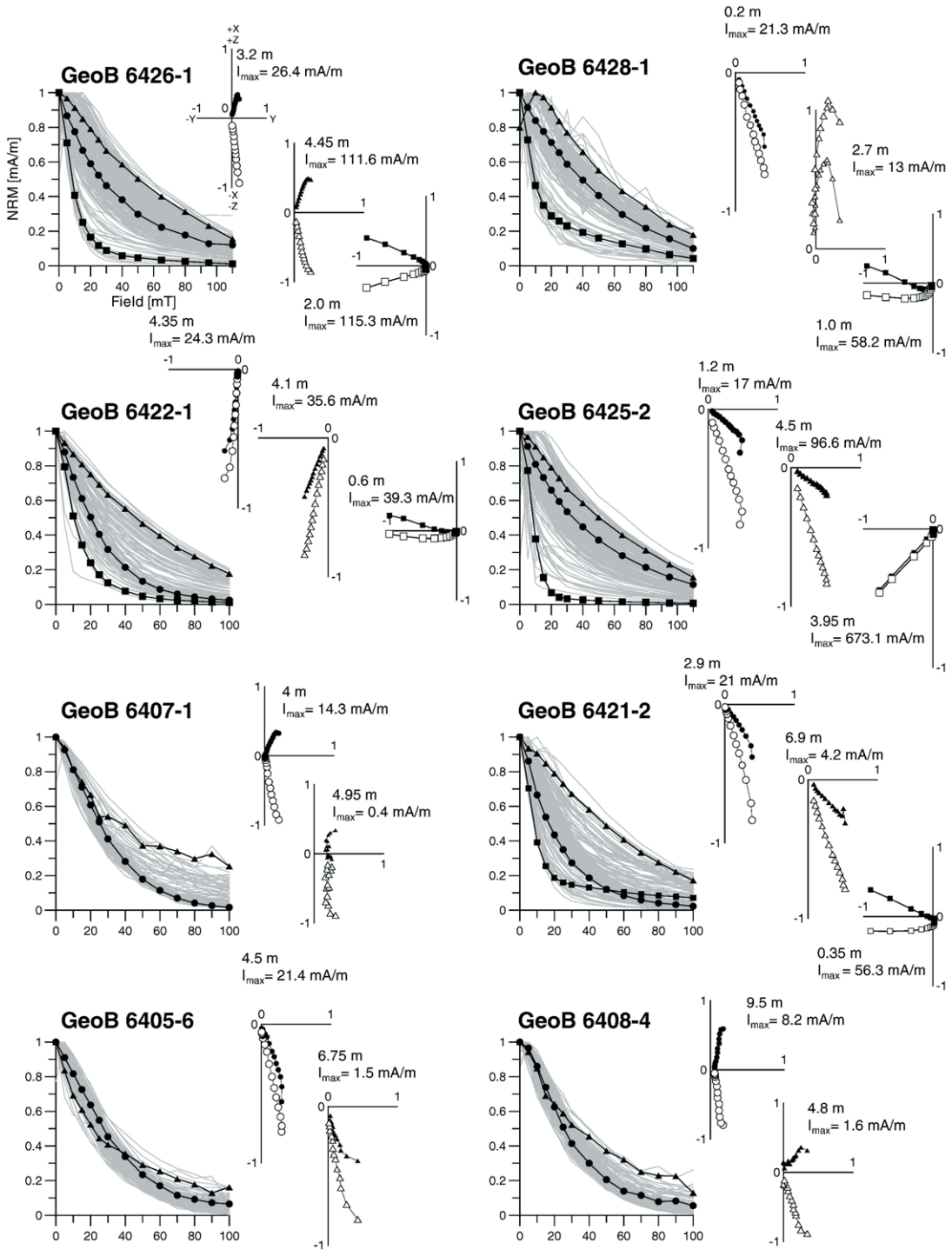

Fig. 6. Gray lines represent the AF demagnetization curves for all samples for each core. Solid black lines with symbols indicate the AF demagnetization curve for the related orthogonal projection curves for representative samples. The open and filled symbols indicate projection of vector endpoints on the vertical and horizontal planes, respectively.

the latter samples is about 10 mT and thus much lower than for non-overprinted samples which typically have MDFs near 25 mT.

The Characteristic Remanent Magnetization (ChRM) was calculated for each sample, using principal component analysis after Kirschvink (1980) (Fig. 2) including at least

four successive demagnetization steps. Superimposed trends on some declination values, e.g. at the end of core GeoB 6426-1, point to rotation during core recovery, peak values coincide with the overprinted samples. Maximum angular deviations are generally below 10° indicating that the magnetization components are well defined. Slightly higher MAD values are found for samples with low NRM intensities, and for samples with viscous overprint.

The origin of the viscous overprint is unknown but it is eliminated by demagnetization fields above 30 mT. Therefore, all further investigations use only NRM demagnetization steps above 30 mT. The three northern cores contain at least one magnetic reversal. NRM intensity is variable across the STF and increases towards the North, while core GeoB 6428-1 has lower NRM values than the other northern cores.

5. Relative paleointensity determination

5.1. Principal component analysis of NRM

As for ARM and IRM, principal component analysis can be applied to isolate a predominant linear NRM signal component, and to assess how many independent components contribute significantly to the total NRM. The quality of NRM is ideal if it can be attributed to a single component which comprises paleomagnetic and environmental influences. Since we know already from Fig. 6 that the magnetite signal in some cores is overprinted by a low coercive viscous signal, and that in other cores higher coercivity minerals are present, we constrain the NRM demagnetization curves to the interval between 30 and 80 mT (Fig. 7) before applying PCA. Comparison with Fig. 6 shows that this restriction considerably reduces the deviations between demagnetization curves within the single cores. Fig. 7 also affirms that the NRM of the 30 to 80 mT coercivity interval is carried by a quite homogenous magnetic mineral fraction which probably is magnetite. However, the above restriction of the demagnetizing interval produces an extremely high noise level for a few curves in Fig. 7 (especially for GeoB 6428-1) because the largest fraction of their NRM is already demagnetized at 30 mT. PCA performed on the 30 to 80 mT demagnetization interval indicates that not only the mineral fraction carrying the NRM, but also the NRM signal itself in most cores consists of more than 90% of one single component. Only the NRM signals of GeoB 6421-2, GeoB 6422-1, and GeoB 6426-1 need more than 5% of a second component in the PCA analysis.

5.2. RPI determination

To obtain an estimate of relative paleointensity (RPI), NRM needs to be normalized to correct for variations of remanence carrier concentration (Levi and Banerjee, 1976). Because we still know very little about sedimentary remanence acquisition, there is no straightforward normalization method (Johnson et al., 1948, 1975; Levi and Banerjee, 1976; King et al., 1983; Meynadier et al., 1992; Tauxe, 1993). Consequently, as we do not have a proven medication, a multitude of different 'snake oil' normalization techniques is in circulation, each of which has its own merits and shortcomings. The seemingly most reasonable

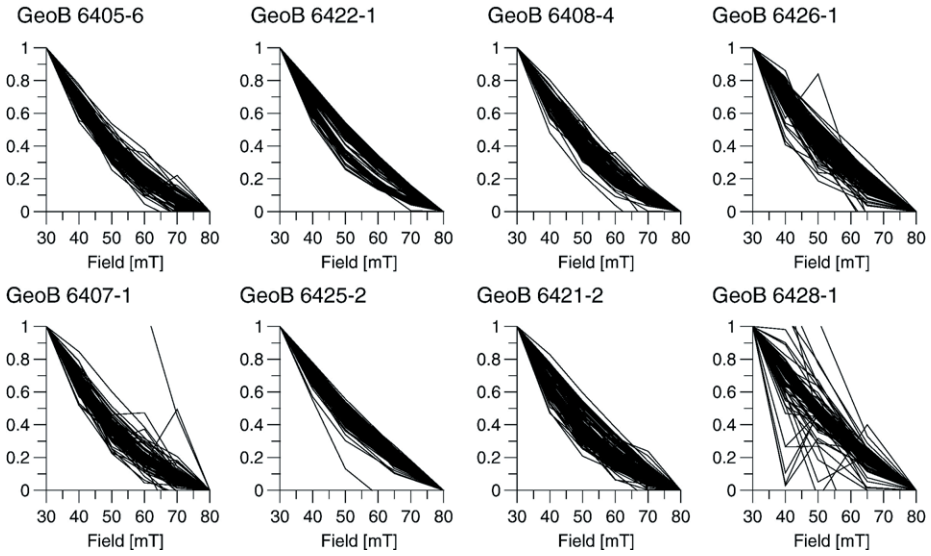

Fig. 7. NRM demagnetization curves of all network cores for the 30 to 80 mT interval normalized on the 30 mT demagnetization step.

normalizers are ARM and IRM, which are remanence based, and often resemble the NRM in their demagnetization behavior. It is therefore assumed that they activate the same grains that carry the NRM (Channell et al., 1997). Magnetic susceptibility is occasionally used as normalizer, but its signal also encompasses paramagnetic, superparamagnetic, and large multi-domain grains which contribute little or nothing to NRM. Yet, just to worry the reader how little we know, it could – and has been – argued that the normalization process is meant to correct for an overall environmental signal rather than just canceling out concentration variations (Fabian, 2006), in which case the more integral susceptibility signal may be even more appropriate than ARM or IRM.

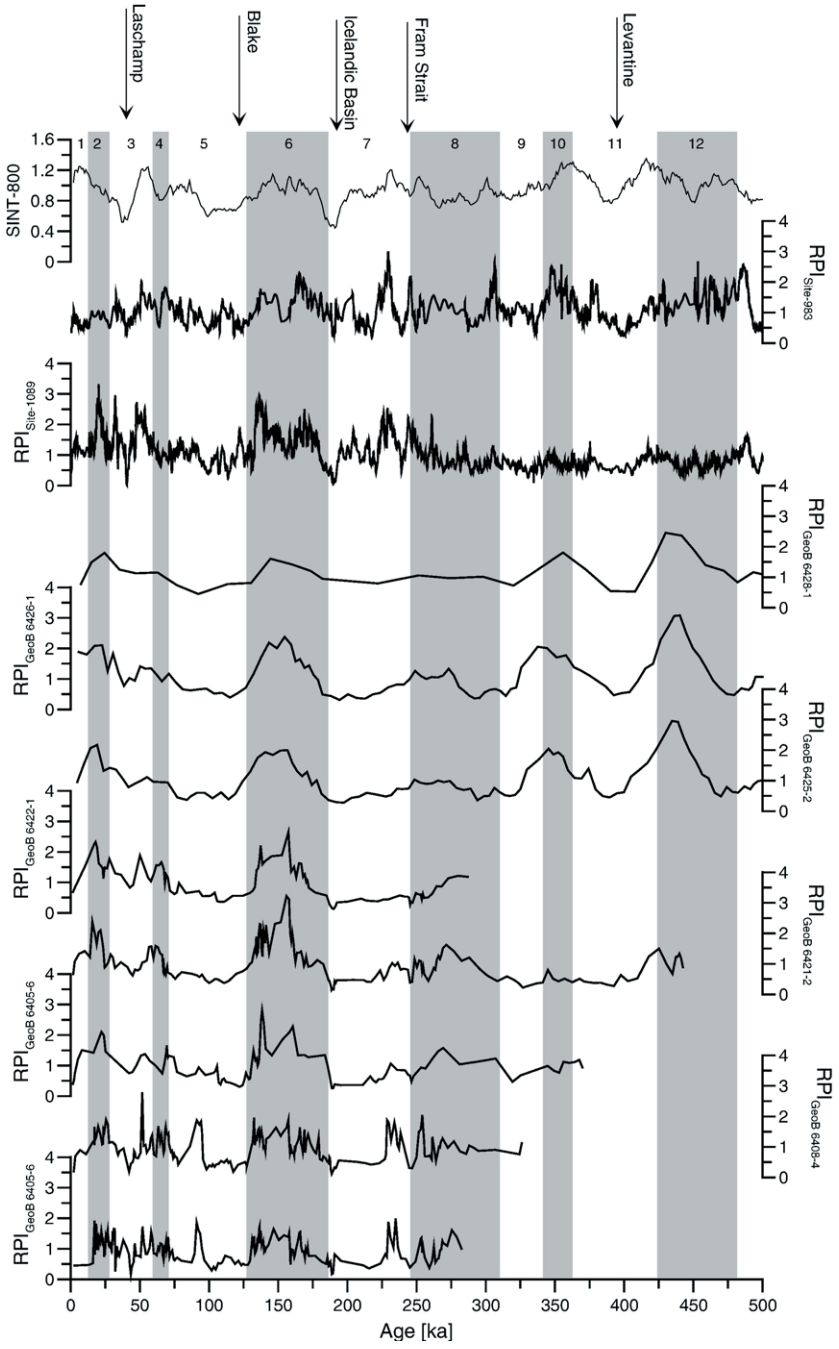

Fig. 8. NRM_{diff}/ARM_{diff} records for the network cores. The RPI records from the network cores are compared to the RPI record from ODP Site 1089, ODP Site 983 and the global RPI stack Sint-800 (Guyodo and Valet, 1996; Stoner et al., 2002a; Channell et al., 2002).

Here we follow the practical approach of using all three parameters as alternative normalizers, hoping that they either yield similar results, or that the resulting records allow to make a well founded choice. Since PCA of all remanences (NRM, ARM and IRM) resulted in a single dominating (>90%) component in the 30 to 80 mT demagnetization interval, we also restricted the RPI determination to this interval by defining

$$\mathrm{NRM}_{\mathrm{diff}} := NRM_{30} - \mathrm{NRM}_{80}, \quad (1)$$

and similarly for $\mathrm{ARM}_{\mathrm{diff}}$ and $\mathrm{IRM}_{\mathrm{diff}}$. By comparing the RPI records obtained from the three different normalization parameters $\mathrm{ARM}_{\mathrm{diff}}$, $\mathrm{IRM}_{\mathrm{diff}}$, and κ, it turned out that, while $\mathrm{NRM}_{\mathrm{diff}}/\mathrm{ARM}_{\mathrm{diff}}$ and $\mathrm{NRM}_{\mathrm{diff}}/\mathrm{IRM}_{\mathrm{diff}}$ lead to very similar results, both can considerably deviate from the susceptibility normalized RPI record $\mathrm{NRM}_{\mathrm{diff}}/\kappa$. Due to the closer resemblance between NRM and ARM demagnetization curves as compared to the IRM demagnetization curves, we will base the following analysis on the $\mathrm{NRM}_{\mathrm{diff}}/\mathrm{ARM}_{\mathrm{diff}}$ records which are collected in Fig. 8.

In most of the network cores lows in paleointensity around 45 ka, corresponding with the Laschamp event, and around 100 ka, corresponding to the Blake event, (Thouveny et al., 1990, 1993; Laj et al., 2000; Channell et al., 2000; Mazaud et al., 2002; Thouveny et al., 2004; Guillou et al., 2004) are observed.

Two further lows in RPI at 190 ka and 250 ka are found in all cores except the three northernmost cores; this could be due to their much lower sedimentation rate. The first low at 190 ka could correspond with the Icelandic Basin event (Channell, 1999) and the low at 250 ka with the Fram Strait event (Nowaczyk and Baumann, 1992; Langereis et al., 1997). In the northern cores another RPI low at 400 ka, corresponding to the Levantine excursion (Langereis et al., 1997; Thouveny et al., 2004) is observed. In all cases, the inclination records are not anomalous. This probably is due to the low sedimentation rates, which smooth out short term field variations. However, it is also possible that the geomagnetic field – though weaker – did not noticeably change its local geometry. Throughout the network cores slightly higher relative paleointensity values are found during glacial times (Fig. 8). In view of the above discussed shortcomings of the RPI methodology, this is more likely to be an artifact of insufficiently cancelled environmental signals, than an indication of climate-field coupling.

5.3. Comparison to RPI records from other locations

In Fig. 8 the individual records from the network cores are compared to the RPI record from ODP Site 1089 (Stoner et al., 2002a), located further south on the southeastern flank of the Agulhas Ridge, the record from ODP Site 983 (Channell, 1999; Channell et al., 2002), located in the Iceland Basin, and to the global paleointensity stack Sint-800 (Guyodo and Valet, 1996). Several of the well known geomagnetic events are found as RPI lows throughout all our records. Interestingly, the Laschamp event is detected in the network cores around 45 ka, while in ODP 1089, ODP 983, and Sint-800 it occurs at 40 ka. While this age difference barely exceeds our maximum age error estimate, the direction of the deviation coincides with the high resolution western North Atlantic study of Lund et al. (2006), which determined a Laschamp age of 41 ka, but also presents a record from the Blake Outer Ridge where the RPI low starts even before 45 ka. The Icelandic Basin event is observed in all cores around 180 ka. At the boundary between marine isotope stage (MIS) 7 and 8 (245 ka), also corresponding with the Fram strait event, beside the intensity low, two peaks with higher RPI values were observed in cores GeoB 6405-6, GeoB 6408-4 and the more northern core GeoB 6421-2. These two peaks are also visible in the RPI records from ODP Sites 1089 and 983, where both fall completely into MIS 7. However, in Sint-800 the second peak falls into MIS 8 similar to our records. Also the Fram Strait event itself occurs at the same time, directly at the boundary between MIS 7 and MIS 8, in our network cores and in the Sint-800 record. Again, both ODP records recorded this event slightly earlier. As with the Laschamp event, these differences may be caused by deviations between the age models. Yet, they also could be a true record of a geometrically complex spatiotemporal pattern of the geomagnetic field during the events.

5.4. A 300 ka South Atlantic relative paleointensity stack

Since the individual RPI records in Fig. 8 were recorded by substantially different sedimentary regimes, they are likely to contain significant signal components which are rather due to local environmental influences than to the regional geomagnetic field. Indeed, it needs no overcareful examination to find several discrepancies between records of different lithological groups in Fig. 8. Yet, the main signal features are similar in all records and one is tempted to again use PCA to extract the common principal component. However, a closer look at the nature of the RPI records as ratios of magnetic properties, shows that important information is contained in the absolute offset in relation to signal amplitude, an information which will be lost by PCA. On the other hand, from the physical point of view it is more desirable to understand the origin of the discrepancies between the records than merely to suppress them by refined signal analysis. Since this analysis of the connection between sediment composition and RPI

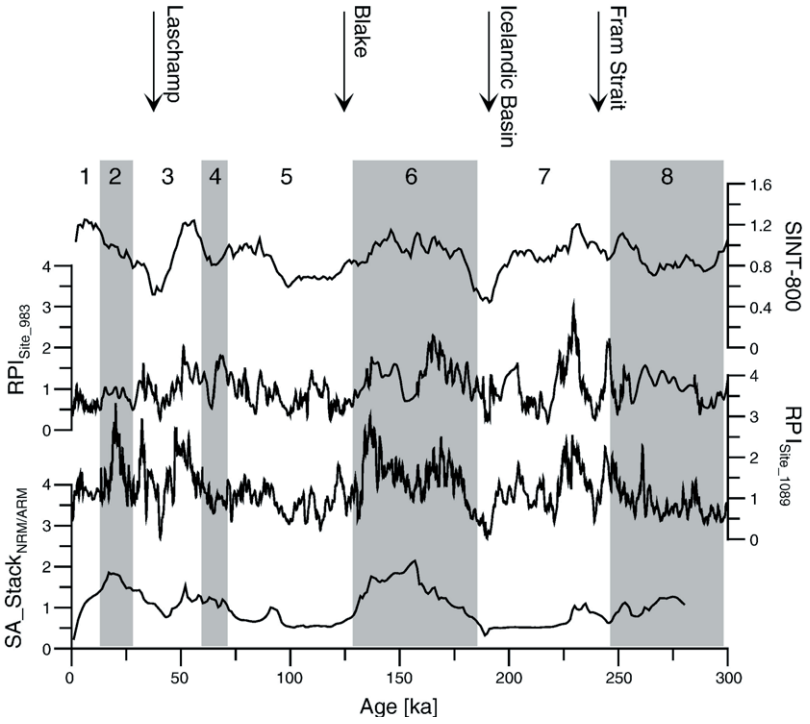

Fig. 9. Stack of the NRM_{diff}/ARM_{diff} records from the eight network cores compared to the RPI Stack Sint-800, the RPI records of ODP Sites 983 and 1089 (Guyodo and Valet, 1996; Channell et al., 2002; Stoner et al., 2002a).

records is beyond the scope of this study, and will be developed in more detail in a forthcoming paper, we here restrict ourselves to a most simple stacking procedure which solely intends to average out the most prominent local influences. We do this by linearly interpolating the individual RPI records on a 1 ka time grid, and then stacking them by using the arithmetic mean over the time interval of the last 300 ka. This procedure results in a first direct RPI stack (SAS-300) for the central South Atlantic. While this stack should contain less local distortion than any single record, it still fully contains environmental distortions from global, or large scale regional variations, and, due to the simple averaging process, enhances the low frequency RPI signal component, while the amplitudes of high frequency components are reduced. The latter effects result from the variation in sedimentation rate across the network, and from inevitable centimeter scale misalignments between the cores. These low-pass filter properties, which apply also to the Sint-800 record, are clearly visible in the comparison between SAS-300 and the nearby RPI record of ODP site-1089 in Fig. 9. Both records show markedly higher RPI values during glacial times, which – to a lesser extent – is also true for the Sint-800 and the site-983 records. However, we tend to attribute this rather to an uncompensated global climatic signal than to a coupling between climate and geomagnetic field.

6. Conclusions

We here present rock magnetic measurements and individual relative paleointensity records of eight sediment cores from a stratigraphic network across the central South Atlantic subtropical front (STF) based on a previously developed precise age model (Hofmann et al., 2005). For this region, with its complex sedimentary regime and low sedimentation rates, no relative paleointensity records have been available up to now. This study is part of a larger project, which intends to improve upon this situation by untangling the geomagnetic field record from lithological influences. Therefore, the stratigraphic network was designed to cover a compositional gradient. Yet, with respect to their position relative to the STF, the cores split into three local groups of relatively similar lithology. Whilst none of the cores ideally fulfills the classical quality criteria for relative paleointensity determination (King et al., 1983; Tauxe, 1993), we were able to isolate by principal component analysis (PCA) a demagnetization interval (30 to 80 mT) where NRM, ARM, and IRM are well defined single homogenous signals. This interval was subsequently used to construct eight individual relative paleointensity records which are connected only by their common network chronology. Despite some marked differences, all eight network cores display paleointensity

lows at the positions of the Laschamp (45 ka), Blake (100 ka), Icelandic Basin (190 ka) and Fram Strait (250 ka) events. Moreover, many individual features of our relative paleointensity records resemble other regional and global RPI records, even though some of the variations appear to still originate from insufficient normalization of climatic signals in the sedimentary sequence, and not from true paleofield variations. To suppress at least local climatic variations, we constructed a regional relative paleointensity stack for the last 300 ka (SAS-300) from our data set. Even if preliminary, this stack provides a first field intensity record for the central South Atlantic and can be used to investigate the still unsatisfactory link between southern and northern RPI records. A detailed study of the influence of sediment composition upon the individual RPI records of the stratigraphic network will appear separately.

Acknowledgements

We thank Thomas Frederichs and Christian Hilgenfeldt for valuable discussions and technical support. Thoughtful reviews by Lisa Tauxe and an anonymous reviewer are thankfully acknowledged. This work was supported by the Deutsche Forschungsgemeinschaft (DFG), SPP 1097: "Geomagnetic variations", grant Fa 408/1-2.

Appendix A. Supplementary data

Supplementary data associated with this article can be found, in the online version, at doi:10.1016/j.epsl.2007.05.042.

References

Bloemendal, J., King, J., Hall, F., Doh, S.-J., 1992. Rock magnetism of late Neogene and Pleistocene deep-sea sediments: relationship to sediment source, diagenetic processes and sediment lithology. J. Geophys. Res. 97 (B4), 4361–4375.

Channell, J., 1999. Geomagnetic paleointensity and directional secular variation at Ocean Drilling Program (ODP) Site 984 (Bjorn Drift) since 500 ka: comparisons with ODP Site 983 (Gardar Drift). J. Geophys. Res. 104 (B10), 22937–22951.

Channell, J., Hodell, D., Lehmann, B., 1997. Relative geomagnetic paleointensity and $\delta^{18}O$ at ODP Site 983 (Gardar Drift, North Atlantic) since 350 ka. Earth Planet. Sci. Lett. 153, 103–118.

Channell, J., Valet, J.-P., Hodell, D., Charles, C., 2000. Geomagnetic paleointensity from late Brunhes-age piston cores from the subantarctic South Atlantic. Earth Planet. Sci. Lett. 175, 145–160.

Channell, J., Mazaud, A., Sullivan, P., Turner, S., Raymo, M., 2002. Geomagnetic excursions and paleointensities in the Matuyama Chron at Ocean Drilling Program Sites 983 and 984 (Iceland Basin). J. Geophys. Res. 107 (B6), 2114. doi:10.1029/2001JB000491.

Day, R., Fuller, M., 1977. Hysteresis properties of titanomagnetites: grain-size and compositional dependence. Phys. Earth Planet. Inter. 13, 260–267.

Fabian, K., 2006. A Linear Theory of Physical Properties in Inhomogeneous Sediments and its Application to Relative Paleointensity Determination. eEarth Discuss 1, 51–62.

Funk, J., von Dobeneck, T., Reitz, A., 2004. Integrated rock magnetic and geochemical quantification of redoxomorphic iron mineral diagenesis in Late Quaternary sediments from the equatorial Atlantic. In: Wefer, G., Mulitza, S., Ratmeyer, V. (Eds.), The South Atlantic in the Late Quaternary: reconstruction of material budgets and current systems. Springer-Verlag, Berlin, pp. 237–260.

Guillou, H., Singer, B., Laj, C., Kissel, C., Scaillet, S., Jicha, B., 2004. On the age of the Laschamp geomagnetic excursion. Earth Planet. Sci. Lett. 227, 331–343.

Guyodo, Y., Valet, J.-P., 1996. Relative variations in geomagnetic intensity from sedimentary records: the past 200,000 years. Earth Planet. Sci. Lett. 143, 23–36.

Guyodo, Y., Richter, C., Valet, J.-P., 1999. Paleointensity record from Pleistocene sediments (1.4–0 ma) off the California Margin. J. Geophys. Res. 104 (B10), 22953–22964.

Guyodo, Y., Acton, G., Brachfeld, S., Channell, J., 2001. A sedimentary paleomagnetic record of the Matuyama chron from the Western Antarctic margin (ODP Site 1101). Earth Planet. Sci. Lett. 191, 61–74.

Hofmann, D., Fabian, K., Schmieder, F., Donner, B., 2005. A stratigraphic network from the subtropical and subantarctic South Atlantic: multiparameter correlation of magnetic susceptibility, bulk density, X-ray fluorescence measurements and $\delta^{18}O$. Earth Planet. Sci. Lett. 240, 694–709.

Imbrie, J., Hays, J.D., Martinson, D.G., McIntyre, A., Mix, A.C., Morley, J.J., Pisias, N.G., Prell, W.L., Shackleton, N.J., 1984. The orbital theory of Pleistocene climate: support from a revised chronology of the marine $\delta^{18}O$ record. In: Berger, A., Imbrie, J., Hays, J., Kukla, G., Saltzman, B. (Eds.), Milankovitch and Climate: Understanding the Response to Orbital Forcing. Reidel Publishing, Dordrecht, pp. 269–305.

Jansen, J., van der Gaast, S., Koster, B., Vaars, A., 1998. CORTEX, a shipboard XRF-scanner for element analysis in split sediment cores. Mar. Geol. 151, 143–153.

Johnson, E.A., Murphy, T., Torreson, O.W., 1948. Pre-history of the earths magnetic field. Terr. Magn. Atmos. Electr. 53, 349–372.

Johnson, H.P., Kinoshita, H., Merrill, R.T., 1975. Rock magnetism and paleomagnetism of some north Pacific deep-sea sediments. Geol. Soc. Amer. Bull. 86, 412–420.

King, J.W., Banerjee, S.K., Marvin, J.A., 1983. A new rock magnetic approach to selecting sediments for geomagnetic paleointensity studies: application to paleointensity for the last 4000 years. J. Geophys. Res. 88, 5911–5921.

Kirschvink, J.L., 1980. The least-squares line and plane and the analysis of paleomagnetic data. Geophys. J. R. Astron. Soc. 62, 699–718.

Laj, C., Kissel, C., Mazaud, A., Channell, J., Beer, J., 2000. North Atlantic paleointensity stack since 75 ka (NAPIS-75) and the duration of the Laschamp event. Philos. Trans. R. Soc. 3358, 1009–1025.

Langereis, C., Dekkers, M., de Lange, G., Paterne, M., van Santvoort, P., 1997. Magnetostratigraphy and astronomical calibration of the last 1.1 Myr from an eastern Mediterranean piston core and dating of short events in the Brunhes. Geophys. J. Int. 129, 75–94.

Lay, D., 2000. Linear Algebra and its Applications. Addison-Wesley, New York.

Lehman, B., Laj, C., Kissel, C., Mazaud, A., Paterne, M., Labeyrie, L., 1996. Relative changes of the geomagnetic field intensity during the last 280 k year from piston cores in the Açores area. Phys. Earth Planet. Inter. 93, 269–284.

Levi, S., Banerjee, S.K., 1976. On the possibility of obtaining relative paleo-intensities from lake sediments. Earth Planet. Sci. Lett. 29, 219–226.

Lund, S., Stoner, J., Channell, J., Acton, G., 2006. A summary of Brunhes paleomagnetic field variability recorded in Ocean Drilling Program cores. Phys. Earth Planet. Inter. 156, 194–204.

Martinson, D., Pisias, N., Hays, J., Imbrie Jr., J., T.M., Shackleton, N., 1987. Age dating and the orbital theory of the Ice Ages: development of a high-resolution 0 to 300.000-year chronostratigraphy. Quat. Res. 27, 1–29.

Mazaud, A., Sicre, M., Ezat, U., Pichon, J., Duprat, J., Laj, C., Kissel, C., Beaufort, L., Michel, E., Turon, J., 2002. Geomagnetic-assisted stratigraphy and sea surface temperature changes in core MD94-103 (Southern Indian Ocean): possible implications for North–South climatic relationships around H4. Earth Planet. Sci. Lett. 201, 159–170.

Meynadier, L., Valet, J.-P., Weeks, R., Shackleton, N., Hagee, V., 1992. Relative geomagnetic intensity of the field during the last 140 ka. Earth Planet. Sci. Lett. 114, 39–57.

Nowaczyk, N., Baumann, M., 1992. Combined high-resolution magnetostratigraphy and nannofossil biostratigraphy for late Quaternary Arctic Ocean sediments. Deep Sea Res. 39, 567–601.

Reid, J., 1989. On the total geostrophic circulation of the South Atlantic Ocean: flow patterns, tracers, and transports. Prog. Oceanogr. 23, 149–244.

Roehl, U., Abrams, L., 2000. High resolution, downhole, and nondestructive core measurements from sites 999 and 1001 in the Caribbean sea: application to the late Paleocene thermal maximum. Proc. Ocean Drill. Program Sci. Results 165, 191–203.

Schmieder, F., 2004. Magnetic signals in Plio–Pleistocene sediments of the South Atlantic: chronostratigraphic usability and paleoceanographic implication. In: Wefer, G., Mulitza, S., Ratmeyer, V. (Eds.), The South Atlantic in the Late Quaternary: reconstruction of material budgets and current systems. Springer-Verlag, Berlin, pp. 269–305.

Stoner, J., Channell, J., Hillaire-Marcel, C., 1995. Late Pleistocene relative geomagnetic paleointensity from the deep Labrador Sea: regional and global correlations. Earth Planet. Sci. Lett. 134, 237–252.

Stoner, J., Channell, J., Hillaire-Marcel, C., 2000. Geomagnetic paleointensity and environmental record from Labrador sea core md95-2024: global marine sediment and ice core chronostratigraphy for the last 110 kyr. Earth Planet. Sci. Lett. 183, 161–177.

Stoner, J., Channell, J., Hodell, D., Charles, C., 2002a. A ~580 kyr paleomagnetic record from the sub-Antarctic South Atlantic (Ocean drilling Program Site 1089). J. Geophys. Res. 108, 1141–1151.

Stoner, J., Laj, C., Channell, J., Kissel, C., 2002b. South Atlantic and North Atlantic geomagnetic paleointensity stacks (0–80 ka): implications for inter-hemispheric correlation. Quat. Sci. Rev. 21, 1141–1151.

Stramma, L., England, M., 1999. On the water masses and mean circulation of the South Atlantic Ocean. J. Geophys. Res. 104 (C9), 20863–20883.

Stramma, L., Peterson, R., 1990. The South Atlantic current. J. Phys. Oceanogr. 20, 846–859.

Talley, L., 1996. Antarctic Intermediate Water in the South Atlantic. In: Wefer, G., Siedler, W.H. (Eds.), The South Atlantic: Present and Past Circulation. Springer Verlag, Berlin, pp. 219–238.

Tauxe, L., 1993. Sedimentary records of relative paleointensity: theory and practice. Rev. Geophys. 31, 319–354.

Tauxe, L., Shackleton, N., 1994. Relative paleointensity records from the Ontong–Java Plateau. Geophys. J. Int. 117, 769–782.

Thouveny, N., Creer, K., Blunk, I., 1990. Extension of the Lac du Bouchet palaeomagnetic record over the last 120000 years. Earth Planet. Sci. Lett. 97, 140–161.

Thouveny, N., Creer, K., Williamson, D., 1993. Geomagnetic moment variations in the last 70000 years, impact on production of cosmogenic isotopes. Glob. Planet. Change 7, 157–172.

Thouveny, N., Carcaillet, J., Moreno, E., Leduc, G., Nerini, D., 2004. Geomagnetic moment variation and paleomagnetic excursions since 4000 kyr BP: a stacked record from sedimentary sequences of the Portuguese margin. Earth Planet. Sci. Lett. 219, 377–396.

Valet, J.-P., 2003. Time variations in geomagnetic intensity. Rev. Geophys. 41.

von Dobeneck, T., 1996. A systematic analysis of natural magnetic mineral assemblages based on modelling hysteresis loops with coercivity-related hyperbolic basis functions. Geophys. J. Int. 124, 675–694.

von Dobeneck, T., Schmieder, F., 1999. Using rock magnetic proxy records for orbital tuning and extended time series analyses into the super and sub-Milankovitch Bands. In: Fischer, G., Wefer, G. (Eds.), Use of Proxies in Paleoceanography: Examples from the South Atlantic. Springer-Verlag, Berlin, pp. 601–633.

Wefer, G., cruise participants, 2001. Report and preliminary results of Meteor Cruise M46/4, Mar del Plata (Argentinia)–Salvador da Bahia (Brazil), February 10–March 13, 2000. With partial results of Meteor cruise M46/2. Berichte, FB Geowissenschaften. Universität Bremen, p. 173.

Worm, H.-U., 1998. On the superparamagnetic-stable single domain transition for magnetite, and frequency dependence of susceptibility. Geophys. J. Int. 133, 201–206.

Yamazaki, T., Ioka, N., Eguchi, N., 1995. Relative paleointensity of the geomagnetic field during the Brunhes Chron. Earth Planet. Sci. Lett. 136, 525–540.

Zijderveld, J., 1995. A.C. Demagnetization of Rocks: Analysis of Results. In: Collinson, D., Creer, K., R., S.K. (Eds.), Methods in Paleomagnetism. Elsevier, Amsterdam, pp. 254–286.

3.3 Correcting relative paleointensity records for variations in sediment composition: Results from a South Atlantic stratigraphic network

Daniela I. Hofmann, K. Fabian,

Correcting relative paleointensity records for variations in sediment composition: Results from a South Atlantic stratigraphic network

Daniela I. Hofmann [a] Karl Fabian [b,a]

[a] *University Bremen, Geoscience, Postbox 330440, 28334 Bremen, Germany*

[b] *Geological Survey of Norway, Leiv Eirikssons vei 39, N-7491 Trondheim, Norway*

Abstract

Marine sediments record direction and intensity of the Earth's magnetic field by the alignment of magnetic particles during deposition. For determining relative paleointensity (RPI) from sediment records it is commonly assumed that their natural remanent magnetization (NRM) is proportional to the Earth's magnetic field during deposition, and also proportional to the concentration of remanence carriers in the sediment layer. However, little is known how varying sediment composition and environmental conditions during deposition influence the NRM. Here we try to identify and quantify such sedimentary influences for eight sediment series from the subtropical and subantarctic South Atlantic. The cores were recovered in a constraint area crossing the subtropical front (STF). They have widely different sediment lithologies, which can be divided into three lithologic groups. Due to their mutual proximity, they have experienced approximately the same magnetic field history, and differences in their RPI signals must be caused by their varying sediment composition and recording properties. Based on high resolution rock magnetic and compositional data from two previous studies it is possible to quantitatively test and compare the influences of different sediment properties upon the NRM. It is found that magnetic grain size, as measured by the magnetic parameter ARM/IRM, is most influential among the parameters tested. Weak to moderate reductive diagenesis, as measured by the parameter Fe/κ, turns out to have minor impact. By comparing the sensitivity of different normalization procedures for RPI determination, it is found that induced remanent magnetization (IRM) is most robust. Based on an extended linear RPI theory, we can calculate a corrected RPI stack for the investigated cores. This correction improves the the correlation with independent global paleointensity stacks in comparison to our previous uncorrected RPI stack (Hofmann and Fabian, 2007). The ratio between corrected and uncorrected RPI stacks reveals a hidden global climate signal, which indicates that climatic variations in sediment composition are inevitably present in non-ideal sediment sequences.

Key words: Paleomagnetism, Relative paleointensity, South Atlantic, sedimentary influence, climate

1 Introduction

Sedimentary sequences are the most important continuous archives of past variations of the Earths magnetic field. Recent advances in palaeomagnetic methods have resulted in precise records of relative paleointensity (RPI) of the Earth's past magnetic field at numerous sites (Lund et al., 2006; Guyodo and Valet, 2006). The current technique to infer paleofield intensity from sedimentary sequences essentially is described by Johnson et al. (1948); Levi and Banerjee (1976); King et al. (1983), and new developments are reviewed in Tauxe (1993); Valet (2003). Quality of individual RPI records is intrinsically assessed in terms of mineralogic and rock magnetic uniformity, diagenetic alteration, and residual correlation of the normalized record with rock magnetic parameters Tauxe (1993). Still missing is a quantitative way to determine the influence of any disturbing factors upon the RPI determination. In Guyodo et al. (1999) this is concisely stated:

> An actual correction of the paleointensity signal would require quantification of the dual dependency of the NRM on the IRM and ARM/k, which is probably not constant throughout the time interval investigated.

This highlights the undesirable fact, that RPI determination is still very descriptive and qualitative, because the fundamental problem to understand the physics of remanence acquisition in sediments has not yet been solved. The need to address these fundamental questions is widely recognized and several recent studies have been focussing on sedimentary remanence acquisition and RPI correction (Katari et al., 2000; Katari and Bloxham, 2001; Franke et al., 2004; Fabian, 2006; Mazaud, 2006). Here, we develop a quantitative method to estimate the influence of sediment composition upon RPI records, which requires a local group of sediment cores having different sediment compositions. Comparing their individual NRM records of the same paleofield permits to estimate the compositional influences. These estimates can then be used to select an optimal normalization parameter for RPI determination, and to build a corrected RPI stack which takes into account variations in sediment composition.

2 Study area and previous results

The records used for this study originate from a stratigraphic network of sediment cores which lie on a north-south traverse across the subtropical Front (STF) in the subtropical and subantarctic South Atlantic. The cores were taken during Meteor Cruise M46/4 (Wefer and cruise participants, 2001) and studies of physical param-

eters, chrono-stratigraphy, rock-magnetic properties, and relative paleointensity are available (Hofmann et al., 2005; Hofmann and Fabian, 2007). Figure 1 briefly summarizes location, grouping, and essential magnetic records of the eight network cores, which resulted from these earlier work.

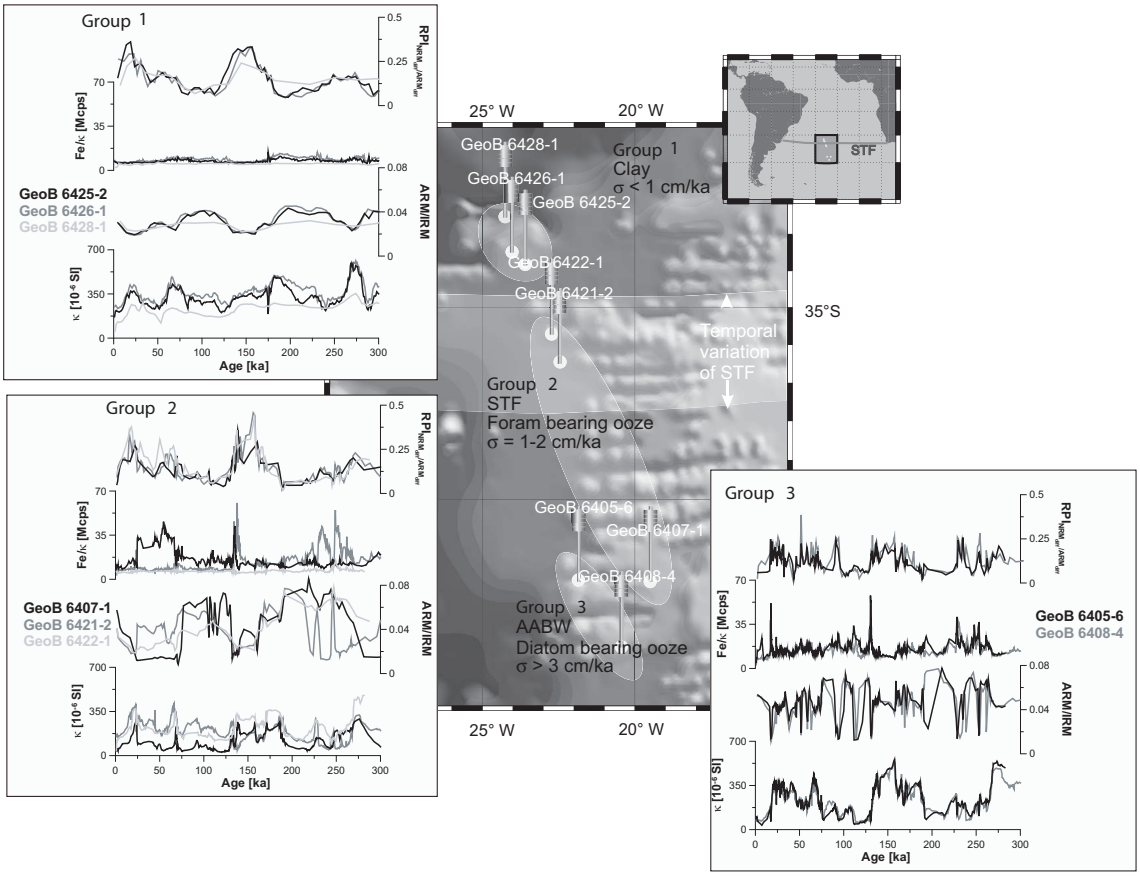

Fig. 1. Location and grouping of the eight network cores. For each core magnetic susceptibility κ, ARM/IRM, Fe/κ and the RPI record ($NRM_{\mathrm{diff}}/ARM_{\mathrm{diff}}$) are presented (details see also Hofmann and Fabian (2007)).

2.1 Study area

Colliding water masses at the STF lead to a sharp North-South contrast of surface temperature and salinity. In the study area, close to the Mid-Atlantic ridge, the STF generates a productivity gradient with low productivity in the North and high productivity in the South Wefer and cruise participants (2001); Franke et al. (2004); Hofmann et al. (2005). This in turn causes significant differences in sediment composition and sedimentation rate. With respect to these variations, the eight cores of the stratigraphic network have been sorted in three lithologic groups (Fig. 1). Group 1 comprises the three cores North of the STF, GeoB 6425-2, GeoB 6426-1 and GeoB 6428-1, which are rich in clay minerals. The central group 2, GeoB 6407-1,

GeoB 6421-2 and GeoB 6422-1, mostly consist of calcareous nannofossil ooze with some foraminifers, whereas The cores in the southernmost group 3, GeoB 6405-6 and GeoB 6408-4, contain a siliceous component of diatoms.

2.2 Previous measurements

Investigating the influence of varying sediment composition upon RPI records requires high resolution records of many different physical and especially magnetic parameters, which are precisely correlated to a common timescale. We here use the data set of Hofmann et al. (2005) and Hofmann and Fabian (2007). It provides magnetic susceptibility (κ), X-ray fluorescence and density measurements of the sediment cores, as well as rock- and paleomagnetic measurements, performed on oriented box samples taken on board in 5 cm intervals (Wefer and cruise participants, 2001). The age model of the stratigraphic network was obtained in Hofmann et al. (2005) by fitting magnetic susceptibility, κ, and δ^{18}O records to the target records SUSAS, SPECMAP (von Dobeneck and F.Schmieder, 1999; Imbrie et al., 1984) and the stack of Martinson et al. (1987).

Natural remanent magnetization (NRM) was AF demagnetized in 5 mT steps up to a peak field of 30 mT and then in 10 mT steps up to 100 mT. Anhysteretic remanent magnetization (ARM), acquired in a 40 μT-bias and an 100 mT-alternating field, was demagnetized using the same field steps as in case of NRM. Isothermal remanent magnetization (IRM) was measured in 18 steps up to 300 mT, and also afterwards stepwise AF demagnetized. Backfield measurements using -300 mT were performed after imposing a hard isothermal remanent magnetization HIRM (Stoner et al., 1996) in +1 T and +2.5 T, in order to calculate the S-ratio (Bloemendal et al., 1992). All remanence measurements were carried out using the fully automated 2G-Enterprises cryogenic rock magnetometer (model 755 R) at the University of Bremen (Hofmann and Fabian, 2007). Grain size and concentration of the magnetic mineral fraction is variable throughout the network cores, with higher amplitudes in the southern cores than in the northern cores. Magnetic mineral concentration is higher during cold, and lower during warm oxygen-isotope stages. The influence of reductive diagenesis, as measured by the parameter Fe/κ (Funk et al., 2004), increases from North to South. High Fe/κ values, representing high diagenetic transformation of primary Fe minerals, are related to lower ARM/IRM values. This consistently indicates the loss of fine grained magnetic minerals during reductive diagenesis. From hysteresis measurements and S-parameter values it can be concluded that the overall magnetic mineralogy of the network cores is dominated by low coercive (titano-)magnetite in the PSD grain-size range (Hofmann and Fabian, 2007).

2.3 Relative paleointensity records

Using the above data set, it is straightforward to calculate the classical relative paleointensity estimates by normalizing NRM with respect to a concentration dependent magnetic parameter (normalizer). Commonly used normalizers are ARM or IRM. NRM, as well as the normalizer, are AF-demagnetized to the same level (10-30 mT) before forming the ratio which serves as RPI estimate (Tauxe, 1993; Valet, 2003). In our previous study (Hofmann and Fabian, 2007), we used principal component analysis of the single demagnetization steps to extract a demagnetization interval where the demagnetized signal consists mostly of a single principal component. This approach was meant to reduce the influence of several independent environmental signals upon the records, and to improve homogeneity. It turned out, that magnetite contributes most to the demagnetizing interval between 30 and 80 mT where NRM, ARM, and IRM show a single clearly predominant principal component. Yet, throughout the network cores increased relative paleointensity values are found during glacial times (Figure 2).

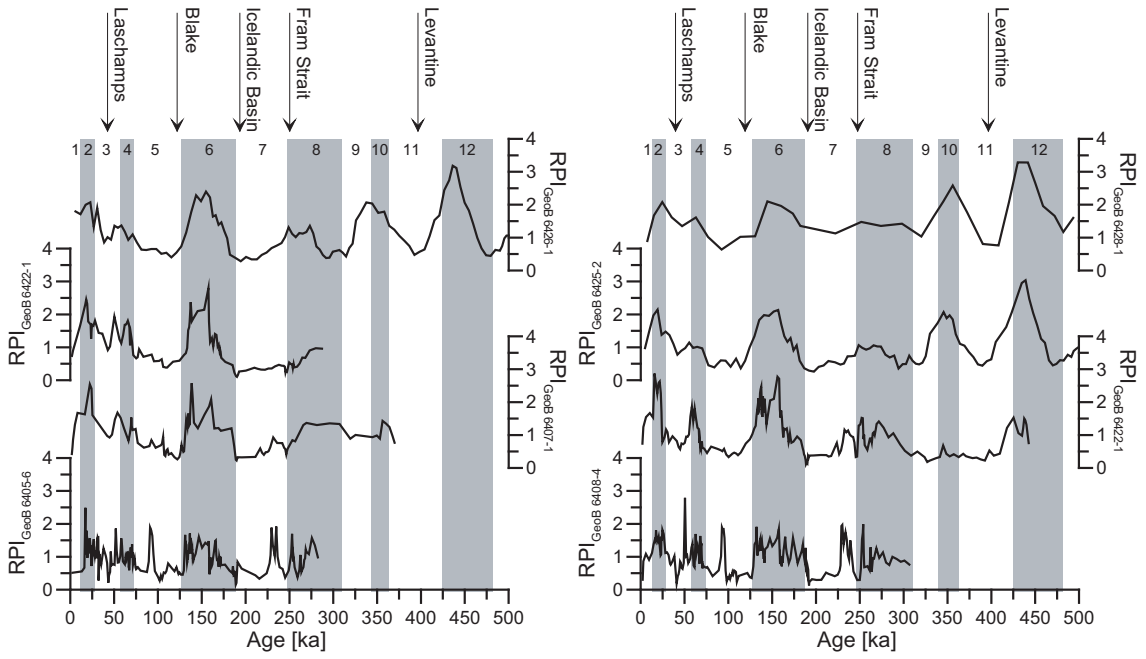

Fig. 2. Relative paleointensity records. NRM is normalized using ARM. Increased paleointensity values are found during glacial times.

In view of the well-known shortcomings of the RPI methodology, this is most likely an artifact of insufficiently cancelled environmental signals, than an indication of climate-field coupling. To study this important topic of environmental influence more completely, the next sections investigate the influences of compositional variations upon the NRM signal in the network cores.

3 How to correct RPI for variations in sediment composition

3.1 Theory of relative paleointensity determination

Relative paleointensity estimation requires that NRM is proportional to the external field and the concentration of remanence carriers. For N network cores ($i = 1, \ldots, N$) this reads

$$NRM_i(z) \;=\; q_i(z)\, H(z)\, c_i(z), \tag{1}$$

where the coefficients $q_i(z)$ describe the efficiency of NRM acquisition. In case of the common RPI determination on a single core it is usually requested that this efficiency $q_i(z)$ is independent of depth z. For any depths z_1, z_2 we must have $q_i(z_1) = q_i(z_2)$. This very strict homogeneity assumption is necessary if in the next step one wants to divide by $c_i(z)$ to obtain the a relative paleointensity

$$\frac{NRM_i(z)}{c_i(z)} \;=\; q_i\, H(z). \tag{2}$$

In this interpretation of the RPI technique, the twofold problem is then to 1) find a sufficiently homogeneous sediment core, and 2) to determine a normalizer which most reliably reproduces $c_i(z)$.

Significant lithologic downcore variation, as is present in our network cores, renders the above approach invalid. In an interesting numerical experiment, Valet (2003) used a variable efficiency $q(z) = (1 + \epsilon(z))$ for a single sediment record, and showed how wavelet analysis can be used to detect climatic influences due to such variability. Valet (2003) recommends that the detected 'disturbed' regions should then be excluded from further analysis. For our network cores, we extend this approach by assuming that the recording efficiency primarily depends on lithology, and that local geographic variations, i.e. variations in lithology between the network cores, have the same effect upon recording efficiency as downcore variations, which reflect variations in time. We can then make use of the fact that we have eight parallel recordings of the same field to identify and correct for the main lithologic contributions to $\epsilon(z)$.

To achieve this, the efficiency of remanence acquisition is explicitely written as a function of lithologic parameters representing variations in sediment composition

$$q_i(z) \;=\; q_i\left(\lambda_i^{(1)}(z), \lambda_i^{(2)}(z), \lambda_i^{(3)}(z), \ldots\right). \tag{3}$$

Here $\lambda_i^{(k)}(z)$ is a normalized downcore measurement of parameter k on core i. E.g. choosing $k = 9$, $i = 4$ may correspond to an XRF scan of the element Ti on core GeoB 6407-1. Then

$$\lambda_4^{(7)}(z) \;=\; \frac{\mathrm{Ti}_4(z) - \overline{\mathrm{Ti}}}{\sigma(\mathrm{Ti})}, \tag{4}$$

where $\overline{\mathrm{Ti}}$ and $\sigma(\mathrm{Ti})$ are average and standard deviation of all Ti-measurements over all cores and all depths, while $\mathrm{Ti}_4(z)$ is the measured record of GeoB 6407-1.

It is now further assumed that the variation of the external field $H(z)$ is the most important contribution to the variation of the concentration-corrected NRM. Thus the compositional variations $\lambda_i^{(k)}(z)$ have only a relatively weak influence on $q_i(z)$, such that (3) can be linearized to yield

$$NRM_i(z) = q\,H(z)\,c_i(z)\,\left(1+\alpha_1\,\lambda_i^{(1)}(z)+\alpha_2\,\lambda_i^{(2)}(z)+\alpha_3\,\lambda_i^{(3)}(z),\ldots\right), \qquad (5)$$

where in case of weak lithologic influence $\alpha_k \ll 1$. To further simplify this expression only the variation of the predominant parameter $\lambda_i(z)$ –i.e. the parameter $\lambda_i^{(k)}(z)$ which turns out to have largest α_k – is retained in this expansion, while the other parameters are neglected. This has two reasons, first it substantially more simple and robust to determine α for a single parameter. The second reason is that the downcore variations of different parameters are very likely to be highly correlated, because all these variations result from a common environmental signal. This argument is elaborated in Fabian (2006). Therefore, concentrating on the single most important lithologic variation will incorporate most of the variation due to the primary environmental signal.

3.2 Determining α for given sediment parameter variations $\lambda_i(z)$

It now remains to determine 1) which $\lambda_i(z)$ is the most important lithologic variation, and 2) what is the corresponding appropriate value of α. We first solve the second problem for an arbitrarily chosen parameter λ with variations $\lambda_i(z)$. If α is known, it is easy to find the corresponding apparent relative paleofield record $H_i^{(\alpha)}(z)$ for each sediment core i according to

$$q\,H_i^{(\alpha)}(z) = \frac{NRM_i(z)}{c_i(z)\;(1+\alpha\,\lambda_i(z))}. \qquad (6)$$

For the optimal choice α^* it is expected that the resulting different paleofield reconstructions $H_i^{(\alpha^*)}(z)$ are as similar as possible. Therefore, it is possible to determine α^* by minimizing the sum $\Delta^2(\alpha)$ of the pairwise total squared distances between the single paleofield estimates $H_i^{(\alpha)}(z)$,

$$\Delta^2(\alpha) \;=\; \sum_{1\le i<j\le N}\int_{t_0}^{t_1}\left(H_i^{(\alpha)}(z(t))-H_j^{(\alpha)}(z(t))\right)^2\,dt \;\stackrel{!}{=}\; \min. \qquad (7)$$

To evaluate this sum one requires well correlated sediment sequences on a common time-interval $[t_0,t_1]$. In case of the South Atlantic stratigraphic network, this common time interval covers the last 270 ka. All further investigations are therefore confined to this age interval. Consequently, we have to exclude the northernmost

core, GeoB 6428-1, because due to its very low sedimentation rate of 0.4 cm/ka, the investigated time interval corresponds to only about 20 data points from its top meter, which results in a much too low resolution. The concentrations $c_i(z)$ in (6) are estimated by $\mathrm{ARM}_i(z)$, following the argument in Hofmann and Fabian (2007) that the demagnetization behavior of the NRM more closely resembles that of ARM than that of IRM. For both, NRM and ARM, we use the values $\mathrm{NRM}_{\mathrm{diff}}$ and $\mathrm{ARM}_{\mathrm{diff}}$ from the 30-80 mT demagnetization interval.

Figure 3 illustrates the envisaged procedure to determine α^* by using the variations $\lambda_i(z) \propto ARM/IRM_i(z)$. The initial state in Fig. 3a consists of the uncorrected individual RPI estimates corresponding to $\alpha = 0$. Now α is varied systematically in the admissible range of about $[-0.5, 0.5]$, and for each value of α the number $\Delta^2(\alpha)$ is calculated. The graph of Δ^2 shows a well defined parabolic minimum from which α^* can be determined. By comparing the corrected RPI records for the optimal $\alpha^* \approx -0.257$ in Fig. 3b with the initial state, it is clearly visible that the coherence between the paleofield reconstructions $H_i^{(\alpha^*)}(z)$ has significantly improved. The correction damps high peaks in several records, and amplifies low regions in others, but tends to reduce the overall amplitude. Choosing $\alpha = -0.05$ for the correction, as in Fig. 3c, does not significantly improve the coherence. A too large correction, using $\alpha = -0.35$, apparently further improves the coherence in some central time-intervals, but completely destroys the coherence in other parts (Fig. 3d).

A measure of the effected decrease in scatter (i.e. quadratic deviation) is $s(\lambda) = \Delta^2(\alpha^*)/\Delta^2(0)$, which only depends on the lithologic parameter λ used for the correction. Smaller values of $s(\lambda)$ reflect a better coherence between the $H_i^{(\alpha^*)}(z)$ after the correction. Because the records $\lambda_i(z)$ are based on a common normalization procedure, the value $\alpha^*(\lambda)$ itself is a quantitative measure of the influence of the corresponding lithologic parameter upon field recording in the network area. A larger $|\alpha^*(\lambda)|$ implies a larger influence of λ, whereas the sign of $\alpha^*(\lambda)$ determines whether an increase in λ increases ($\alpha^* > 0$) or decreases ($\alpha^* < 0$) the efficiency of NRM acquisition in the sediment.

4 Building a corrected RPI network stack

4.1 Scanning the available sediment parameters

By the method of the previous section it is straightforward to calculate the optimal efficiencies $\alpha^*(\lambda)$ for all available sediment parameters λ, listed in table 1. Comparing their effected decrease in scatter $s(\lambda)$, and their influence upon field recording, $|\alpha^*(\lambda)|$ makes it possible to decide which λ is most influential for RPI determination, which solves then the first problem stated at the beginning of the previous section.

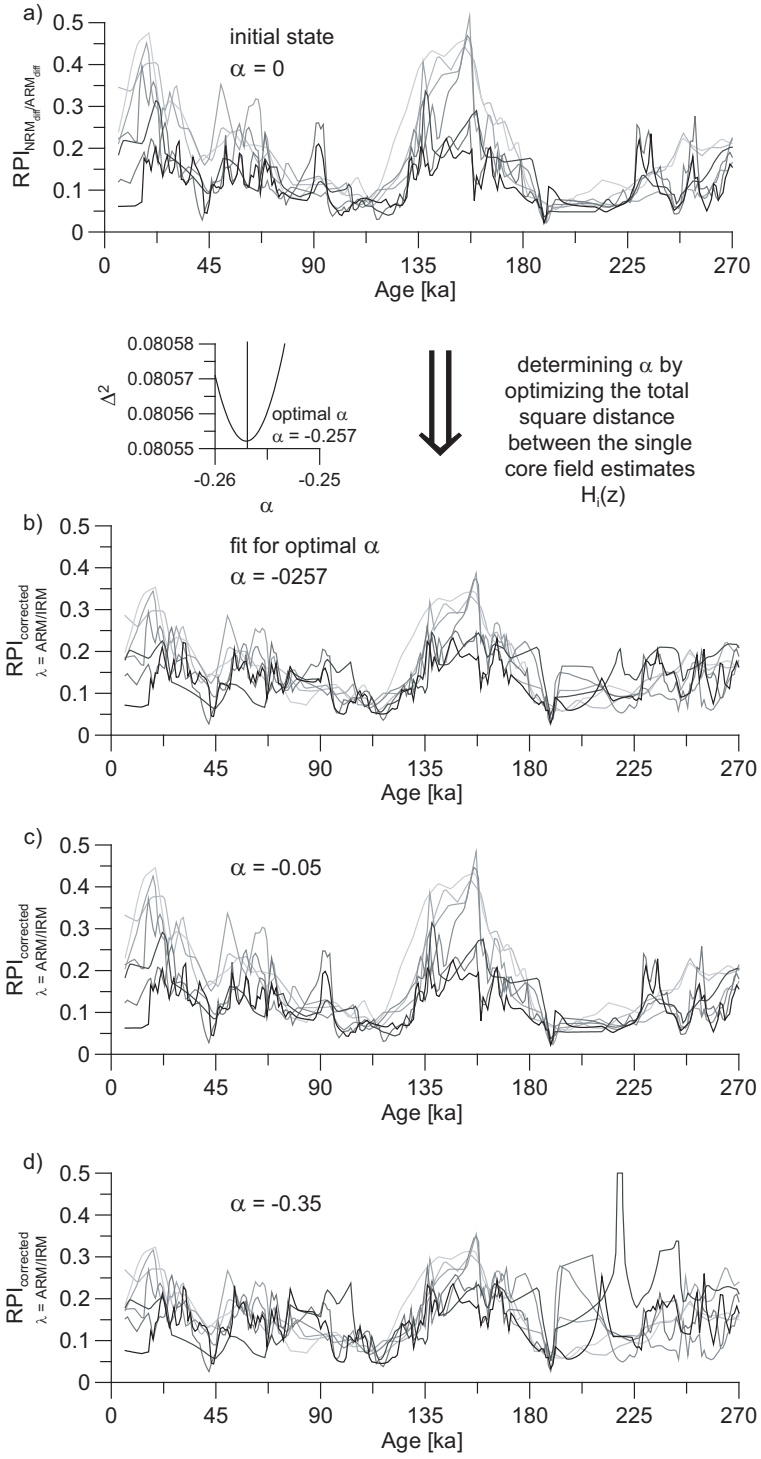

Fig. 3. Determining α by minimizing the total squared distance between the single core field estimates $H_{\mathrm{i}}(z)$. (a) RPI records ($NRM_{\mathrm{diff}}/ARM_{\mathrm{diff}}$) for the seven network cores are presented before correction (initial state $\alpha = 0$), (b) for the optimal fit after correction (fit for optimal α = -0-257), (c) and (d) for two non-optimal fits (α = -0.05 and α = -0.35).

Table 1
Available sediment parameters, indicating variations in sediment composition. After normalizing according to (4), they yield standardized variation records λ used for RPI correction. The following abbreviations are used: CORTEX: XRF core scanner developed at the Netherlands Institute for Sea Research at Texel for elemental analyses of split sediment cores (Jansen et al., 1998). 2G: 2G Enterprises cryogenic rock magnetometer 755 R, Bremen. MS2-E: Bartington MS2 magnetic susceptibility meter linked to E-Probe sensor having a 3.8×10.5 mm area of response for surface measurements on split cores. WENNER: Handheld Wenner electrical resistivity probe with ≈ 5 mm electrode spacing for surface measurements on split cores.

Parameter	Indicating	Instrument(s)	Sampling distance [cm]	Resolution [cm]
Fe	iron content	CORTEX	1	5 ??
Fe/κ	diagenetic iron reduction	CORTEX, MS2-E	1	5??
Ca	carbonate content	CORTEX	1	5 ??
ARM/IRM	magnetic grain size	2G	5	5
$\mathrm{MDF_{NRM}}$	coercivity of NRM	2G	5	5
$\mathrm{MDF_{ARM}}$	coercivity of ARM	2G	5	5
$\mathrm{MDF_{IRM}}$	coercivity of IRM	2G	5	5
ARM/κ	magnetic grain size	2G , MS2-E	5	5
Ti	Ti content	CORTEX	1	5 ??
Mn	Mn content	CORTEX	1	5 ??
Density ρ	porosity (compaction)	WENNER	2.0	3.0 ??

This approach is used in Tab. 2 to find one or more parameters, which are most influential for the RPI record of our South Atlantic stratigraphic network.

The results in Tab. 2 show that the lowest scatter of RPI records is obtained after correcting for ARM/IRM, yielding $s(ARM/IRM) = 49\%$ of the uncorrected scatter. Together with the analysis in Fig. 3 this leads to two conclusions. First, in our stratigraphic network the efficiency of NRM acquisition is dominated by magnetic grain size as measured by ARM/IRM. Second, due to $\alpha^* < 0$, the efficiency of NRM acquisition is higher for coarser magnetic particles, having smaller ARM/IRM, than for finer magnetic particles. While few researchers in RPI will be astonished about the first result, it is likely that most would have guessed the opposite of the second.

Table 2
Influence upon field recording $\alpha^*(\lambda)$, and decrease in scatter $s(\lambda)$ for different sediment parameters p, where $\lambda_i(z) = (p_i(z) - \overline{p})/\sigma(p)$. Relative paleointensity is determined using (6), where $c_i(z)$ is approximated by $\mathrm{ARM}_{i,\mathrm{diff}}(z)$. $\mathrm{NRM}_{i,\mathrm{diff}}(z)$ and $\mathrm{ARM}_{i,\mathrm{diff}}(z)$ refer to the 30 to 80 mT demagnetization interval.

Parameter p	unit	$\overline{p}$	$\sigma(p)$	$\alpha^*(\lambda)$	$s(\lambda)$
ARM/IRM	-	0.042	0.016	-0.257	0.49
ARM/κ	kA/m	0.29	0.15	-0.111	0.95
$\mathrm{MDF_{ARM}}$	mT	28.29	3.11	-0.181	0.72
$\mathrm{MDF_{NRM}}$	mT	27.96	8.29	0.161	0.66
$\mathrm{MDF_{IRM}}$	mT	23.61	3.88	0.17	0.66
Fe	cps	2788.21	1286.07	-0.157	0.8
Ca	cps	4819.51	2619.66	0.219	0.68
Ti	cps	82.15	42.39	-0.196	0.71
Mn	cps	127.13	126.49	0.261	0.797
Fe/κ	10^6 cps	13.09	6.79	-0.071	0.86
ρ	$\mathrm{kg/m^3}$	1420.65	43.99	0.169	0.86

4.2 Choosing the optimal normalizer

Further study of Tab. 2 shows that several other parameters, like $\mathrm{MDF_{IRM}}$, $\mathrm{MDF_{NRM}}$, or Ca also lead to a noticeable reduction in scatter. It therefore appears reasonable to reconsider the simplification of (5) by taking into account two or more compositional parameters at the same time. We have tested this approach on the above data set, but did not find a significantly larger reduction in scatter by using two correction parameters as compared to one. Only at first sight, this finding seems to contradict Tab. 2. On a second look one recognizes that the corrections performed by the individual parameters in Tab. 2 are highly correlated. E.g. both, ARM/IRM and $\mathrm{MDF_{IRM}}$ correct for variations in the magnetic particle assembly, and both variations are related to a common environmental signal controlling sediment composition. It is thus not astonishing, that after correcting for one of these parameters, an additional correction for the second is much less effective, because most of its variation has already been taken care of by correcting for the first parameter.

Astonishingly, a different approach to correct for a second parameter works better. It relies on the observation that correcting for ARM/IRM with a negative α approximately means correcting for IRM/ARM with a positive α, which essentially leads

Table 3
Influence upon field recording $\alpha^*(\lambda)$, and decrease in scatter $s(\lambda)$ for different sediment parameters p, where $\lambda_i(z) = (p_i(z) - \overline{p})/\sigma(p)$. Relative paleointensity is determined using (6), where $c_i(z)$ is approximated by $\mathrm{IRM}_{i,\mathrm{diff}}(z)$. $\mathrm{NRM}_{i,\mathrm{diff}}(z)$ and $\mathrm{IRM}_{i,\mathrm{diff}}(z)$ refer to the 30 to 80 mT demagnetization interval.

Parameter p	unit	$\overline{p}$	$\sigma(p)$	$\alpha^*(\lambda)$	$s(\lambda)$
ARM/IRM	-	0.042	0.016	-0.021	0.99
ARM/κ	kA/m	0.29	0.15	0.118	0.92
$\mathrm{MDF_{ARM}}$	mT	28.29	3.11	0.033	0.98
$\mathrm{MDF_{NRM}}$	mT	27.96	8.29	0.031	0.98
$\mathrm{MDF_{IRM}}$	mT	23.61	3.88	-0.014	0.99
Fe	cps	2788.21	1286.07	-0.073	0.93
Ca	cps	4819.51	2619.66	0.057	0.96
Ti	cps	82.15	42.39	-0.072	0.93
Mn	cps	127.13	126.49	-0.024	0.99
Fe/κ	10^6 cps	13.09	6.79	-0.09	0.87
ρ	kg/m^3	1420.65	43.99	0.078	0.93

to an RPI estimate of the form

$$H(z) \sim \frac{NRM(z)}{r\,\mathrm{ARM}(z) + q\,\mathrm{IRM}(z)}. \tag{8}$$

The observed large influence of ARM/IRM on the ARM-normalized RPI could indicate that $q \ll r$, and that it is better to normalize RPI by IRM. Repeating the correction analysis using the network-RPI records normalized by $\mathrm{IRM}_{i,\mathrm{diff}}(z)$, leads to Tab. 3, which is markedly different from Tab. 2 in that correcting for ARM/IRM has nearly no effect. Instead, now Fe/κ and ARM/κ are the most efficient correction parameters. On the background of constant IRM, both are related to reductive diagenesis, either through transformation of ferrimagnetic to paramagnetic minerals (increasing Fe/κ), or by average coarsening of the ferrimagnetic grain sizes (decreasing ARM/κ).

Fig. 4 gives a graphical overview of the different correction approaches using either ARM or IRM as a normalizer.

It is clearly visible that initial normalization by ARM leads to higher amplitudes of the reconstructed RPI signal, which are damped only by correcting for ARM/IRM. On the other hand, initial normalization by IRM already starts out with consider-

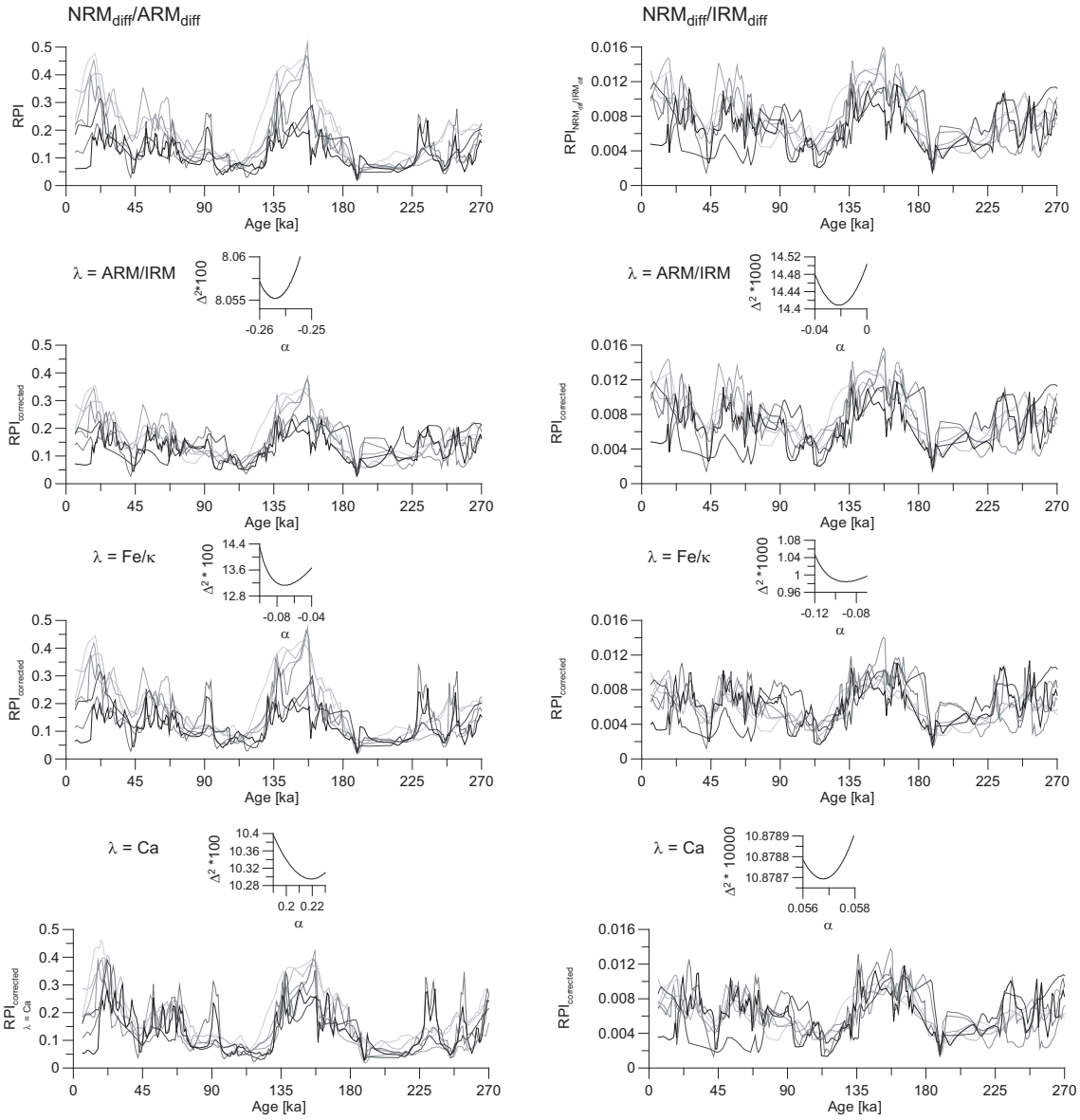

Fig. 4. Different compositional corrections to the network RPI records. The RPI records in the left column are calculated from $NRM_{\mathrm{diff}}/ARM_{\mathrm{diff}}$, those in the right column from $NRM_{\mathrm{diff}}/IRM_{\mathrm{diff}}$. The index "diff" refers to the demagnetization interval 30 to 80 mT. The four rows show all individual RPI records with either (1) no correction applied, or correction for variations $\lambda_i(z)$ of the parameters (2) ARM/IRM, (3) Fe/κ, and (4) Ca. The insets show the scatter parabola used to determine the value of α^* on which the correction is based.

ably smaller RPI amplitudes, and less scatter between the individual records. The improvement due to further correction using Fe/κ consists mainly in detrending the first 100 ka of the record. Correction by Ca has a qualitatively similar, but weaker effect. It thus appears that normalization by IRM accounts best for variation of the relevant magnetic grains which carry the NRM, while correcting for Fe/κ reduces the influence of different relative age positions of the diagenetic front near the core

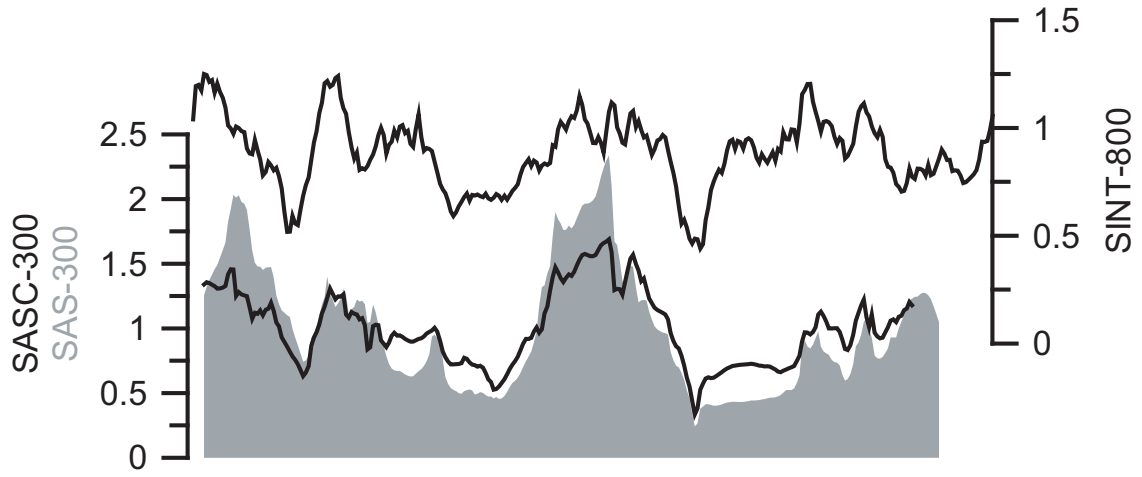

Fig. 5. RPI stack based on IRM normalization and corrected for Fe/κ.

top. This latter correction is missing in previous intensity stacks which may imply that the often observed increase of intensity from 20-30 ka towards the present is an artifact related to averaged positions of diagenetic fronts.

4.3 A corrected RPI stack for the central South Atlantic

The above analysis of compositional influences upon RPI suggests the construction of a corrected RPI-network stack, based on the informed choice of IRM as normalizer, and with Fe/κ as correction parameter. This stack is obtained by averaging the individual IRM-based RPI estimates after correcting them for Fe/κ by using the found influence coefficient α^* from tab. 3. In Fig. 5 the thus obtained stack of corrected RPI is compared to the uncorrected stack of Hofmann and Fabian (2007), and to the global SINT-800 record (Guyodo and Valet, 1999). Although in its general features the corrected RPI stack is similar to the uncorrected stack, it displays a considerably smaller amplitude variation and significant differences in several details.

The correction proves that a large fraction of the original amplitude variation originated from lithologic factors, and not from the paleofield. This clearly shows that environmental variations are strongly reflected in the uncorrected RPI stack, and could not be averaged out. While environmental influence upon RPI records via ARM/IRM has been suspected for a long time, this study for the first time gives a quantitative verification of this effect. Near 20 ka the relative field amplitude is corrected from 2.1 to 1.4, which means that it was originally overestimated by a factor of 1.5. However, there are also time intervals where the corrected RPI estimate is higher than the uncorrected. This is mainly the case before 160 ka. Interestingly, the correction nearly everywhere moves the RPI stack towards the – completely independent– SINT-800 record of (Guyodo and Valet, 1999), even though details of the pattern are significantly different.

The aim of this study was to determine the RPI from sediment cores with varying sediment compositions. Therefore all cores were used regardless if they fulfill all standard criteria for RPI investigation (Tauxe (1993)). Now it is possible to look at the single corrected RPI records (Fig. 6). The single corrected RPI records using IRM as normalizer and Fe/κ as correction parameter are quite similar. The cores from the South show much more small scale variations than the northern cores, due to the decreasing sedimentation rate towards North. The Laschamp and Icelandic Basin excursions occur in all RPI records, while the Blake and Fram Strait excursions are only visible in the southern cores. Core GeoB 6407-1 shows a much different RPI signal. This core is highly influenced by reductive diagenesis (Hofmann et al. (2005)). This core is excluded from further paleointensity investigations.

Based on the different sedimentation rates it is possible to create a RPI stack using only the six best records. Three stacks were performed using first the two northern cores GeoB 6425-2 and GeoB 6426-1, second the two cores within the STF transition GeoB 6421-2 and GeoB 6422-1 and third the two southernmost cores GeoB 6405-6 and GeoB 6408-4 (Fig. 7).

It is clearly visible that the high frequency variations decrease with decreasing sedimentation rate. Correlating the three stacks with the corrected stack using all cores it can be seen, that the high frequency variations are smoothed out. The Fram Strait excursion which is clearly visible in the stack from the southern cores is not visible in the two other stacks and also not visible in the complete stack (SASC-300).

5 Discussion

5.1 Environmental influence upon RPI records

The correction removed a relatively large environmental influence which was contained in the uncorrected stack. This leads to the question how this environmental signal looks like, and whether it could have been detected by other means. The removed environmental signal is best seen in the ratio of corrected to uncorrected stack in Fig. 8.

Comparison with the SPECMAP record of Martinson et al. (1987) and the insolation signal of Juli 21 at 65°N indicates that correction removed a *global* climate signal from the stack which was not directly visible in any of the individual RPI records.

The observation that the detected climate influence is due to a global signal has important ramifications for the interpretation of sedimentary relative paleointensity records. First, it poses a problem for direct global stacks which intend to remove environmental influence by averaging a wide variety of globally distributed RPI

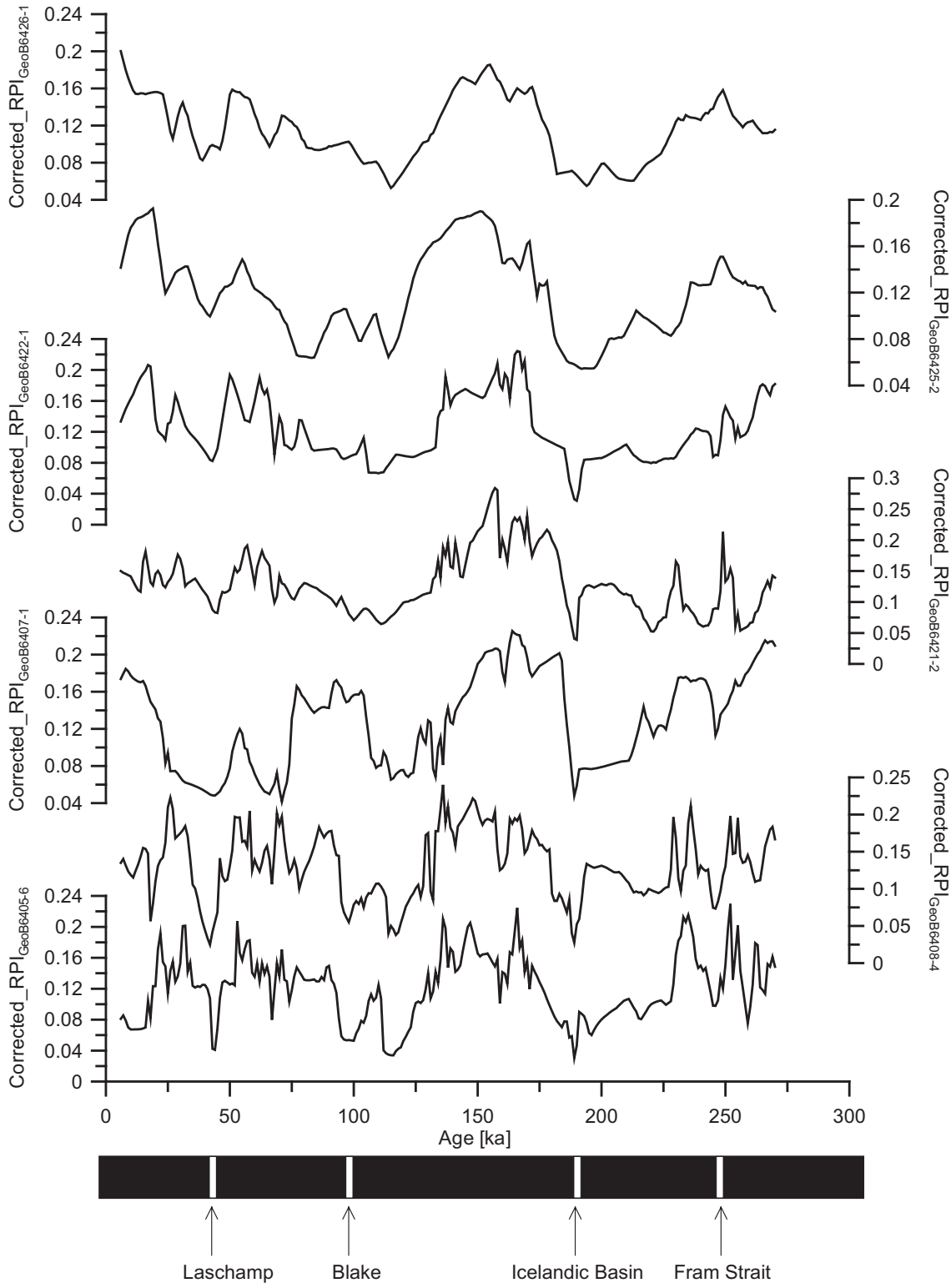

Fig. 6. Single corrected RPI records of all network cores. IRM is used as normalizer and the correction parameter is Fe/κ
and α = -0.09. The cores GeoB 6425-2 and GeoB 6426-1 indicate a much lower frequency variation than the two southern cores GeoB 6405-6 and GeoB 6408-4. The cores from the vicinity of the subtropical front show median frequency variations. In addition core Geo 6407-1 presents a much different RPI signal.

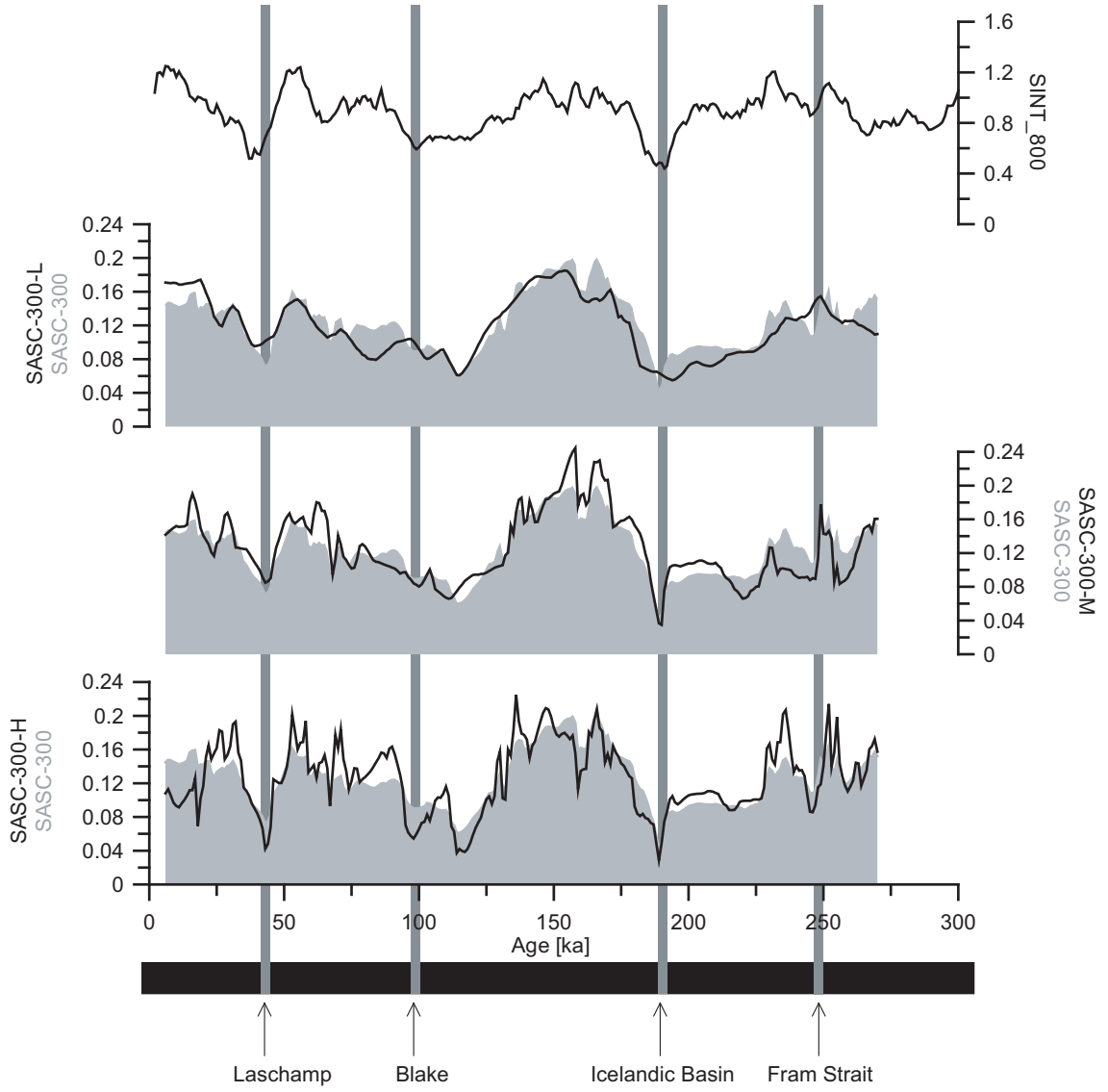

Fig. 7. Based on the six best records, three different stacks are constructed, each of which represents two cores with similar sedimentation rates. The first, SASC-300-L, comprises low sedimentation rates < 1 cm/ka in GeoB 6425-2 and GeoB 6426-1. The second, SASC-300-M, averages GeoB 6421-2 and GeoB 6422-1 with sedimentation rates $1 - 2$ cm/ka, and the third, SASC-300-H, stacks high sedimentation rates of > 3 cm/ka in GeoB 6405-6 and GeoB 6408-4. The gray background presents the corrected stack SASC-300 using all cores.

records. This approach, however, cannot succeed when the environmental signal itself is global. In the light of our finding, the presence of a hidden global environmental signal, appears highly likely in most individual RPI records. Second, a hidden global climatic influence upon the recording medium makes it much more difficult to study possible real correlations between variations of the geomagnetic field and climate.

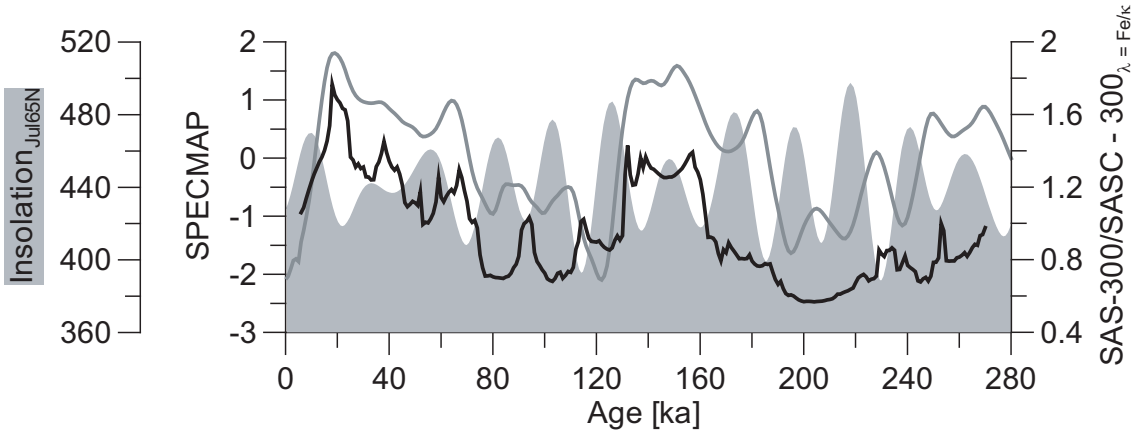

Fig. 8. The black line shows the ratio between the uncorrected RPI stack SAS-300 based on IRM normalization and the corrected stack SASC-300$_{\lambda=\mathrm{Fe}/\kappa}$. The gray line is the normalized SPECMAP curve after Imbrie et al. (1984), and the gray shaded background is the july insolation at 65° N (W/m^2). The two latter curves indicate global climate, related to either ice cover, or ice growth and global atmospheric circulation.

5.2 Influence of magnetic grain size

The most significant influence found, is magnetic grain size as measured by ARM/IRM, where small values of ARM/IRM lead to increased NRM. Especially the fact that RPI obtained from normalization of $\mathrm{NRM}_{\mathrm{diff}}(z)$ to $\mathrm{IRM}_{\mathrm{diff}}(z)$ depends significantly less on magnetic grain size than normalization to $\mathrm{ARM}_{\mathrm{diff}}(z)$ requires a physical explanation.

Apparently the very plausible criterion of Levi and Banerjee (1976), to choose the normalization parameter whose demagnetization curve most closely approximates that of the NRM, is flawed.

A convincing explanation for two facts is needed, (1) that when the grain size of the remanence carrier decreases, the efficiency of NRM acquisition also decreases, and (2) that ARM-demagnetization curve which rather reflects smaller particles, still resembles the NRM demagnetization curve better.

This essentially means that, even if an artificial process, like ARM acquisition, magnetizes the sediment with a coercivity spectrum which closely resembles the NRM, this does not guarantee that the two remanences are carried by the same particles. A possible physical reason for this discrepancy is that the detrital remanence is carried by particles which initially acquired a TRM and later rotated their moment in the field. Especially in pseudo-single domain grains, TRM is much more efficient than ARM (Dunlop and Argyle, 1997; Witt et al., 2005), but it also demagnetizes easier.

Another possibility is that fine particles are transported to the sediment in flocs which contribute little to the total NRM while larger grains orient better towards

the paleofield. These flocs then contribute significantly to the ARM but little to the NRM.

In addition, ARM acquisition is influenced by magnetotstatic interactions (**?**). Normalization by ARM can therefore overcompensate for the concentration of magnetic grains and cause significant coherence between normalized intensity and normalizer.

The SASC-300 stack is based on sediment series which do not ideally fulfill the classical quality criteria for relative paleointensity investigations. The here developed correction for sediment composition still enables to use sedimentary records of less quality related to the supposed reliability criteria by Tauxe (1993). Correcting for the most influential sediment parameter still leads to reliable paleointensity records and even to a sedimentation rate dependent sequence of relative paleointensity stacks based on a common correction scheme, which makes use of information from all involved sediment cores. Naturally, a stack using cores with a high sedimentation rate shows higher frequency variations than a stack using low sedimentation rate. An improved stacking method should account for this effect, maybe by stacking in different frequency regimes. In any case compositional correction in comparison to direct stacking leads to a noticeable improvement in RPI amplitude and partly even to a change in RPI signal shape.

6 Conclusion

Seven lithologic different sediment records from a constraint area, which exhibit a precise age control have been used for a new approach for determining the influence of varying sediment composition upon relative paleointensity. Using this approach we reach the following conclusions:

(1) ARM/IRM has slightly lower values during glacial times, indicating coarser grain sizes. The correction for the RPI stack using NRM/ARM indicates a decrease for the glacial times using ARM/IRM as correction parameter.
(2) Diagenesis causes dissolution of magnetite. The observed small influence upon ARM-based RPI may be explained because diagenetic alteration is a non-linear effect which is not detected using a linear approach. In case of IRM-based RPI Fe/kappa turns out to be the most influential sediment parameter.
(3) Second order effects have not been included into the presented linear approach. A test by synchronously using two or more parameters λ did not significantly improve the results.
(4) The uncorrected RPI records are influenced by an environmental signal related to the recording process. Comparing the ratio of the uncorrected stack to the corrected stacked shows a clear correlation to SPECMAP and the global summer insolation signal from 65deg North.
(5) Since the ARM demagnetization curves more closely resembles that of NRM,

first ARM was selected as normalizer for paleointensity investigation. Using the correction method it turned out, that the more stable normalizer is IRM. The presented correction method therefore represents a quantitative method to select the most appropriate normalizer.

(6) After finding the most influential sediment parameter it is possible to build a corrected relative paleointensity stack for the last 300 ka (SASC-300). SASC-300 is an improved stack for the central South Atlantic and compares to other local or global paleointensity records. The different sediment rates allow to create stacks with different sedimentation rates, but based on the correction parameters from all records. As expected, high - frequency variations are smoothed out in the sub - stack of the cores with low sedimentation rate.

Acknowledgements

We thank U. Bleil, T. von Dobeneck and Thomas Frederichs for valuable discussions. Financial support was provided by the Deutsche Forschungsgemeinschaft (DFG), SPP 1097: "Erdmagnetische Variationen", in the framework of proposal Fa 408/1-2.

References

Bloemendal, J., King, J., Hall, F., Doh, S.-J., 1992. Rock magnetism of late neogene and pleistocene deep-sea sediments: Relationship to sediment source, diagenetic processes and sediment lithology. J. Geophys. Res. 97 (B4), 4361–4375.

Dunlop, D. J., Argyle, K. S., 1997. Thermoremanence, anhysteretic remanence and susceptibility of submicron magnetites: Nonlinear field dependence and variation with grain size. J. Geophys. Res. 102 (B9), 20199–20210.

Fabian, K., 2006. A linear theory of physical properties in inhomogeneous sediments and its application to relative paleointensity determination. eEarth Discuss. 1, 51–62.

Franke, C., Hofmann, D., von Dobeneck, T., 2004. Does lithology influence the paleointensity record? A statistical analysis on South Atlantic pelagic sediments. Phys. Earth Planet. Inter. 147, 285–296.

Funk, J., von Dobeneck, T., Reitz, A., 2004. Integrated rock magnetic and geochemical quantification of redoxomorphic iron mineral diagenesis in late quaternary sediments from the equatorial Atlantic. In: Wefer, G., Mulitza, S., Ratmeyer, V. (Eds.), *The South Atlantic in the Late Quaternary: reconstruction of material budgets and current systems*. Springer-Verlag, Berlin, pp. 237–260.

Guyodo, Y., Gaillot, P., Channell, J., 1999. Wavelet analysis of relative geomagnetic paleointensity at ODP Site 983. Earth Planet. Sci. Lett. 184, 109–123.

Guyodo, Y., Valet, J.-P., 1999. Global changes in the intensity of the Earth's magnetic field during the past 800 kyr. Nature 399, 249–252.

Guyodo, Y., Valet, J.-P., 2006. A comparison of relative paleointensity records of the Matuyama Chron for the period 0.75-1.25 ma. Phys. Earth Planet. Inter. 156, 205–212.

Hofmann, D., Fabian, K., 2007. Rock-magnetic properties and relative paleointensity stack for the last 300 ka based on a stratigraphic network from the subtropical and subantarctic south atlantic. EARTHL 260, 297–312.

Hofmann, D., Fabian, K., Schmieder, F., Donner, B., 2005. A stratigraphic network from the subtropical and subantarctic South Atlantic: Multiparameter correlation of magnetic susceptibility,bulk density, X-ray fluorescence measurements and δ^{18}O. Earth and Planetary Science Letters 240, 694–709.

Imbrie, J., Hays, J. D., Martinson, D. G., McIntyre, A., Mix, A. C., Morley, J. J., Pisias, N. G., Prell, W. L., Shackleton, N. J., 1984. The orbital theory of pleistocene climate: support from a revised chronology of the marine δ^{18}O record. In: Berger, A., Imbrie, J., Hays, J., Kukla, G., Saltzman, B. (Eds.), *Milankovitch and Climate: Understanding the Response to Orbital Forcing*. Reidel Publishing, Dordrecht, pp. 269–305.

Jansen, J., van der Gaast, S., Koster, B., Vaars, A., 1998. CORTEX, a shipboard XRF-scanner for element analysis in split sediment cores. Marine Geology 151, 143–153.

Johnson, E. A., Murphy, T., Torreson, O. W., 1948. Pre-history of the earths magnetic field. Terr. Mag. Atmos. Elec. 53, 349–372.

Katari, K., L.Tauxe, King, J., 2000. A reassessment of post-depositional remanent magnetism: preliminary experiments with natural sediments. EARTHL 183, 147–160.

Katari, S., Bloxham, J., 2001. Effects of sediment aggregate size on drm intensity: A new theory. Earth Planet. Sci. Lett. 186, 113–122.

King, J. W., Banerjee, S. K., Marvin, J. A., 1983. A new rock magnetic approach to selecting sediments for geomagnetic paleointensity studies: application to paleointensity for the last 4000 years. J. Geophys. Res. 88, 5911–5921.

Levi, S., Banerjee, S. K., 1976. On the possibility of obtaining relative paleointensities from lake sediments. Earth Planet. Sci. Lett. 29, 219–226.

Lund, S., Stoner, J., Channell, J., Acton, G., 2006. A summary of Brunhes paleomagnetic field variability recorded in Ocean Drilling Program cores. Phys. Earth Planet. Inter. 156, 194–204.

Martinson, D., Pisias, N., Hays, J., Imbrie, J., Jr., T. M., Shackleton, N., 1987. Age dating and the orbital theory of the Ice Ages: Development of a high-resolution 0 to 300.000-Year chronostratigraphy. Quaternary Research 27, 1–29.

Mazaud, A., 2006. A first-order correction to minimize environmental influence in sedimentary records of relative paleointensity of the geomagnetic field. Geochem. Geophys. Geosyst. 7, Q07002, doi: 10.1029/2006GC001257.

Stoner, J., Channell, J., Hillaire-Marcel, C., Kissel, C., 1996. The magnetic signature of rapidly deposited detrital layers from the deep Labrador Sea: Relationship to North Atlantic Heinrich layers. Paleoceanography 11 (3), 309–325.

Tauxe, L., 1993. Sedimentary records of relative paleointensity: theory and practice. Rev. Geophys. 31, 319–354.

Valet, J.-P., 2003. Time variations in geomagnetic intensity. Rev. Geophys. 41, 1–44.

von Dobeneck, T., F.Schmieder, 1999. Using rock magnetic proxy records for orbital tuning and extended time series analyses into the super- and sub-Milankovitch Bands. In: Fischer, G., Wefer, G. (Eds.), *Use of proxies in paleoceanography: Examples from the South Atlantic*. Springer-Verlag, Berlin, pp. 601–633.

Wefer, G., cruise participants, 2001. Report and preliminary results of Meteor Cruise M46/4, Mar del Plata (Argentinia)-Salvador da Bahia (Brazil), February 10-March 13, 2000. With partial results of Meteor cruise M46/2. Berichte, FB Geowissenschaften, Universität Bremen 173.

Witt, A., Fabian, K., Bleil, U., 2005. Three-dimensional micromagnetic calculations for naturally shaped magnetite: Octahedra and magnetosomes. Earth Planet. Sci. Lett. 233, 311–324.

3.4 Does lithology influence the paleointensity record? A statistical analysis on South Atlantic pelagic sediments

Christine Franke, D.I. Hofmann, T. von Dobeneck,

Available online at www.sciencedirect.com
SCIENCE DIRECT®
Physics of the Earth and Planetary Interiors 147 (2004) 285–296
PHYSICS OF THE EARTH AND PLANETARY INTERIORS
www.elsevier.com/locate/pepi

Does lithology influence relative paleointensity records? a statistical analysis on South Atlantic pelagic sediments

Christine Franke[a,b,*], Daniela Hofmann[a], Tilo von Dobeneck[a,b]

[a] *Department of Geosciences, University of Bremen, P.O. Box 330 440, D-28334 Bremen, Germany*
[b] *Paleomagnetic Laboratory 'Fort Hoofddijk', Utrecht University, Budapestlaan 17, 3584 CD Utrecht, The Netherlands*

Received 24 November 2003

Abstract

The relative paleointensity (RPI) method assumes that the intensity of post depositional remanent magnetization (PDRM) depends exclusively on the magnetic field strength and the concentration of the magnetic carriers. Sedimentary remanence is regarded as an equilibrium state between aligning geomagnetic and randomizing interparticle forces. Just how strong these mechanical and electrostatic forces are, depends on many petrophysical factors related to mineralogy, particle size and shape of the matrix constituents. We therefore test the hypothesis that variations in sediment lithology modulate RPI records. For 90 selected Late Quaternary sediment samples from the subtropical and subantarctic South Atlantic Ocean a combined paleomagnetic and sedimentological dataset was established. Misleading alterations of the magnetic mineral fraction were detected by a routine Fe/κ test (Funk, J., von Dobeneck, T., Reitz, A., 2004. Integrated rock magnetic and geochemical quantification of redoxomorphic iron mineral diagenesis in Late Quaternary sediments from the Equatorial Atlantic. In: Wefer, G., Mulitza, S., Ratmeyer, V. (Eds.), The South Atlantic in the Late Quaternary: reconstruction of material budgets and current systems. Springer-Verlag, Berlin/Heidelberg/New York/Tokyo, pp. 239–262). Samples with any indication of suboxic magnetite dissolution were excluded from the dataset. The parameters under study include carbonate, opal and terrigenous content, grain size distribution and clay mineral composition. Their bi- and multivariate correlations with the RPI signal were statistically investigated using standard techniques and criteria. While several of the parameters did not yield significant results, clay grain size and chlorite correlate weakly and opal, illite and kaolinite correlate moderately to the NRM/ARM signal used here as a RPI measure. The most influential single sedimentological factor is the kaolinite/illite ratio with a Pearson's coefficient of 0.51 and 99.9% significance. A three-member regression model suggests that matrix effects can make up over 50% of the observed RPI dynamics.

Keywords: Relative paleointensity; PDRM; Sediment lithology; Statistical analysis; South Atlantic

1. Introduction

High-resolution records of the paleointensity of the Earth's magnetic field have been successfully obtained from marine (Roberts et al., 1997; Valet and

* Corresponding author. Tel.: +49 421 218 8922; fax: +49 421 218 8671.
E-mail address: cfranke@uni-bremen.de (C. Franke).
URL: http://www.geophysik.uni-bremen.de/, http://www.geo.uu.nl/∼forth (C. Franke).

0031-9201/$ – see front matter © 2004 Elsevier B.V. All rights reserved.
doi:10.1016/j.pepi.2004.07.004

Meynardier, 1993; Tauxe and Shackleton, 1994) and lacustrine sediment (Creer and Morris, 1996; Nowaczyk et al., 2001) sequences. These so-called 'relative paleointensities' (RPI) are determined by normalizing the natural remanent magnetisation (NRM) by the concentration of the magnetic carriers, quantified by parameters such as anhysteretic remanent magnetization (ARM), isothermal remanent magnetization (IRM) or magnetic susceptibility (κ) (Verosub, 1977; Kent, 1982; Tauxe, 1993).

The most widely accepted relative paleointensity reference for the last 800 kyr is the Sint-800 record (Guyodo and Valet, 1999), a global composite of 33 marine records. The RPI records used for this stack correlate well with each other, but not with paleoclimate, and therefore seem to carry a nearly unbiased paleointensity signal. However, on a global scale, very little sediments show such coherent patterns in RPI. In practice, many RPI records routinely obtained from pelagic sediments deviate partly or fully from Sint-800 for mostly unknown reasons. Regionally confined sets of RPI records with similar lithology typically match considerably well internally, but may correlate poorly to records of different origin and composition (Tauxe and Wu, 1990). In some cases, rock magnetic and diagenetic effects are responsible, but it has also been observed that the lithology of the sediment matrix appears to have an influence on the character of the RPI signal (Creer and Morris, 1996).

Laboratory resedimentation experiments by Lu et al. (1990) and Lu (1992) have shown that clay mineralogy and pore water salinity strongly affect PDRM intensity. Lower RPI values result from higher clay mineral, in particular kaolinite, concentration as well as from higher salinity. The authors explain the influence of mineral-dependent surface charges and interparticle forces on magnetic particle alignment by a so-called 'heterocoagulation model'.

Here, we take an analytical and statistical approach to investigate the importance of such 'matrix effects' under natural conditions. RPI data from various deep-sea sediments that were sampled across the frontal systems of the subtropical and subantarctic South Atlantic are compared. The six sites are regionally so well confined, that they should have experienced the same paleofield history, in particular if a (fairly small) dipole based latitudinal correction is applied. These very continent-far locations on the western slope of the Mid-Atlantic ridge receive mainly eolian magnetic mineral input from Patagonian sources (Schmieder et al., 2000) and therefore carry similar magnetic mineral inventories. A detailed environmental magnetic study of this region by Hofmann and Fabian is in preparation. Characteristic differences between the RPI values should therefore reflect the influence of the sediment matrix on magnetic particle alignment.

Extensive sedimentological data were collected for a total of 90 samples from six Late Quaternary sediment series. The sediment matrix was characterized with respect to lithology and grain size. Using bi- and multi-variate statistics, we challenge the prevailing working (and 'null') hypothesis that the mentioned sediment characteristics have no influence on PDRM intensity. In more mathematical terms, we investigate, whether RPI records can be expressed as a product of paleofield intensity, magnetic carrier concentration and a specific 'lithology factor' introducing the influence of the sediment matrix.

2. Material and methods

The proposed paleomagnetic and sedimentological investigations require undisturbed oxic sediments with differing lithologies, but a common field history, hence a narrow spatial distribution. For the deposits of the selected investigation area, the subtropical and subantarctic South Atlantic, all these conditions are largely fulfilled.

The material originates from the western slope of the Mid-Atlantic Ridge (MAR) between 44–32°S and 25–22°W and was taken by gravity coring during the R/V Meteor Cruise M 46/4 (Collaborative Research Center 261, University of Bremen) in March 2000 (Fig. 1). Six out of 29 recovered sediment cores (Table 1) from water depths of 3500–4300 m were selected on basis of their distinct physical properties (porosity, p-wave velocity, magnetic susceptibility and color reflectance) investigated by shipboard logging techniques (Wefer et al., 2001). According to shipboard core descriptions (Wefer et al., 2001), all sediment series appear to be free from disturbances such as hiati or turbidities. Due to a strong southwards increase in primary productivity, there is a tenfold N–S increase in sedimentation rate (0.43–4.56 cm/kyr) from the olig-

Table 1
Core information

Core	Longitude (S)	Latitude (W)	Water depth (m)	Core length (m)	Sedimentation rate (cm/kyr)
GeoB 6428-1	32°30.60	24°14.91	4015	7.26	0.43
GeoB 6425-2	33°49.51	23°35.24	4352	10.73	1.05
GeoB 6422-1	35°42.45	22°44.01	3972	5.32	1.77
GeoB 6407-1	42°02.70	19°30.00	3384	5.36	1.76
GeoB 6405-6	42°00.00	21°51.19	3862	11.94	4.56
GeoB 6408-4	43°00.00	20°26.46	3817	10.55	3.77

otrophic subtropical to the mesotrophic subantarctic South Atlantic.

The six selected cores fall into three different lithological categories; the two northernmost cores from the oligotrophic subtropics (GeoB 6425-2 and 6428-1) have elevated clay mineral contents. The two cores at the subtropical front (GeoB 6407-1 and 6422-1) mostly contain calcareous nannofossil ooze with some foraminifers due to higher primary productivity. The two southernmost cores (GeoB 6405-6 and 6408-4) are under influence of the subantarctic front and have an additional siliceous component contributed by diatoms. In the following, these three sediment types are called clay bearing, foram bearing, and diatom bearing nannofossil oozes. A total of 90 discrete samples, about 15 per core, were taken from maxima and minima of the marine isotope stages 2–8, always from matching age positions back to 280 ka.

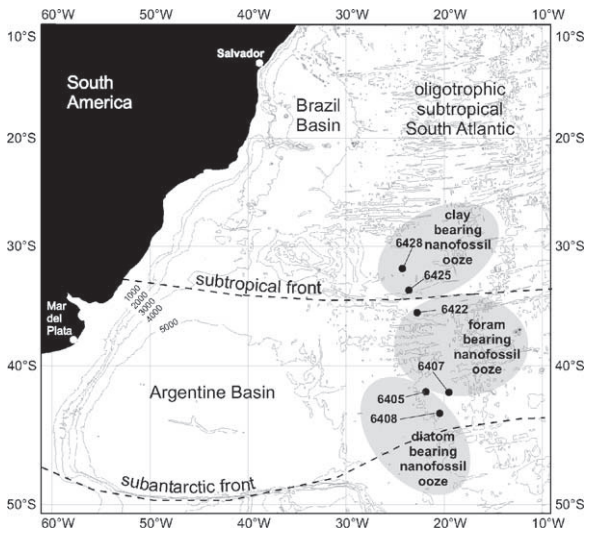

Fig. 1. Core locations in the subtropical and subantarctic South Atlantic on the western slope of the Mid-Atlantic Ridge. Sedimentation conditions are controlled by the frontal systems.

The age models of the two northernmost sediment cores GeoB 6425-2 and GeoB 6428-1 (Schmieder, 2004) were based on a correlation of susceptibility κ to the 'Subtropical South Atlantic Susceptibility Stack' (SUSAS) established by von Dobeneck and Schmieder (1999). The age models of cores GeoB 6405-6, GeoB 6407-1, GeoB 6422-1 and GeoB 6408-4 depend on a multi-parameter correlation (Hofmann et al., in preparation) of κ and element logs, which were tied to the SUSAS and SPECMAP stack (Imbrie et al., 1984). The maxima and minima of the susceptibility signal follow Quaternary climate cycles and correlate very well with available $\delta^{18}O$ isotope records (Donner, unpublished data).

The total carbonate content (Müller, unpublished data) was determined with a Herateus CHN-O-RAPID element analyzer (Weser, 1983). Carbonate content ranges between 6.4 and 86.3 wt.% and is the major matrix component in all investigated sediments. Biogenic opal was analyzed by the automated wet leaching method of Müller and Schneider (1993) and reaches up to 17.7 wt.%. The mineralogy of the clay size fraction of our selected sediment samples was investigated by X-ray powder diffraction. Texture preparations of the centrifuged, decalcified and dried sediment were analyzed in a Phillips PW 1820 diffractometer (Co Kα) and modeled with the Mac Diff 4.2.3 computer program by Petschick (2000). Iron and other element contents were identified with an automated X-ray fluorescence half-core (XRF) scanner (Jansen et al., 1998). Relative element concentrations are given in counts per second with a range from potassium (K) to iron (Fe) (Röhl and Abrams, 2000).

Grain size distribution was analyzed on ultrasonically resuspended wet bulk sediment using a Fritsch Economy Analysette 22 laser particle sizer (Fritsch,

1994). This quick method yields a good representation of the fine sand and silt fraction, but systematically underestimates the submicron clay fraction (Konert and Vandenberghe, 1997). As this effect regards all sediments in a similar way, the obtained grain size fractions should nevertheless be valuable for differentiation.

For a combined paleo- and rock-magnetic analysis (Hofmann and Fabian, in preparation), NRM, IRM and ARM AF demagnetization curves were measured on cubic samples at 5 cm spacing using an automated 2G Enterprises 755 R pass-through cryogenic magnetometer. The issue of the best available NRM standardizer for paleointensity estimates has been widely discussed (Tauxe, 1993; Tauxe, 1995; Levi and Banerjee, 1976). IRM represents the concentration of all magnetic grain sizes. Susceptibility additionally includes the dia- and para-magnetic fraction. ARM, like PDRM, is linked to the fine magnetic particle spectrum as indicated by their similar coercivity spectra. In this study the RPI signals of the sediment samples were calculated by normalizing NRM with ARM after a 20 mT AF treatment to remove viscous overprints. The alternative normalizers yield similar signals except for core GeoB 6407-1.

Early diagenetic magnetite dissolution proceeds even under mildly suboxic conditions (Karlin and Levi, 1983; Canfield, 1989; Leslie et al., 1990). It affects especially the finest magnetite particles, the main carriers of PDRM, and leaves an imprint on the RPI records. Diagenetically affected core sections had to be excluded for the purpose of this study. They were identified by the magnetite dissolution index Fe/κ proposed by Funk et al. (2004). Stable plateau values of Fe/κ throughout the sediment column are indicative of unaltered magnetic mineralogy, while locally elevated values indicate partial magnetite losses due to reductive dissolution. The rationale of this index is the diminution of the magnetic susceptibility κ relative to iron content caused by the diagenetic transformation of (ferric) ferrimagnetic into (ferrous) paramagnetic iron.

The Fe/κ plateau values of the investigated sediment cores increase by a factor of three from North to South (Franke, 2002). Two different Fe/κ levels were therefore applied to a northern (GeoB 6422-1, 6425-1, 6428-1) and southern (GeoB 6405-6, 6407-1, 6408-4) core group (Fig. 2), below which samples are considered as unaffected by reductive diagenesis. According to this criterion, more than one third of originally 90 samples gave subtle to pronounced indication of iron mineral reduction and was excluded from further consideration.

3. Results

The sedimentological characterization of the samples was based on analyses of the major components, grain size distribution and clay mineralogy. Ranges, means and N–S trends of all investigated parameters have been compiled as box-and-whisker plots in Fig. 3a–c. Foraminiferal and coccolithophorid carbonate make up 45–85% of the four northernmost cores and is complemented by terrigenous silicates (Fig. 3a). Temporal downcore variations are related to glacial-interglacial changes of the calcite lysocline (Schmieder et al., 2000). Near the subantarctic front, carbonate contents decrease 20–55% and give way to a much higher terrigenous content and additional siliceous components, mainly diatoms and radiolarians. In terms of the standard grain size classification 55–85% of the sediment falls into the

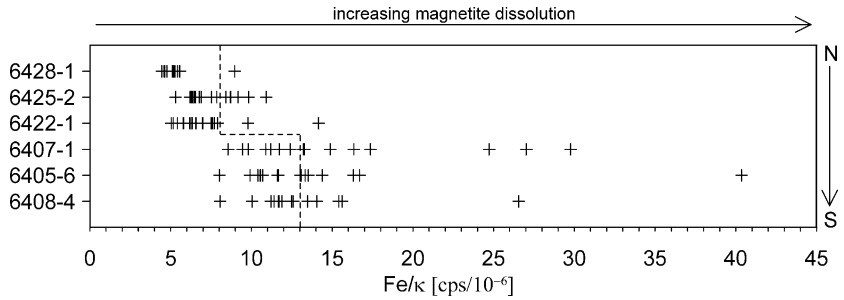

Fig. 2. Sample rejection based upon partial magnetic mineral dissolution according to regional Fe/κ criterion (Funk et al., 2004). Due to increasing Fe/κ plateau values from N to S, two separate threshold values for the northern and southern core group were chosen (dashed line).

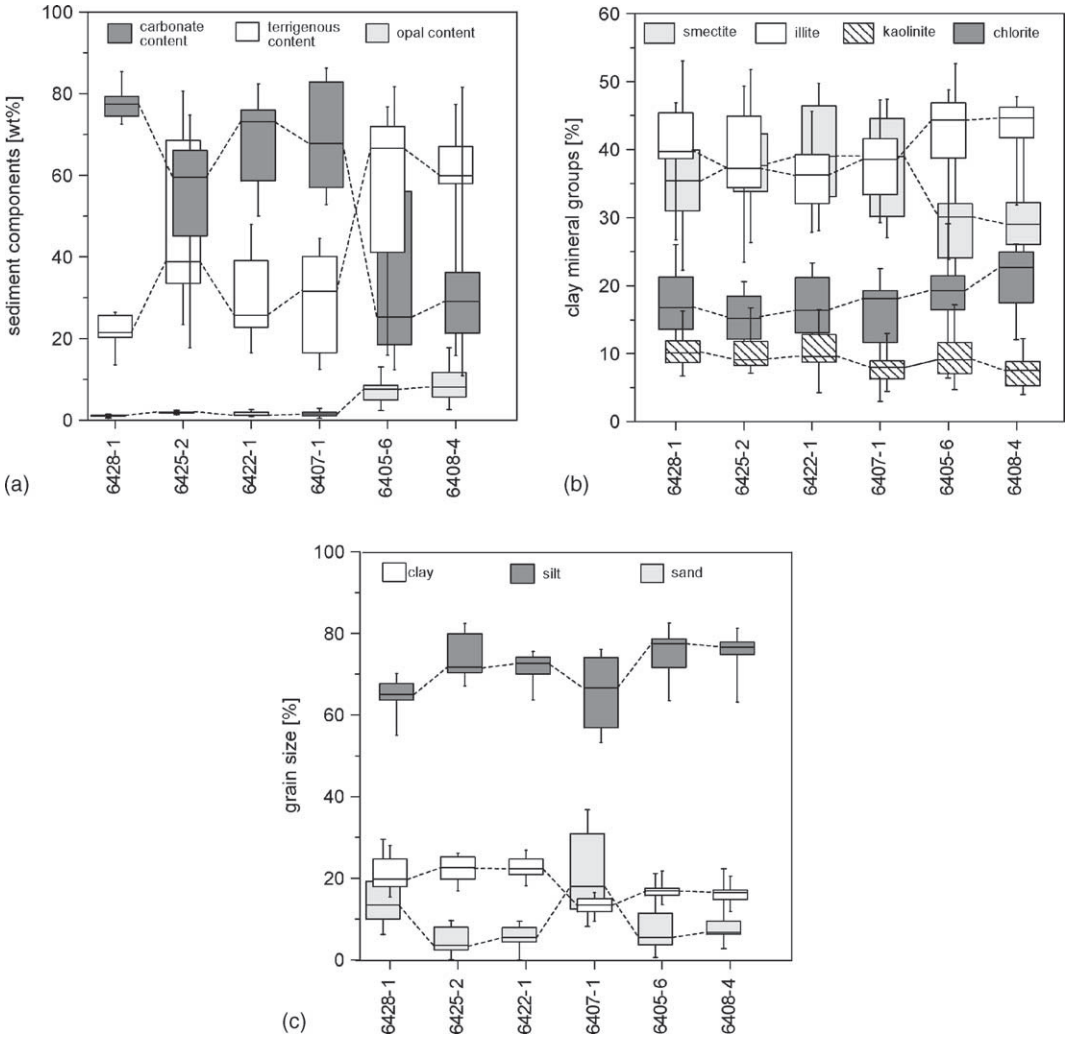

Fig. 3. Univariate box-and-whisker plots of (a) major components, (b) grain size distribution (c) clay mineralogy for the discrete samples from N to S. The boxes represent the median value and interquartile range; the whiskers mark the total data range.

silt fraction (2–63 μm), while sand (>63 μm) and clay (<2 μm) are subordinate (Fig. 3b). The terrigenous clay size fraction is higher in the subtropical than in the subantarctic zone. Winnowing effects explain the relatively high sand content at the shallowest site GeoB 6407-1 exposed to bottom-current erosion. The clay mineral analysis yields relative contents of the clay mineral groups smectite, illite, chlorite and kaolinite. Smectite and illite are the dominant phases and provide some 60–80% of the total content (Fig. 3c). In the subtropical zone, both minerals are nearly equally represented. The subantarctic region is characterized by a lower smectite and higher illite and chlorite content. Chlorite and kaolinite are subordinate, where chlorite is approximately twice as common as kaolinite. A source area and transport pathway of the clay minerals was investigated by Petschick et al. (1996).

All lithological parameters described above contribute to the sedimentary fabric and could be influential on PDRM acquisition. The dependency of the RPI values on each individual parameter was assessed on basis of a linear bivariate correlation analysis (Swan

and Sandilands, 1995). We take the standard approach in geostatistics and use Pearson's product-moment correlation coefficient

$$r_{xy} = \frac{\sum_{i=1}^{n}(x_i - \bar{x})(y_i - \bar{y})}{(N-1)s_x s_y}$$

where x_i are the independent sedimentological parameters, y_i the RPI values, $\bar{x}$ and $\bar{y}$ their respective means, s_x and s_y their standard deviations and N the size of the statistical sample. The significance of any determined r_{xy} value, which may range from 0 (uncorrelated) to ± 1 (strictly linearly dependent), is controlled by the extent of the relationship r and by the number of cases N contributing to the analysis. The test statistics for significance of the correlation coefficient,

$$t = r\sqrt{\frac{N-2}{1-r^2}}$$

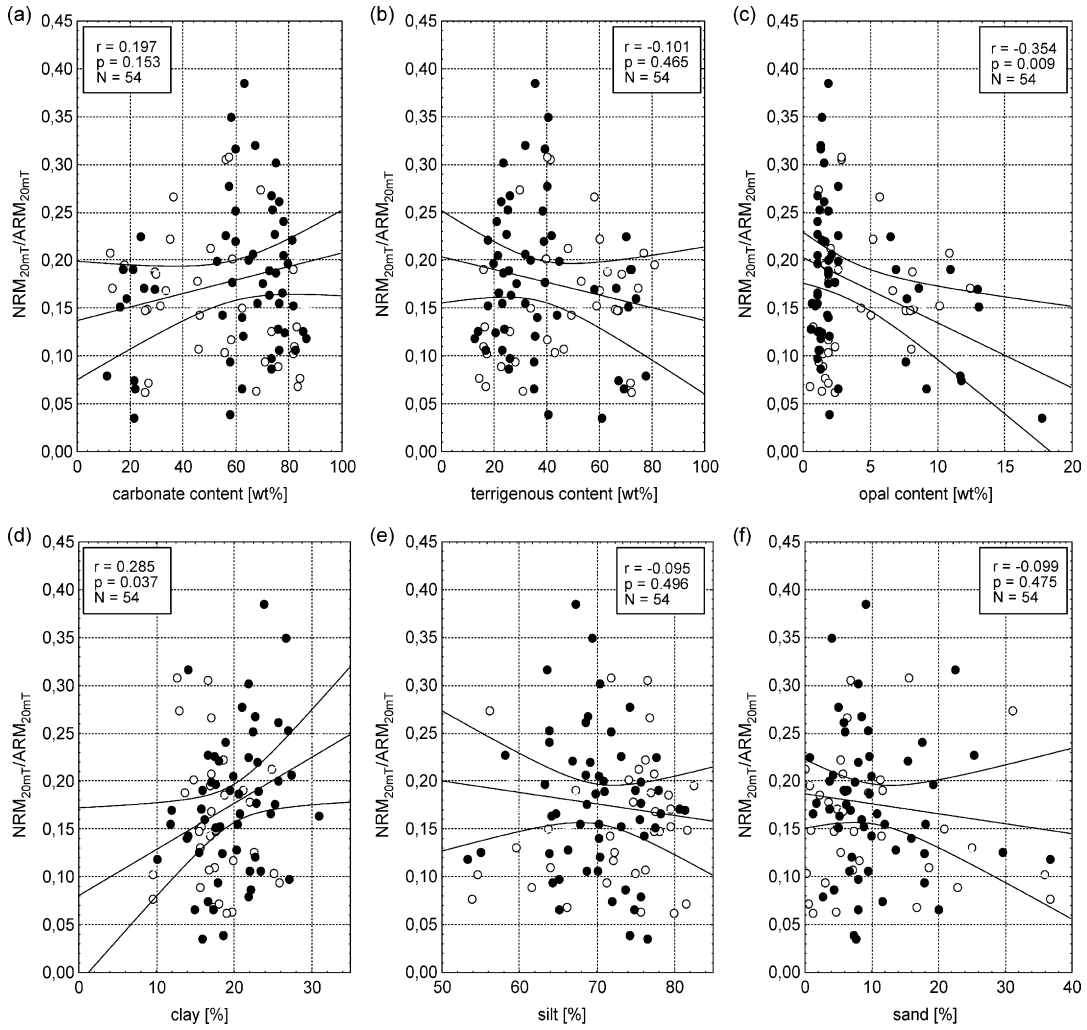

Fig. 4. Biplots of NRM_{20mT}/ARM_{20mT} vs. (a) carbonate, (b) terrigenous, (c) opal, (d) clay, (e) silt and (f) sand content. Pearson's correlation coefficients r, the probabilities p for randomness and samples sizes N are given in the figure headers. The gentle slopes of the regression lines and their broad 95% confidence range are indicative of large bivariate scatter. The correlations were exclusively based on the unaltered samples (solid symbols). The samples rejected by the diagenesis criterion (empty symbols) do not principally fall out of the major trend, but lower correlations and their significance.

leads to a probability measure, p, quantifying the likeliness, that an observed correlation is purely incidental. p-values of 0.05, 0.01 and 0.001 correspond to 95, 99 and 99.9% significance, respectively. Instead of using these fixed significance levels, we state the individual probability for randomness in each analysis.

The probability p is also reflected by the slope and width of the 95% confidence range of the linear regression line shown in the biplots. In contrast to the correlation coefficient r, the linear bivariate regression calculation assumes a causal relationship between lithology and relative paleointensity and therefore minimizes the (squared vertical) deviation of the dependent variable, i.e. NRM_{20mT}/ARM_{20mT}. Because of the impact of geomagnetic field variations and the complexity of lithological controls, each individual sedimentological factor can only exert a partial and rather feeble influence on RPI. We therefore do not present each bivariate regression equation separately and give a multiple regression analysis below.

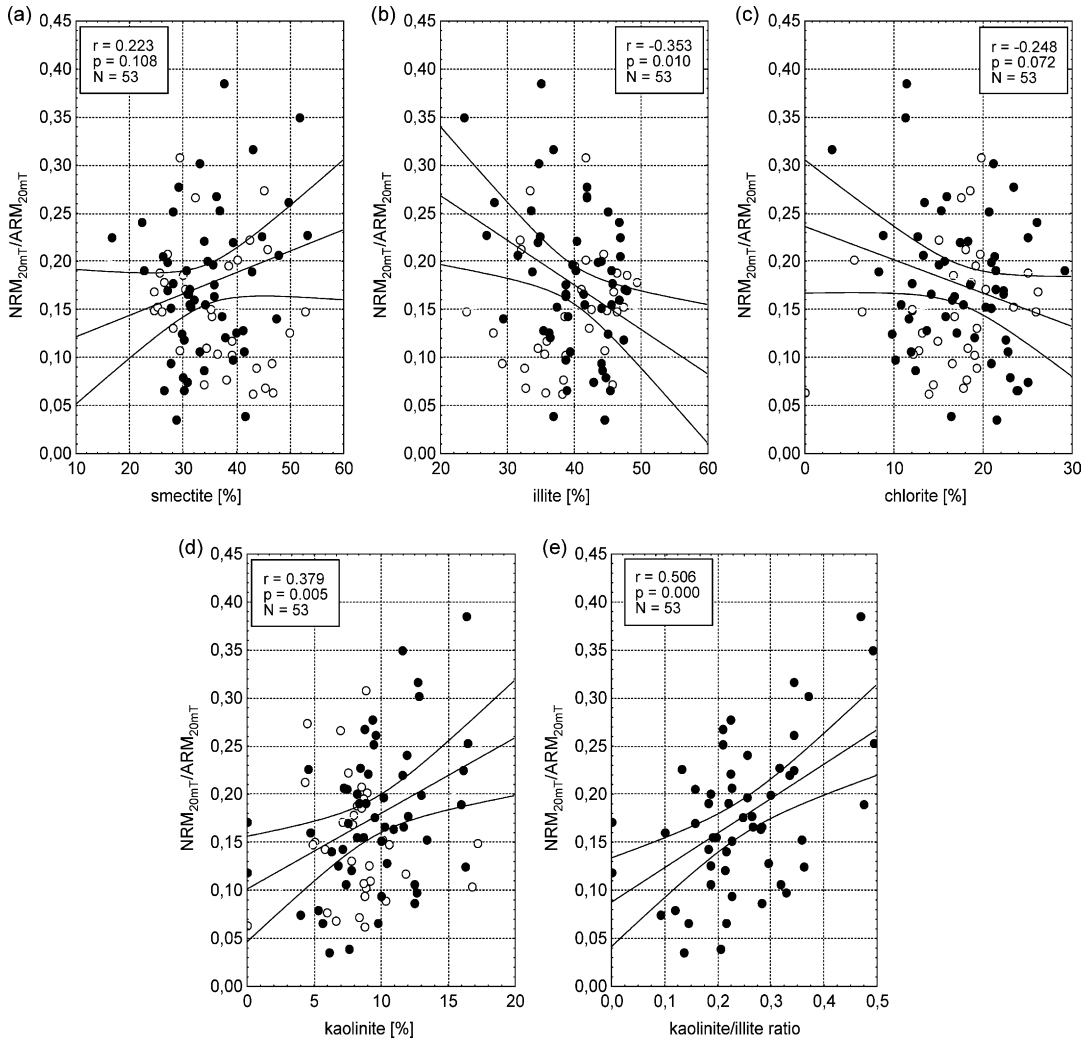

Fig. 5. Biplots of NRM_{20mT}/ARM_{20mT} vs. (a) smectite, (b) illite, (c) chlorite, (d) kaolinite content and (e) kaolinite/illite ratio. For legends and symbols see Fig. 4.

For the following correlation analyses, the data of all 54 samples from the six cores were pooled to encompass a sufficiently large lithological variability and case number. The correlations of major components and grain size fractions with the NRM_{20mT}/ARM_{20mT} ratio are depicted in Fig. 4a–f. In four of the cases, carbonate and terrigenous content, silt and sand content, the correlations are practically insignificant. There is a low (r = 0.29) positive correlation with clay at significance level of about 97% and a moderate (r = −0.35) negative correlation with opal content at 99% significance level. Fig. 5a–e show the correlations of relative clay mineral contents with the NRM_{20mT}/ARM_{20mT} ratio. In the case of smectite, the correlation is insignificant, while chlorite shows a low (r = −0.25) negative correlation at about 93% significance. Illite (r = −0.35) and kaolinite (r = 0.38) contents are moderately correlated with NRM_{20mT}/ARM_{20mT}, at significance levels of ∼99%. Because of the inverse relationships with kaolinite and illite, their ratio is more strongly

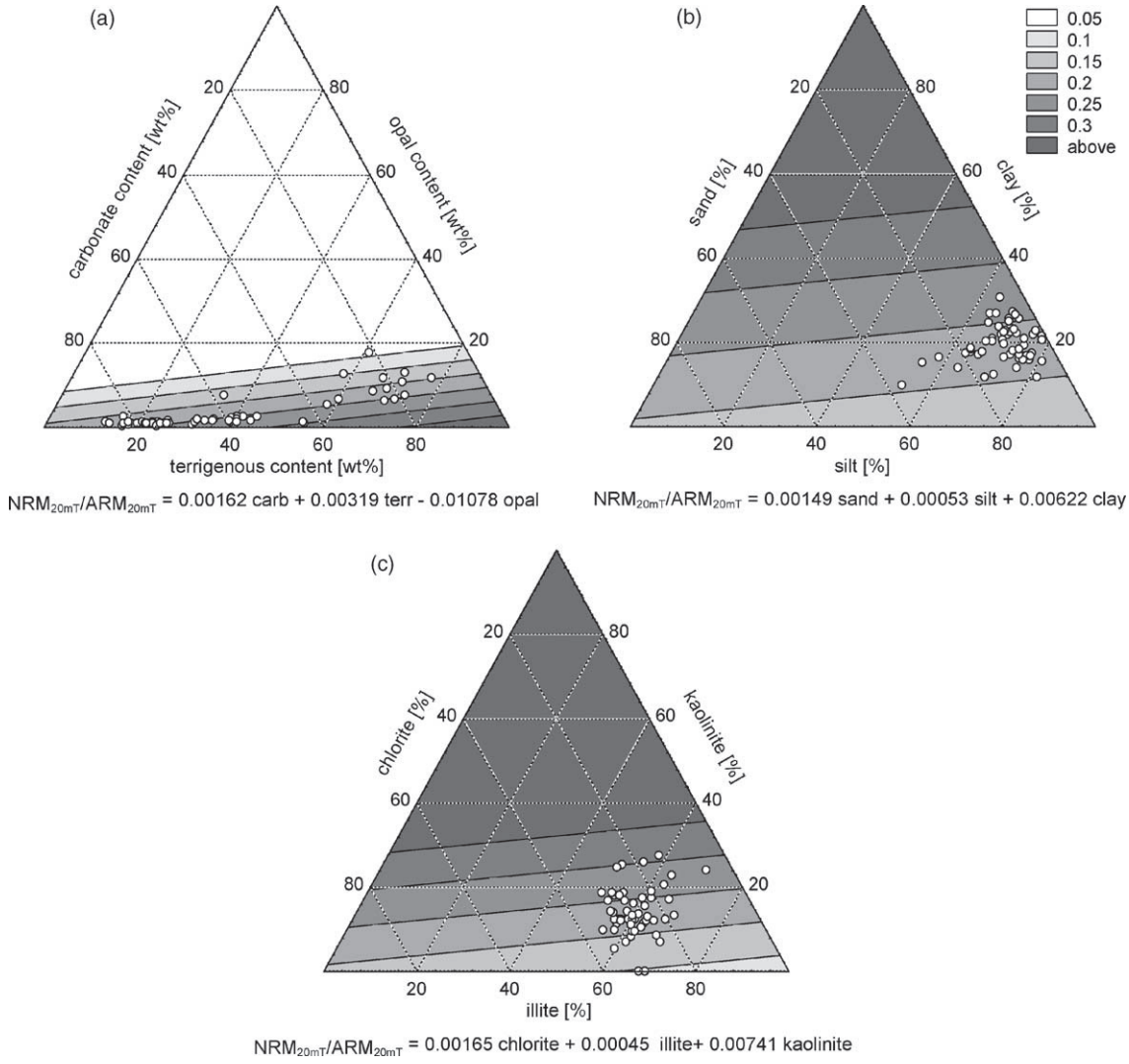

Fig. 6. Trend surface plots of NRM_{20mT}/ARM_{20mT} in the ternary systems of (a) carbonate, opal and terrigenous content, (b) sand, silt and clay percentage, (c) chlorite, illite and kaolinite.

(r = 0.51) and significantly (>99.9%) correlated with NRM_{20mT}/ARM_{20mT} than either single value.

The three lithological parameter groups can be formulated as ternary systems, in which the observed NRM_{20mT}/ARM_{20mT} values are approximated by a regression plane (Fig. 6a–c). In the case of clay mineralogy, the apparently insignificant mineral smectite was excluded and the analysis was performed in the kaolinite–illite–chlorite system. The compilation of all three ternary plots clearly hints at the decisive factors. Rather small opal content seems to lower the RPI signal, while clay content and particularly the relative kaolinite content raise its value. The defining equations of the three ternary planes are given in the diagrams.

The bivariate analyses indicate that several of the investigated sedimentological parameters show a moderate but significant correlation with the RPI signal. Since all of these parameters are to some degree mutually independent, a multiple linear regression model of all factors can be established which quantifies the combined lithological controls on the RPI signal. The difficulty of distinguishing between meaningful and redundant parameters is a well-known problem (Swan and Sandilands, 1995). Here we use the 'backward elimination' method by which an initially overdetermined regression model is successively depleted from regressors with insignificant partial correlation. Multicollinearity is avoided by omitting at least one within a group of complementary parameters from the analysis. With reasonable settings, a multiple regression solution based on the three lithological parameters opal content, terrigenous content and kaolinite/illite ratio was found. The significance level of each individual regressor is equal to or better than 95% (Table 2). The goodness-of-fit R number is 0.59 and the probability of non-randomness exceeds 99.99%. The impact of lithology on RPI is demonstrated in Fig. 7. As the NRM_{20mT}/ARM_{20mT} record doubtlessly holds considerable paleofield information, any better predictability solely based on lithological parameters would seem unrealistic.

Table 2
Summary of multiple linear regression analysis using the 'backward elimination' method

Regressors	Regression coefficient	SD of coefficient	P-Level
Intercept	0.068	±0.034	0.052
opal content	−0.009	±0.004	0.015
Terrigenous content	0.002	±0.001	0.031
Koalinite/illite ratio	0.316	±0.091	0.001

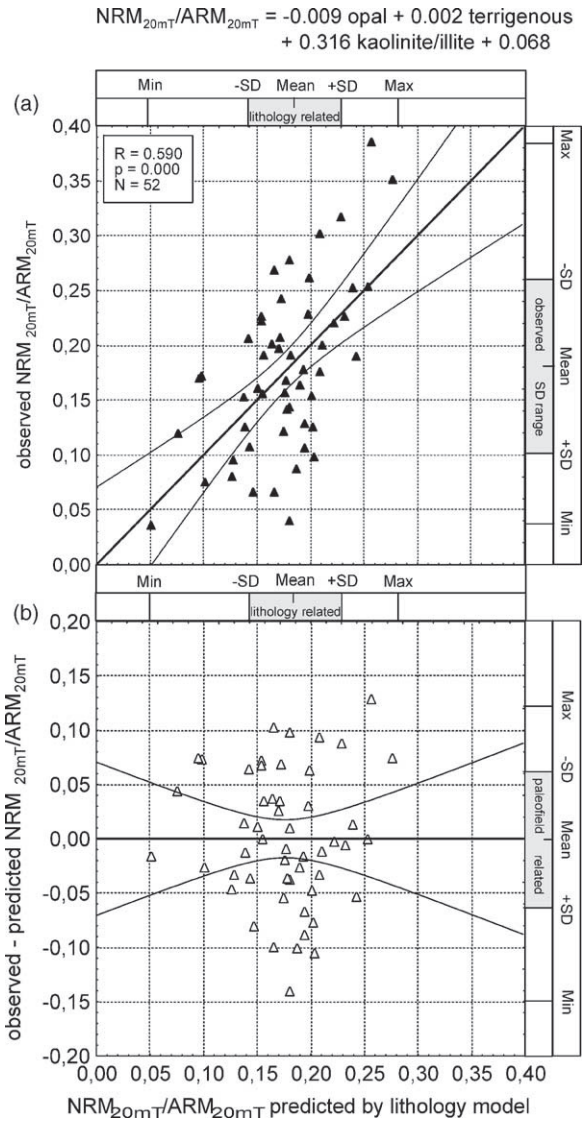

Fig. 7. Biplots of (a) observed and (b) residual NRM_{20mT}/ARM_{20mT} vs. predicted NRM_{20mT}/ARM_{20mT} resulting from the multiple regression model given above. Goodness of fit R, significance level p and sample size N is given in the figure header. All axes are equally scaled. Standard deviation (SD) ranges of the three shown parameters outline the average contributions of lithology and paleofield to the observed RPI signal.

As an alternative approach to quantifying lithology effects, the raw RPI (NRM_{20mT}/ARM_{20mT}) data of the

selected sediment samples were divided by isochronal values of the Sint-800 paleointensity stack. When plotted against the various lithology parameters, these 'paleofield corrected' RPI data show approximately the same scatter as the raw RPI data. It was initially expected, that correlations should be markedly improved by this data treatment. Probable causes for the failure are discrepancies in chronology and temporal resolution of the investigated and reference records.

4. Discussion and conclusions

Current quality requirements of RPI records as established by Levi and Banerjee (1976), King et al. (1983) and Tauxe (1993) are essentially based on rock- and paleomagnetic criteria, namely (1) magnetite as predominant magnetic carrier, homogeneity of (2) concentration and (3) magnetic grain size, as well as absence of (4) inclination errors and (5) magnetic mineral diagenesis. Ongoing analyses indicate, that criteria (1)–(4) are locally fulfilled by groups, the three northern and the three southern cores. Only for the pooled core set, the variations in magnetite concentration exceed the Tauxe (1993) 'one order of magnitude' rule. However, combining diverse lithologies was one basic requirement for the feasibility of this study. Criterion (5) was also respected: By rigorous application of the Fe/κ parameter all samples affected by (mild) chemical overprint, altogether one third of the initial collection, were excluded from the statistical analysis. What else influences paleointensity estimates?

Our statistical results suggest, that the sedimentary magnetic recording process of post-depositional particle alignment is not exclusively an expression of geomagnetic field history, but also controlled by the strong and complex interactions of magnetic carriers with their non-magnetic matrix. These mechanical and electrostatic forces are responsible for the relatively low intensity of PDRM in comparison with laboratory remanences such as ARM. The NRM_{20mT}/ARM_{20mT} ratio of the investigated samples averages at around 0.18 (Table 3). The RPI signal dynamics due to varying matrix effects are considerable; if we compare the standard deviation (SD) range of the RPI data set (±0.077) to the SD range of our lithology-dependent regression model (±0.045) and to the paleofield-dependent residue (±0.063), we find that matrix-related effects could possibly influence signal dynamics to nearly the same extend as geomagnetic field intensity variations.

Of course, the lithological spectrum encountered in our pooled sample set exceeds that of most published RPI records by far and therefore marks an upper limit of matrix-related signal biasing. Nevertheless, any paleointensity record claiming 'high fidelity' should additionally fulfil a criterion (6) related to lithological homogeneity, in particular with respect to clay mineralogy and major components. If RPI data are collected for stratigraphic purposes, we should expect sedimentologically induced patterns at lithological boundaries, e.g. at climate transitions. Our regression equations point towards the possibility of establishing multi-parameter based correction formulas to discard lithological overprint. A broader and more representative database such as the Sint-800 core set would be desirable for this objective. The numerous high-quality records should open the possibility to apply similar regression analyses on singular time slices sharpening the definition of the approach.

It is worth considering, why some of the sedimentological parameters seem to have greater influence on sedimentary magnetic recording than others. Our regionally restricted results indicate an inhibition of magnetic particle alignment by the presence of siliceous microfossils. This could be simply due to the porous structure of diatoms, radiolaria and sponge spicules which favor a high initial porosity followed by extreme postdepositional compaction. In addition, Florindo et al. (2003) suggested that magnetite alteration to authigenic smectite under oxic to suboxic conditions is favored by high silica concentrations. The growth of authigenic smectite directly on diatom

Table 3
Statistical properties of parameters in (Fig. 7)

Variable	Mean	Minimum	Maximum	SD
Observed NRM_{20mT}/ARM_{20mT}	0.183	0.035	0.385	0.077
Predicted NRM_{20mT}/ARM_{20mT}	0.183	0.049	0.281	0.045
Residual NRM_{20mT}/ARM_{20mT}	0.000	−0.153	0.126	0.063

Table 4
Comparative properties of common silicate clay minerals (adapted from Brady and Weil, 1996)

Property	Smectite	Illite	Kaolinite
Size (μm)	0.01–1.0	0.02–2.0	0.5–5.0
Shape	Flakes	Irregular Flakes	Hexagonal Crystals
External surface area (m^2/g)	70–120	70–100	10–30
Internal surface area (m^2/g)	550–650	–	–
Plasticity	High	Medium	Low
Cohesiveness	High	Medium	Low
Swelling capacity	High	Low to None	Low
Unit-layer charge	0.5–0.9	1.0–1.5	0
Interlayer spacing (nm)	1.0–2.0	1.0	0.7
Bonding	Van der Waal's	Potassium Ions	Hydrogen
Net negative charge ($cmol_c/kg$)	80–120	15–40	2–5

frustules has been described by Badaut and Risacher (1983). Clay mineralogy also appears to have a tight grip on magnetic particle orientation. We find that kaolinite has a positive and illite a negative effect on magnetic alignment, while smectite is more indifferent. This is certainly related to the unit-layer charges of the three clay minerals, eventually also to their crystalline versus flaky structure and low versus medium to high plasticity (Table 4). Specific investigations are needed to consolidate these hypotheses. We can nevertheless conclude, that lithology of the sedimentary matrix is an influential and widely underrated factor in the signal formation of relative paleointensity records.

Acknowledgements

Bernhard Diekmann from the Alfred-Wegener-Institute for Marine and Polar Research Bremerhaven/Potsdam was a great support for the clay mineral analyses. Rainer Petschick from Johann–Wolfgang Goethe University, Frankfurt a.M., kindly provided the 'MacDiff 4.2.3.' computer program for XRD analysis. Automated signal correlation for age modelling was performed with the unpublished computer programs 'Automated Signal Correlation, v.07' by Karl Fabian and 'Correlation Tool, v.6' by Thomas Frederichs from University of Bremen, Marine Geophysics group, to whom we owe also thanks for their support of the measurements. Monika Breitzke from GEOMAR Kiel supervised the laser granulometry. We thank Peter Müller for providing unpublished carbonate content data and Barbara Donner for unpublished $\delta^{18}O$ isotopy records. Financial support was provided by the Deutsche Forschungsgemeinschaft (DFG), SPP 1097, in the framework of proposals Do 705/1-1 and Fa 408/1-2. Tilo von Dobeneck acknowledges a visiting research fellowship by the Netherlands Research Centre for Integrated Solid Earth Science (ISES). Christine Franke presently enjoys a stipend of the EUROPROX graduate college (Universities of Bremen, Utrecht and Amsterdam). All data presented in this study are available at the PANGEA database (www.pangea.de, search string: FrankeC).

References

Badaut, D., Risacher, F., 1983. Authigenic smectite on diatom frustules in Bolivian saline lakes. Geochim. Cosmochim. Acta 47, 363–375.

Brady, N.C., Weil, R.R., 1996. The nature and properties of soils, 11th edition. Prentice-Hall International, Inc., New Jersey.

Canfield, D.E., 1989. Reactive iron in marine sediments. Geochim. Cosmochim. Acta 53, 619–632.

Creer, K.M., Morris, A., 1996. Proxy-climate and geomagnetic palaeointensity records extending back to ca. 75,000 BP derived from sediments cored from Largo Grande Di Monticchio. Southern Italy, Quaternary Sci. Rev. 15, 167–188.

Florindo, F., Roberts, A.P., Palmer, M.R., 2003. Magnetite dissolution in siliceous sediments. Geochem. Geophys. Geosyst., 4: 1053. doi: 10.1029/2003GC000516.

Franke, C., 2002. Der Einfluß der Lithologie auf die Rekonstruktion der "relativen Paläointensität" des Erdmagnetfeldes an spätquartären Sedimenten des subtropischen und subantarktischen Südatlantiks, Diploma thesis, Department of Geosciences, University of Bremen, 117 pp.

Fritsch GmbH Laborgerätebau, 1994. Benutzer-Handbuch Laser Particle Sizer Analysette 22, Idar Oberstein, pp. 30–37.

Funk, J., von Dobeneck, T., Reitz, A., 2004. Integrated rock magnetic and geochemical quantification of redoxomorphic iron mineral diagenesis in Late Quaternary sediments from the

Equatorial Atlantic. In: Wefer, G., Mulitza, S., Ratmeyer, V. (Eds.), The South Atlantic in the Late Quaternary: reconstruction of material budgets and current systems. Springer-Verlag, Berlin/Heidelberg/New York/Tokyo, pp. 239–262.

Guyodo, Y., Valet, J.P., 1999. Global changes in intensity of the earth's magnetic field in the past 800 kyr. Nature 399, 249–252.

Hofmann, D., Fabian, K., Schmieder, F., Donner, B., in preparation. A South Atlantic stratigraphic network.

Hofmann, D. and Fabian, K., in preparation. Investigation of the relative paleointensity parameters with respect to lithological influences.

Imbrie, J., Hays, J.D., Martinson, D.G., McIntyre, A., Mix, A.C., Morley, J.J., Pisias, N.G., Prell, W.L., Shackleton, N.J., 1984. The orbital theory of Pleistocene climate: support from a revised chronology of the marine $\delta^{18}O$ record. In: Berger, A.L., Imbrie, J., Hays, G., Kukla, G., Saltzman, B. (Eds.), Milankovitch and climate., 1. D. Reidel Publ. Comp, pp. 269–305.

Jansen, J.H.F., Van der Gaast, S.J., Koster, A.J., 1998. CORTEX, a shipboard XRF-scanner for element analyses in split sediment cores. Marine Geology 151, 143–153.

Karlin, R., Levi, S., 1983. Diagenesis of magnetic minerals in recent haemipelagic sediments. Nature 303, 327–330.

Kent, D.V., 1982. Apparent correlation of paleomagnetic intensity and climate records in deep-sea sediments. Nature 299, 538–539.

King, J.W., Banerjee, S.K., Marvin, J., 1983. A new rock-magnetic approach to selecting sediments for geomagnetic paleointensity studies: application to paleointensity for the last 4000 years. J. Geophys. Res. 88, 5911–5921.

Konert, M., Vandenberghe, J., 1997. Comparisation of laser grain size analysis with pipette and sieve analysis: a solution for the underestimation of the clay fraction. Sedimentology 44, 523–535.

Leslie, B.W., Hammond, D.E., Berelson, W.M., Lund, S.P., 1990. Diagenesis in anoxic sediments from the California Continental Borderland and its influence on iron, sulfur and magnetite behavior. J. Geophys. Res. 95B, 4453–4470.

Levi, S., Banerjee, S.K., 1976. On the possibility of obtaining relative paleointensities from lake sediments. Earth Planet. Sci. Lett. 29, 219–226.

Lu, R., Banerjee, S.K., Marvin, J., 1990. Effects of clay mineralogy and the electrical conductivity of water on the acquisition of depositional remanent magnetization in sediments. J. Geophys. Res. 95B, 4531–4538.

Lu, R., 1992. A study of the effect of matrix properties on postdepositional remanent magnetization (pDRM) acquisition in sediments, Ph.D. thesis, University of Minnesota, 171 pp.

Müller, P.J., Schneider, R., 1993. An automated leaching method for the determination of opal in sediments and particulate matter. Deep-sea Res. 1, 425–444.

Nowaczyk, N.R., Harwart, S., Melles, M., 2001. Impact of early diagenesis and bulk particle grain size distribution on estimates of relative geomagnetic palaeointensity variations in sediments from Lama Lake, northern Central Siberia. Geophys. J. Int. 145, 300–306.

Petschick, R., Kuhn, G., Gingele, F., 1996. Clay mineral distribution in surface sediments of the South Atlantic: sources, transport and relation to oceanography. Marine Geology 130, 203–229.

Petschick, R., 2000. MacDiff 4.2.3, unpublished computer program, Johann-Wolfgang Goethe Universität, Frankfurt a. M.

Roberts, A.P., Lehman, B., Weeks, R.J., Verosub, K.L., Laj, C., 1997. Relative paleointensity of the geomagnetic field over the last 200,000 years from ODP Sites 883 and 884, North Pacific Ocean. Earth Planet Sci. Let. 152, 11–23.

Röhl, U., Abrams, L.J., 2000. High-resolution down hole and non-destructive core measurements from sites 999 and 1001 in the Caribbean Sea: application to the late Paleocene thermal maximum. In: Leckie, R.M., Sigurdsson, H., Acton, G.D., Draper, G. (Eds.), ODP Sci. Res., 165, pp. 191–203.

Swan, A.R.H., Sandilands, M., 1995. Introduction to geological data analysis. Blackwell Science Ltd., Oxford, London.

Schmieder, F., von Dobeneck, T., Bleil, U., 2000. The Mid-Pleistocene climate transition as documented in the deep South Atlantic Ocean: initiation, interim state and terminal event. Earth Planet. Sci. Lett. 179, 539–549.

Schmieder, F., 2004. Magnetic signals in Plio-Pleistocene sediments of the South Atlantic: chronostratigraphic usability and paleoceanographic implications. In: Wefer, G., Mulitza, S., Ratmeyer, V. (Eds.), The South Atlantic in the Late Quaternary: reconstruction of material budgets and current systems. Springer-Verlag, Berlin/Heidelberg/New York/Tokyo, pp. 263–279.

Tauxe, L., Wu, G., 1990. Normalized remanence in sediments of the western equatorial Pacific: relative paleointensity of the geomagnetic field? J. Geophys. Res. 95B, 12.337-12.350.

Tauxe, L., 1993. Sedimentary records of relative paleointensity of the geomagnetic field: theory and practice. Rev. Geophys. 31, 319–354.

Tauxe, L., Shackleton, N.J., 1994. Relative paleointensity records from the Ontong-Java Plateau. Geophys. J. Int. 117, 769–782.

Tauxe, L., 1995. Relative paleointensity in sediments: a pseudo-Thellier approach Geophys. Res. Let. 22, 2885–2888.

Valet, J.-P., Meynardier, L., 1993. Geomagnetic field intensity and reversals during the past four million years. Nautre 366, 234–238.

Verosub, K.L., 1977. Depositional and postdepositional processes in the magnetization of sediments. Geophys. Space Phys. 15, 129–143.

von Dobeneck, T., Schmieder, F., 1999. Using rock magnetic proxy records for orbital tuning and extended time series analysis into the super- and sub-Milankovitch bands. In: Wefer, G., Fischer, G. (Eds.), Use of proxies in paleooceanography: examples from the South Atlantic. Springer-Verlag, Berlin/Heidelberg, pp. 601–633.

Wefer, G. and cruise participants, 2001. Report and preliminary results of Meteor-cruise M 46/4, Mar del Plata (Argentina)—Salvador (Brazil), 10.2-13.3.2000, Reports of the Department of Geosciences, University of Bremen, 173, 136 pp.

Weser, G., 1983. CHN-Elementanalyse im Halbmikromaßstab, Heraeus-Sonderdruck, Leybold-Heraeus GmbH, pp. 14–43.

4 Summary and outlook

This study was conducted within the framework of a special priority program "*Geomagnetic Variation: Space-Time Structure, Processes, and Effects on System Earth*", conducted by the Deutsche Forschungsgemeinschaft (DFG) between 2000 and 2006. The program combined many different disciplines such as geomagnetism, paleomagnetism, geology, theoretical physics, solar physics, astrophysics, applied mathematics, magnetospheric physics and atmospheric physics. One aim of the program was to study the dynamics of the variations in intensity of the Earth's magnetic field. In addition the high - resolution records of paleointensity obtained in course of the program can be used as global correlation tool for magnetostratigraphic studies and also as basis to refine dynamo models for a better understanding of the variations of the Earth's magnetic field.

Sedimentary sequences provide continuous, high - resolution and global records for paleointensity investigations. The quality of sedimentary records for relative paleointensity investigations is still under discussion and no common theory of remanence acquisition in sediments exists. Classical relative paleointensity estimates are calculated by normalizing the natural remanent magnetization (NRM) with respect to a concentration dependent magnetic parameter, such as anhysteretic or isothermal remanent magnetization (ARM, IRM). However, there is still an ongoing discussion which parameter is the best normalizer. The here presented work provides a broad study of rock - magnetic and relative paleointensity investigations on eight sediment series from a constraint area in the subtropical and subantarctic South Atlantic. Due to the very complex sedimentation environment they exhibit quite different sediment lithologies. This varying sedimentary compositions, which for the reconstruction of geomagnetic variation usually is a most unwanted effect, was a prerequisite for this study. Assuming that because of their regional proximity the sediments have experienced approximately the same magnetic field history, differences in their relative paleointensity signal must be caused by their varying sediment composition and recording properties. Based on this data set a completely new approach is made to quantitatively identify which sediment parameters significantly influences relative paleointensity determination. A newly developed computer aided multi - parameter signal correlation method was used to construct a common high - precision age model for the eight different sedimentary recordings based on high - resolution records of magnetic volume susceptibility κ, wet bulk density ρ, δ^{18}O and X-ray fluorescence scans. By optimizing the correlations over all parts, the final stratigraphic network provides a detailed joint chronology for all cores with an internal consistency that ensures a relative median age error of less then 5 ka. This stratigraphic network provides a comprehensive study of rock - and paleomagnetic investigations to quantify the differences in magnetic mineral content and grain size throughout the cores and resulted in high - resolution records of natural remanent magnetization (NRM) and rock - magnetic properties. As mentioned above the quality of sedimentary records for relative paleointensity investigations is still under discussion and several quality criteria were assumed ([9]) to asses the quality. In this study an additional quality criteria was developed to enhance the quality of the records by performing a principal component analysis (PCA) of the natural remanent magnetization (NRM) and also on the anhysteretic and isothermal remanent magnetization (ARM, IRM) to determine a homogeneity interval, where remanences are only affected by a single environmental signal. For all network cores it turned out that in the 30 to 80 mT

demagnetization interval all remanences indicate, that their signal is mainly explained by a single environmental influence. This method further reduced lithologic and climatic influence upon the relative paleointensity record. For each single network core, relative paleointensity was calculated in the previously determined homogeneity interval, by using the standard normalization technique using either ARM, IRM or susceptibility κ. These different normalizations lead to quite similar results and stacking this individual relative paleointensity records provided a first field intensity record for the central South Atlantic spanning the last 300 ka (SAS-300) and can be used to investigate the link between southern and northern relative paleointensity records. Although several features of this stack are still clearly controlled by the strongly varying lithologies, many of the characteristics can be related to other relative paleointensity stacks, such as SINT-800, SAPIS or the record from ODP-Site 1089 ([46, 18, 19])

The final aim of this comprehensive study was to asses the influence of sediment composition upon relative paleointensity. The obtained results form the basis of a new approach towards correction of relative paleointensity records with respect to sediment composition. Therefore, a linear extension of the standard relative paleointensity determination was developed, taking into account the influence of different sediment parameters. Application of this new method for paleointensity determination for different sediment parameters allows to quantitatively identify the most significant influences upon relative paleointensity. Correcting relative paleointensity with the most influential parameter allows to perform a corrected relative paleointensity stack for the central South Atlantic (SASC-300). Additionally the ratio of the uncorrected stack to the corrected stack shows clear correlations to global climate curves like SPECMAP and the summer insolation signal from 65deg North. This leads to the conclusion that the correction method removed a global climate signal from the stack. A further result of this study is to provide a solution of determining the better normalizer for relative paleointensity determination, because by normalizing NRM with IRM it was found that other lithologic sediment parameters are less influential than after normalizing with respect to ARM.

Overall, the presented study enables to select sedimentary records for relative paleointensity investigations even if they do not fulfill all so far used criteria ([9]) and it provides the opportunity to enhance the theory of remanence acquisition in sediments. Since this is the first approach to correct relative paleointensity with respect to lithologic parameters and it also includes only cores from a constraint area, the future aim will be to study other, for example global, sedimentary records and also other compositional or lithologic parameters to refine the method. Finally, corrected relative paleointensity records can be used as a global correlation tool for magnetostratigraphic studies and also as basis to refine dynamo models to understand more about the variations of the Earth's magnetic field.

References

[1] S. Cande, D. Kent, Revised calibration of the geomagnetic polarity time scale for the Late Creraceous and Cenozoic, J. Geophys. Res. 100 (1995) 6093–6095.

[2] F. D. Stacey, On the role of brownian motion in the control of detrital remanent magnetization in sediments, Pure and Applied Geophysics 98 (1972) 139–145.

[3] M. van Vreumingen, The influence of salinity and flocculation upon the acquisition of remanent magnetization in some artificial sediments, Geophys. Journal Int. 114 (1993) 607–614.

[4] M. van Vreumingen, The magnetization intetsity of some artificial suspensions while flocculating in a magnetic field, Geophys. Journal Int. 114 (1993) 601–606.

[5] S. Katari, J. Bloxham, Effects of sediment aggregate size on drm intensity: A new theory, Earth Planet. Sci. Lett. 186 (2001) 113–122.

[6] E. A. Johnson, T. Murphy, O. W. Torreson, Pre-history of the earths magnetic field, Terr. Mag. Atmos. Elec. 53 (1948) 349–372.

[7] L. Tauxe, D. Kent, Properties of a detrital remanence carried by hematite from study of modern river deposits and laboratory redeposition experiments, Geophys. J. R. Astron. Soc. 77 (1984) 543–561.

[8] G. Anson, K. Kodama, Compaction-induced inclination shallowing of the post-depositional remanent magnetization in a synthetic sediment, Geophys. J.R. Astron. Soc. 88 (1987) 673–692.

[9] L. Tauxe, Sedimentary records of relative paleointensity: Theory and practice, Rev. Geophys. 31 (1993) 319–354.

[10] S. Levi, S. K. Banerjee, On the possibility of obtaining relative paleointensities from lake sediments, Earth Planet. Sci. Lett. 29 (1976) 219–226.

[11] J. W. King, S. K. Banerjee, J. A. Marvin, A new rock magnetic approach to selecting sediments for geomagnetic paleointensity studies: application to paleointensity for the last 4000 years, J. Geophys. Res. 88 (1983) 5911–5921.

[12] Y. Guyodo, J.-P. Valet, Global changes in the intensity of the Earth's magnetic field during the past 800 kyr, Nature 399 (1999) 249–252.

[13] J. Valet, L. Meynadier, A comparison of different techniques for relative paleointensity, Geophys. Res. Lett. 25 (1998) 89–92.

[14] J. Channell, J.-P. Valet, D. Hodell, C. Charles, Geomagnetic paleointensity from late Brunhes-age piston cores from the subantarctic South Atlantic, Earth Planet. Sci. Lett. 175 (2000) 145–160.

[15] J. Tarduno, S. L. Wilkison, Non-steady state magnetic mineral reduction, chemical lock-in, and delayed remanence acquisition in pelagic sediment, Earth Planet. Sci. Lett. 144 (1996) 315–326.

[16] M. Schwartz, S. P. Lund, T. C. Johnson, Environmental factors as complicating influences in the recovery of quantitative geomagnetic field paleointensity estimates from sediments, Geophys. Res. Lett. 23 (19) (1996) 2693–2696.

[17] A. Smirnov, J. Tarduno, Low-temperature magnetic properties of pelagic sediments (ocean drilling program site 805c): Tracers of maghemitization and magnetic mineral reduction, J. Geophys. Res. 105, (B7) (2000) 16457–16471.

[18] J. Stoner, C. Laj, J. Channell, C. Kissel, South Atlantic and North Atlantic geomagnetic paleointensity stacks (0- 80 ka): implications for inter-hemispheric correlation., Quaternary Science Reviews 21 (2002) 1141–1151.

[19] J. Stoner, J. Channell, D. Hodell, C. Charles, A ∼580 kyr paleomagnetic record from the sub-Antarctic South Atlantic (Ocean drilling Program Site 1089), J. Geophys. Res. 108 (2002) 1141–1151.

[20] S. Lund, J. Stoner, J. Channell, G. Acton, A summary of Brunhes paleomagnetic field variability recorded in Ocean Drilling Program cores, Phys. Earth Planet. Inter. 156 (2006) 194–204.

[21] N. Thouveny, J. Carcaillet, E. Moreno, G. Leduc, D. Nerini, Geomagnetic moment variation and paleimagnetic excursions since 4000 kyr BP: a stacked record from sedimentary sequences of the Portuguese margin, Earth and Planetary Science Letters 219 (2004) 377–396.

[22] R. Weeks, C. Laj, L. Endignoux, A. Mazaud, L. Labeyrie, A. Roberts, C. Kissel, E. Blanchard, Normalised natural remanent magnetisation intensity during the last 240000 years in piston cores from the central North Atlantic Ocean: geomagnetic filed intensity or environmental signal?, Phys. Earth Planet. Inter. 87 (1995) 213–229.

[23] S. Brachfeld, S. Banerjee, A new high resoultion geomacnetic relative paleointensity record for the North Atlantic Holocene: A comparision of sedimentary and absolute intensity data, Journal of Geophysical research 105, (B1) (2000) 821–834.

[24] K. Katari, L.Tauxe, J. King, A reassessment of post-depositional remanent magnetism: preliminary experiments with natural sediments, Earth Planet. Sci. Lett. 183 (2000) 147–160.

[25] Y. Yu, L. Tauxe, A. Genevey, Toward an optimal geomagentic field intensity determination technique, Geochemistry, Geophysics,Geosystems 5, Q02H07 (2) (2004) doi:10.1029/2003GC000630.

[26] L. Tauxe, J. Steindorf, A. Harris, Depositional remanent magnetization: Towards an improved theoretical and experimental foundation 244 (2006) 515–529.

[27] A. Mazaud, A first-order correction to minimize environmental influence in sedimentary records of relative paleointensity of the geomagnetic field, Geochem. Geophys. Geosyst. 7, Q07002 (2006) doi: 10.1029/2006GC001257.

[28] G. Wefer, cruise participants, Report and preliminary results of Meteor Cruise M46/4, Mar del Plata (Argentinia)-Salvador da Bahia (Brazil), February 10- March 13, 2000. With partial results of Meteor cruise M46/2., Berichte, FB Geowissenschaften, Universität Bremen 173.

[29] J. Reid, On the total geostrophic circulation of the South Atlantic Ocean: Flow patterns, tracers, and transports, Progress in Oceanography 23 (1989) 149–244.

[30] L. Talley, Antarctic Intermediate Water in the South Atlantic, in: G. Wefer, W. D. Siedler, W.H. (Eds.), *The South Atlantic: Present and Past circulation*, Springer Verlag, Berlin, 1996, pp. 219–238.

[31] L. Stramma, R. Peterson, The South Atlantic current, J. phys. Ocean. 20 (1990) 846–859.

[32] L. Stramma, M. England, On the water masses and mean circulation of the South Atlantic Ocean, J. Geophys. Res. 104 (C9) (1999) 20863–20883.

[33] C. Franke, D. Hofmann, T. von Dobeneck, Does lithology influence the paleointensity record? A statistical analysis on South Atlantic pelagic sediments, Phys. Earth Planet. Inter. 147 (2004) 285–296.

[34] S. Robinson, The late pleistocene paleocliamtic record of North-Atlantic deep sea sediments revealed by mineral magnetic measurements, Phys. Earth Planet. Inter. 42 (1986) 22–47.

[35] S. Robinson, Applications for whole-core-magnetic susceptibility measurements of deep-see sediments, Proc ODP Sci Results 115 (1990) 737–771.

[36] R. Thompson, F. Oldfield, Environmantal magnetism, Allen and Unwin, London (1986) 1–227.

[37] F. Heider, A. Zitzelberger, K. Fabian, Magnetic susceptibility and remanent coercive force in grown magnetit crystals from 0.1 μm to 6 mm, Earth Planet. Sci. Lett. 93 (1996) 239–256.

[38] F. Schmieder, Magnetic signals in plio-pleistocene sediments of the South Atlantic: Chronostratigraphic usability and paleoceanographic implication, in: G. Wefer, S. Mulitza, V. Ratmeyer (Eds.), *The South Atlantic in the Late Quaternary: reconstruction of material budgets and current systems*, Springer-Verlag, Berlin, 2004, pp. 269–305.

[39] H.-U. Worm, On the superparamagnetic–stable single domain transition for magnetite, and frequency dependence of susceptibility, Geophys. J. Int. 133 (1998) 201 – 206.

[40] J. Jansen, S. van der Gaast, B. Koster, A. Vaars, CORTEX, a shipboard XRF-scanner for element analysis in split sediment cores, Marine Geology 151 (1998) 143–153.

[41] U. Roehl, L. Abrams, High resolution, downhole, and nondestructive core measurements from sites 999 and 1001 in the caribbean sea: Application to the late paleocene thermal maximum, Proc. ODP Sci. Results 165 (2000) 191–203.

[42] R. Boyce, Electrical resitivity of modern marine sedimetn from bering sea, J. Geophys. Res. 73 (1968) 4759–4766.

[43] R. Boyce, Sound velocity-density parameters of sediment and rock from dsdp drill sites 315-318 on the line islands chain, manihiki plateau, and tuamotu ridge in the pacific ocean, In: Schlanger, S.O., E.D. Jackson et al., Init. Repts. DSDP 33 (1976) 695–728.

[44] T. v. Dobeneck, A systematic analysis of natural magnetic mineral assemblages based on modelling hysteresis loops with coercivity-related hyperbolic basis functions, Geophys. J. Int. 124 (1996) 675–694.

[45] J. Bloemendal, J. King, F. Hall, S.-J. Doh, Rock magnetism of late neogene and pleistocene deep-sea sediments: Relationship to sediment source, diagenetic processes and sediment lithology, J. Geophys. Res. 97 (B4) (1992) 4361–4375.

[46] Y. Guyodo, J.-P. Valet, Global changes in the intensity of the Earth's magnetic field during the past 800 kyr, Nature 399 249–252.

[47] J. Channell, A. Mazaud, P. Sullivan, S. Turner, M. Raymo, Geomagnetic excursions and paleointnesities in the Matuyama Chron at Ocean Drilling Program Sites 983 and 984 (Iceland Basin), J. Geophys. Res. 107 (B6) (2002) 2114.

[48] D. Hofmann, K. Fabian, Rock-magnetic properties and relative paleointensity stack for the last 300 ka based on a stratigraphic network from the subtropical and subantarctic south atlantic, EARTHL 260 (2007) 297–312.

Danksagung

Die vorliegende Arbeit wurde in der Arbeitsgruppe Marine Geophysik im Fachbereich Geowissenschaften der Universität Bremen erstellt. Für die Vergabe und Betreuung, sowie die stete Gesprächs- und Diskussionsbereitschaft, bedanke ich mich sehr herzlich bei Herrn Prof. Dr. Ulrich Bleil und Herrn Dr. habil. Karl Fabian.
Des Weiteren möchte ich mich bei Frau PD. Dr. Sabine Kasten für Ihre Unterstützung und konstruktive Fachgespräche sowie die Übernahme des Zweitgutachtens ganz herzlich bedanken.

Bei allen aktuellen und ehemaligen Mitarbeitern der Arbeitsgruppe Marine Geophysik der Universität Bremen möchte ich mich bedanken für die stete Hilfsbereitschaft bei der Durchführung der Messungen und bei technischen Problemen im Labor.
Besonderer Dank gilt Herrn Dr. Thomas Frederichs und Herrn Dr. Frank Schmieder für die vielen wissenschaftlichen Gespräche.

Ich möchte mich bei Frau Dr. Babara Donner für die Bereitstellung von z.T. unveröffentlichtem Datenmaterial und bei Frau Dr. Ursula Röhl für die Hilfbereitschaft bei den Messungen am XRF - Scanner bedanken.

Bedanken möchte ich mich bei Melanie, Tilmann und Christine für ihre stete Disskussions- und Hilfsbereitschaft sowie bei allen anderen die in irgendeiner Art und Weise zum Gelingen dieser Arbeit beigetragen haben.

Ein besonderer Dank gilt meinen Eltern, die mir uneingeschränkt ihre Unterstützung gegeben haben und die immer für mich da waren und sind.

Bibliography

Section 3.1:
Hofmann D.I., Fabian K., Schmieder F., Donner B. (2005), A stratigraphic network from the subtropical and subantarctic South Atlantic: Multiparameter correlation of magnetic susceptibility, density, X-ray fluorescence measurements and δ^{18}O, Earth and Planetary Science Letters, 240, 694-709, doi:10.1016/j.epsl.2005.09.048

Section 3.2:
Hofmann D.I., Fabian K. (2007), Rock-magnetic properties and relative paleointensity stack for the last 300 ka based on a stratigraphic network from the subtropical and subantarctic South Atlantic, Earth and Planetary Science Letters, 260, 297-312, doi:10.1016/j.epsl.2007.05.042

Section 3.3:
Hofmann D.I., Fabian K., Correcting relative paleointensity records for variations in sediment composition: Results from a South Atlantic stratigraphic network, submitted to Earth and Planetary Science Letters

Section 3.4:
Franke C., Hofmann D.I., von Dobeneck T. (2004), Does lithology influence the paleointensity record? A statistical analysis on South Atlantic pelagic sediments, Physics of the Earth and Planetary Interiors, 147, 285-296, doi:10.1016/j.pepi.2004.07.004